PROBABILISTIC SEISMIC HAZARD ASSESSMENT OF ILGAZ - ABANT SEGMENTS OF NORTH ANATOLIAN FAULT USING IMPROVED SEISMIC SOURCE MODELS

A THESIS SUBMITTED TO
THE GRADUATE SCHOOL OF NATURAL AND APPLIED SCIENCES
OF
MIDDLE EAST TECHNICAL UNIVERSITY

BY

MERT LEVENDOĞLU

IN PARTIAL FULFILLMENT OF THE REQUIREMENTS
FOR
THE DEGREE OF THE MASTER OF SCIENCE
IN
CIVIL ENGINEERING

JANUARY 2013

Approval of the thesis:

PROBABILISTIC SEISMIC HAZARD ASSESMENT OF ILGAZ – ABANT SEGMENTS OF NORTH ANATOLIAN FAULT USING IMPROVED SEISMIC SOURCE MODELS

submitted by **MERT LEVENDOĞLU** in partial fulfillment of the requirements for the degree of **Master of Science in Civil Engineering Department, Middle East Technical University** by,

Prof. Dr. Canan Özgen _____
Dean, Graduate School of **Natural and Applied Science**

Prof. Dr. Ahmet Cevdet Yalçıner _____
Head of Department, **Civil Engineering**

Asst. Prof. Dr. Zeynep Gülerce _____
Supervisor, **Civil Engineering Dept., METU**

Examining Committee Members:

Prof. Dr. M. Yener Özkan _____
Civil Engineering Dept., METU

Assoc. Prof. Dr. Zeynep Gülerce _____
Civil Engineering Dept., METU

Prof. Dr. Kemal Önder Çetin _____
Civil Engineering Dept., METU

Assoc. Prof. Dr.Aysegül Askan Gündoğan _____
Civil Engineering Dept., METU

Dr. Fuat Şaroğlu _____
Kayen Kayı Energy Investments Inc.

Date: 28.01.2013

I hereby declare that all information in this document has been obtained and presented in accordance with academic rules and ethical conduct. I also declare that, as required by these rules and conduct, I have fully cited and referenced all material and results that are not original to this work.

Name, Last name : Mert Levendoğlu

Signature :

ABSTRACT

PROBABILISTIC SEISMIC HAZARD ASSESSMENT OF ILGAZ - ABANT SEGMENTS OF NORTH ANATOLIAN FAULT USING IMPROVED SEISMIC SOURCE MODELS

Levendoğlu, Mert
M.Sc., Department of Civil Engineering
Supervisor: Asst. Prof. Dr. Zeynep Gülerce

January 2013, 85 pages

Bolu-Ilgaz region was damaged by several large earthquakes in the last century and the structural damage was substantial especially after the 1944 and 1999 earthquakes. The objective of this study is to build the seismic source characterization model for the rupture zone of 1944 Bolu-Gerede earthquake and perform probabilistic seismic hazard assessment (PSHA) in the region. One of the major improvements over the previous PSHA practices accomplished in this study is the development of advanced seismic source models in terms of source geometry and reoccurrence relations. Geometry of the linear fault segments are determined and incorporated with the help of available fault maps. Composite magnitude distribution model is used to properly represent the characteristic behavior of NAF without an additional background zone. Fault segments, rupture sources, rupture scenarios and fault rupture models are determined using the WG-2003 terminology. The Turkey-Adjusted NGA-W1 (Gülerce et al., 2013) prediction models are employed for the first time on NAF system. The results of the study is presented in terms of hazard curves, deaggregation of the hazard and uniform hazard spectrum for four main locations in the region to provide basis for evaluation of the seismic design of special structures in the area. Hazard maps of the region for rock site conditions and for the proposed site characterization model are provided to allow the user perform site-specific hazard assessment for local site conditions and develop site-specific design spectrum. The results of the study will be useful to manage the future seismic hazard in the region.

Keywords: Probabilistic Seismic Hazard Assessment, Seismic Source Modeling, Ground Motion Prediction Equations, North Anatolian Fault, 1944 Bolu-Gerede Earthquake

ÖZ

GELİŞTİRİLMİŞ SİSMİK KAYNAK MODELLERİ OLUŞTURULARAK KUZEY ANADOLU FAY HATTI BOLU-ILGAZ BÖLÜMUNUN OLASILIKSAL SİSMİK TEHLİKE ANALİZİ

Levendoğlu, Mert
Yüksek Lisans, İnşaat Mühendisliği Bölümü
Tez Yöneticisi: Yrd. Doç. Dr. Zeynep Gülerce

Ocak 2013, 85 sayfa

Bolu-Ilgaz Bölgesi geçen yüzyıl boyunca çok sayıda büyük depremler ile sarsılmıştır, özellikle 1944 Bolu-Gerede ve 1999 Düzce depremlerinden sonra gözlenen yapısal hasar oldukça büyüktür. Bu çalışmanın amacı, 1944 Bolu-Gerede depreminin kırılma bölgesi için sismik kaynak karakteristiği modelinin oluşturması ve bölgede olasılıksal sismik tehlike analizinin (OSTA) yapılmasıdır. Bu çalışmanın bölgede daha önce yapılmış OSTA çalışmalarına göre en önemli üstünlüğü, geliştirilmiş çizgisel kaynak geometrisi ve tekrarlanma ilişkisi modellerinin ve Türkiye'ye uyarlanmış kuvvetli yer hareketi tahmin denklemlerinin kullanılmasıdır. Çalışma kapsamında düzlemsel fay segmentlerinin geometrisi belirlenmiş ve varolan fay haritaları yardımıyla Coğrafi Bilgi Sistemi'ne aktarılmıştır. Kompozit deprem büyüklüğü dağılımı modeli, ek bir arkaplan sismik kaynağı olmaksızın, Kuzey Anadolu Fay (KAF) Hattı'nın karakteristik davranışını yansıtmaya olanak tanımıştır. Fay segmentleri, kırılma kaynakları, kırılma senaryoları ve fay kırılma modeli USGS Çalışma Grubu-2003 terminolojisi kullanılarak belirlenmiştir. Türkiye'ye uyarlanmış yeni nesil (NGA-W1) (Gülerce ve diğerleri, 2013) kuvvetli yer hareketi tahmin denklemleri ilk olarak bu çalışma kapsamında KAF sisteminde kullanılmıştır. Bölgedeki özel yapıların depreme dayanıklı tasarımı ve değerlendirilmesi için temel oluşturmak amacıyla dört ana nokta için OSTA eğrileri ve tasarım spekturumları verilmiştir. Kullanıcının yerel bölge koşullarında sismik tehlike değerlendirmesi yapabilmesi ve bölgeye özgü tasarım spektrumu geliştirebilmesi için yerel kaya sınıflandırması modeli önerilmiş ve yerel zemin koşullarını içeren sismik tehlike haritaları yapılmıştır. Bu çalışma sonuçlarının bölgedeki gelecek sismik hazardinin değerlendirilmesi ve yönetilebilmesi için yararlı olacağı düşünülmektedir.

Anahtar Kelimeler: Olasılıksal Sismik Tehlike Analizi, Sismik Kaynak Modeli, Kuvvetli Yer Hareketi Tahmin Denklemleri, Kuzey Anadolu Fay (KAF) Hattı, 1944 Bolu-Gerede Depremi

To My Beloved Family

ACKNOWLEDGEMENTS

I would like to thank my advisor Asst. Prof. Dr. Zeynep Gülerce for her guidance, support and understanding of working in private sector throughout the preparation of this thesis. I would also like to thank Dr. Norman Abrahamson, for his invaluable guidance in providing the hazard code.

I am very grateful to our geologist consultant Dr. Fuat Şaroğlu, especially for preparation of the chapter-2, source model used in this study and the motivation throughout the preparation this study.

I thank to Prof. Dr. Kemal Önder Çetin who educated me about geotechnical science in my undergraduate and graduate education.

I am very grateful to my colleagues Cemre Harzem Yardım and Soner Ocak for their priceless help about taking the courses together and the preparation of this study. I would also thank to Burcu Çamtekne, Altuğ Şahin and Emre Değirmenci for their support at even the most desperate times during the preparation of this thesis.

Special thanks to my ex-general manager Dr. A. Nihat Dilek, for his understanding and tolerance throughout taking the graduate courses. Also, special thanks to my bosses Rıfat Göksu and Ahmet Oktay Kavas for their understanding throughout the preparation of this thesis.

I thank to unknown robber, who steal my laptop and hard disc including my thesis from my car during the preparation of this thesis. If this never happened, I would never finish this study.

At last but truly the first, sincere thanks to my beloved family Mine Engineer R. Engin Levendoğlu and Civil Engineer Sibel Levendoğlu who grow me up until now and who do not avoid their help, support, guidance, understanding and protection at any time during my life.

TABLE OF CONTENTS

LIST OF TABLES

TABLES

LIST OF FIGURES

FIGURES

CHAPTER 1

INTRODUCTION

Earthquakes are natural events with random characteristics. Due to the distribution of tectonic structures around the globe, some countries are affected by large and destructive earthquakes while some of them are seismically quiet. Location of national borders of Turkey is in one of the most active tectonic regions of the world. Accumulation of the strain energy along the major fault systems of Turkey, especially the North Anatolian Fault (NAF) caused huge and destructive earthquakes in the past and future large earthquakes to discharge this on-going accumulating strain are a certainty. NAF system ruptured progressively by eight large and destructive earthquakes in the last century; events between 1939-1967 had broken approximately 900 kilometers of a uniform eastern trace whereas Kocaeli and Düzce Earthquakes in 1999 ruptured a total fault spray of approximately 200 kilometers on the west where NAF system is divided into a number of branches as shown in Figure 1.1.

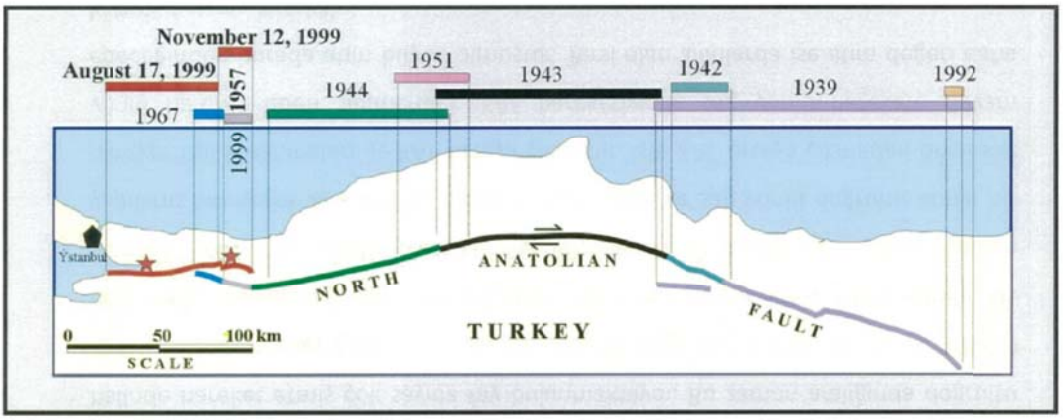

Figure 1.1 1939-1999 earthquake sequence on North Anatolian Fault (Şaroğlu, 2010)

Accurate evaluation of the seismic hazard in Turkey is essential because of increasing number of special project (i.e. nuclear power plants, high rise buildings, viaducts, etc.) Previously, deterministic seismic hazard assessment was the common method in seismic hazard assessment however the common method in seismic hazard assessment is probabilistic in these days. Kramer (1996) explained that probabilistic seismic hazard assessment (PSHA) approach allows the experts to consider the uncertainties in the size, location and rate of recurrence of earthquakes and in the variation of ground motion characteristics explicitly in the evaluation of seismic hazards. Thus, PSHA studies become complete and reliable by means of assessing the seismic hazard.

The published PSHA studies for Turkey were limited (Erdik et al. 1985; Gülkan et al. 1993) before the 1999 events. Several researchers published estimates of seismic hazard and hazard for Marmara Region and for Istanbul after these events (Atakan et al. 2002; Erdik et al. 2004; Crowley and Bommer 2006; Kalkan et al. 2009). The main seismic source characterization was based on earthquake catalogue data using areal sources in early seismic hazard assessment studies and the magnitude distributions of these areal sources were modeled with truncated exponential (GR) relationship. In recent studies (Erdik et al. 2004; Crowley and Bommer 2006; Kalkan et al. 2009), seismic sources were modeled by defining linear fault segments with the assumption that the seismic energy along these fault

segments was released by characteristic events. The magnitude distribution functions of linear sources were considered to be fully characteristic. In addition, a background source representing the small-to-moderate magnitude earthquakes were added to the source model and the earthquake reoccurrence of the background source was modeled using truncated exponential magnitude distribution model. Due to the lack of local predictive models, early-stage global ground motion prediction equations (GMPEs) such as Boore et al. (1997), Campbell (1997), and Sadigh et al. (1997) were used in earlier studies to represent the ground motion variability. A only the recent study by Kalkan et al. (2009) used NGA-W1 ground motion prediction models along with a regional GMPE developed for Turkey after the 1999 events by Kalkan and Gülkan (2004).

The main components of PSHA methodology and framework for PSHA are rapidly improving by increase in the number of studies about seismic source and ground motion characterization for special structures and awareness of earthquake hazard reduction. The primary objective of this study is to evaluate the seismic hazard around the 1944 Bolu-Gerede Earthquake Rupture Zone using improved seismic source models and regionalized global ground motion prediction equations within a probabilistic framework. Once published, this study will be one of the foremost probabilistic seismic hazard analysis studies performed on the rupture zones of 1939-1944 earthquake sequence on NAF system.

1.1 Research Statement and Problem Significance

Bolu is one of the industrialized cities of Turkey, located on the second degree earthquake zone according to the earthquake zonation map of Turkish Earthquake Code (2007). Being in the cross section of Düzce, Bolu-Gerede and Mudurnu-Abant segments of NAF, the city was damaged by several large earthquakes in the last century, however the structural damage in the city and its surroundings were substantial especially after the 1944 Bolu-Gerede Earthquake (Mw = 7.2) and 1999 Düzce Earthquake (Mw = 7.1). Therefore, to reduce the damage in the structures and loss of lives in future earthquakes beside a sensible and economical design practice, accurate evaluation of seismic hazard for this region is vital. When compared to the Marmara Region and İstanbul Metropolitan Area on the west, the number of PSHA studies in the Bolu-Gerede Region is quite limited, only available PSHA study covering the region was performed decades ago by Erdik et al. (1985).

One of the major improvements over the previous seismic hazard assessment practice accomplished in this study; is the development of advanced seismic source models in terms of source geometry and reoccurrence relations. Linear fault segments are defined for 1944 earthquake rupture zone, geometry of the sub-segments (length, width, and segmentation points) are determined and incorporated with the help of updated active fault maps of General Directorate of Mineral Research and Exploration (2012).In this study, to represent the characteristic behavior of NAF, composite magnitude distribution model by Youngs and Coppersmith (1985) is used for all seismic sources without an additional background zone. Fault segments, rupture sources, rupture scenarios and fault rupture models are determined using the WG-2003 terminology and multi-segment rupture scenarios are considered. Events in the earthquake catalogue are attributed to the individual seismic sources and scenario weights are determined by balancing the accumulated seismic energy by the catalog (Statistical evaluation of Turkey earthquake catalog, Kalafat, 2010) seismicity.

Gülerce et al. (2013) proposed that next generation Attenuation (NGA-W1) models are new and improved in terms of additional prediction parameters (such as depth of the source, basin effects, magnitude dependent standard deviations, etc.), statistical approach, and a well constrained global database. The applicability of the NGA-W1 models developed for California (US) is a controversial topic for PSHA studies conducted in other tectonic environments. Said study modified and used the recently developed Turkish Strong Motion Database (TSMD, Akkar et al., 2010) to check the compatibility of the magnitude, distance, and site amplification scaling of NGA-W1 horizontal prediction models with the ground motions recorded in Turkey and adjusted necessary coefficients of these models to reflect

the regional characteristics for the PSHA applications in Turkey. Within the contents of this study, the Turkey-Adjusted NGA-W1 prediction models are employed for the first time on NAF system.

The results of the study is presented in terms of hazard curves, deaggregation of the hazard and uniform hazard spectrum for four main locations in the region (Bolu City Centre, Bolu Mountain Tunnel, Sarıyar Dam, and Hasanlar Dam) to provide basis for evaluation of the seismic design of special structures in the area. To perform site specific hazard assessment and to develop design spectrum for local site conditions, the site characterization model at the accepted hazard levels by TEC-2007 and the region's hazard maps for rock and soil site conditions are provided. Moreover, the uniform hazard spectrum for selected locations compared with the results of TEC-2007 design spectrum.

1.2 Scope of the Work

Contents of the chapters of this study can be summarized to reveal the scope of this thesis as follows;

In Chapter 1, the research statement and the scope of the study is provided with an emphasis on the problem significance and limitations of the previous PSHA procedures in the region.

Chapter 2 briefly summarizes the geology of the study area and seismo-tectonic characteristics of the Ilgaz-Ismetpaşa Segment (1944 Rupture) of North Anatolian Fault System. Site characteristics model based on the 1/1,000,000 scaled geology map is also introduced in this section.

The seismic source characterization model developed for the PSHA analysis is provided in Chapter 3. Source geometry, segmentation points, slip rates and moment accumulation in each sub-segment, magnitude recurrence relations and activity rates are detailed within the content of this chapter.

Chapter 4 briefly introduces the PSHA framework and selection of the ground motion prediction models. Results of the study are presented in terms of hazard maps at selected hazard levels for general rock and soil site conditions. Site-specific design spectra for a few special locations in the region are also provided in this chapter.

Chapter 5 includes a brief summary of the study and discussion of the result. The site characterization map given in Chapter 2 and the hazard maps at selected hazard levels for rock and soil site conditions given in Chapter 4 are interconnected and site specific hazard maps for different hazard levels are also presented in this chapter.

CHAPTER 2

GENERAL GEOLOGY, GEOMORPHOLOGY AND TECTONIC SETTINGS OF NAF BOLU- ILGAZ SEGMENT

The objective of this chapter is to present the seismo-tectonic features of the Bolu- Ilgaz Segment of North Anatolian Fault (NAF) for building a solid background on the seismic source characterization. A brief summary of the geology and geomorphology of Bolu Region is also provided to implement a general site characterization model on top of the probabilistic seismic hazard assessment (PSHA) results for rock site conditions. Starting from early 1940s, many geological investigations were performed in Bolu-Gerede region (Blumenthal, 1948, Tokay, 1952, Pınar, 1953, Abdüsselamoğlu, 1959). Currently, the main sources for any PSHA study performed in Turkey are the general geology map articulated on a 1/500000 scale by the MTA General Directorate in 2002 and North Anatolian Fault Inventory published in 2003 (Herece and Akay, 2003). Within the contents of this chapter, studies by Tokay et al. (1973) and Şaroğlu et al. (1987, 1995) are utilized in addition to these sources for a detailed evaluation.

There are several rock units in Bolu-Gerede region, whose ages are different but they came together lastly in Eocene as a result of the close up of continents and oceans among them. Consequently, rock units in the area are separated into some packets such as the Istanbul Paleozoic, Pontites, the Sakarya Continent Sequence and Suture Zone, which are similar to ophiolitic sequences. Sediments coming after these four sequences are described as cap rocks. The Istanbul Paleozoic consists of Archeozoic sediments, sandstones and shale, and its age is lower Paleozoic. The Pontites are composed of Mesozoic limestone, sandstone, claystone and volcanite. Additionally, the Sakarya continent sequence has Mesozoic sandstone, siltstone at the bottom, gravelstone, limestone, clayed limestone and volcanites at the upper part of it. Lastly, the suture zone rock units consist of ophiolite, ophiolitic mélange and relatively big scaled limestone blocks among them, whose age is Mesozoic. Different kind of lithologies have been developed within the cap rocks starting from upper cretase until today; Eocene sandstone, siltstone, gravelstone, tuff, andesites and basaltic lavas; Miocene sandstone, gravelstone, claystone; Quaternary alluviums, lacustrine sediments, stream sediments and landslides, from bottom to the upper.

The units described above are deformed, folded and faulted in different times. They have been deformed by the earthquakes caused by the NAF for the last 4 million years. Details of these units will be described later in this chapter.

2.1 General Geology and Tectonic Settings of NAF Bolu-Ilgaz Segment

The part of North Anatolian Fault (NAF) between Abant and Ilgaz (Figure 2.1) was ruptured during 1944 Bolu Earthquake. The surface trace of the rupture starts at Ilgaz-Mehmetler village continues until Bolu Plain. In some areas the surface trace of the rupture is divided into a few branches forming a fault zone up to 5 kms. Between Ilgaz and Abant Lake, the surface traces of the fault segment cannot be observed significantly. Large magnitude earthquakes occurred in last 100 years (1944 Gerede, 1953 Cerkes, 1957 Abant and 1967 Dokurcun), on the NAF Bolu – Ilgaz segment are shown on Figure 2.1. Within the contents of this study, the fault segment between Abant and Ilgaz (1944 Rupture) is considered as a whole fault segment and divided into three sub-segments: Ilgaz-Ismetpaşa Segment, Ismetpaşa-Yenicağa Segment, and Yeniçağa-Abant Segment.

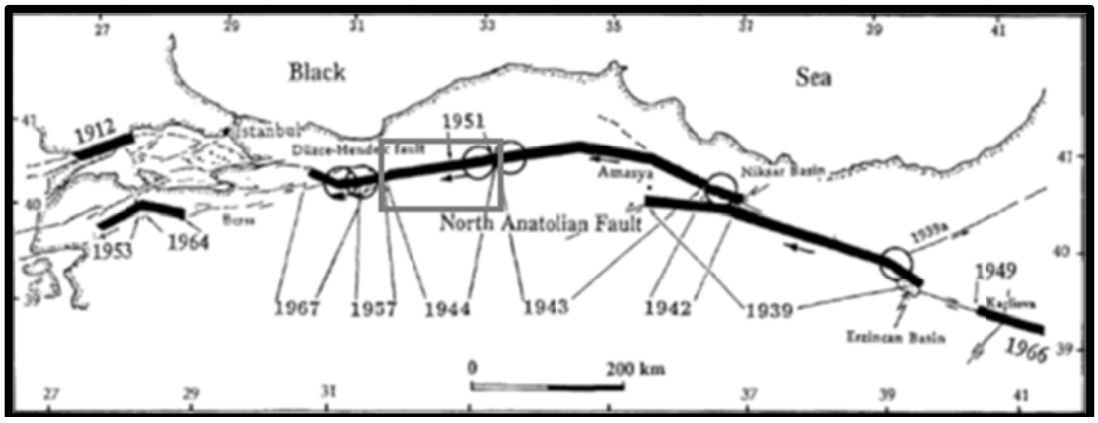

Figure 2.1 Rupture zones of 1939 to 1967 earthquakes along NAF (after Barka 1996)

2.1.1 Ilgaz – Ismetpaşa Segment

The segment of the NAF system in this area starts from the east of Mehmetler Village and continues towards Ismetpaşa Station on the west. Ilgaz – Ismetpaşa Segment is approximately 69 km long, striking towards N10E. Fault geometry is formed as a large zone between the Mehmetler Village and Erencik Villages and maximum width of the fault zone is approximately 3 km in east of the Bayramören as shown in Figure 2.2. The fault is partially linear in the area between the Erencik and north east of the Örenli, however the fault trace is concaved toward North in general. There is a 2 km step-over between Orenli and the Ismetpaşa (Şaroglu et al., 1987). The fault length parallel to the Gerede Stream is 8 km. There are fault set lakes (sag ponds) and landslides along the fault in the North of the Kısaç. It is clear that the fault cuts alluviums in this region.

In the north of this segment, the Eocene limestone including some volcanic material, sandstone and gravelstone, Eocene sediments and Miocene volcanic units exist. On the other hand, the south block has ophiolitic mélange and Jura-Cretase limestone according to MTA 1/5000 scaled geological map. In this section, Eocene aged rock units at the north and Jura-Cretaceus aged rock units at the south have faced with each other due to the formation of NAF. Some fault mirrors and milonitic zones are shaped up along the fault zone. Outcrops of Eocene limestone and serpantinite-peridotite blocks may be seen on the surface of the fault zone. Geological information on this segment of the fault is adopted from Tokay (1973), Şaroğlu et al. (1987, 1995).

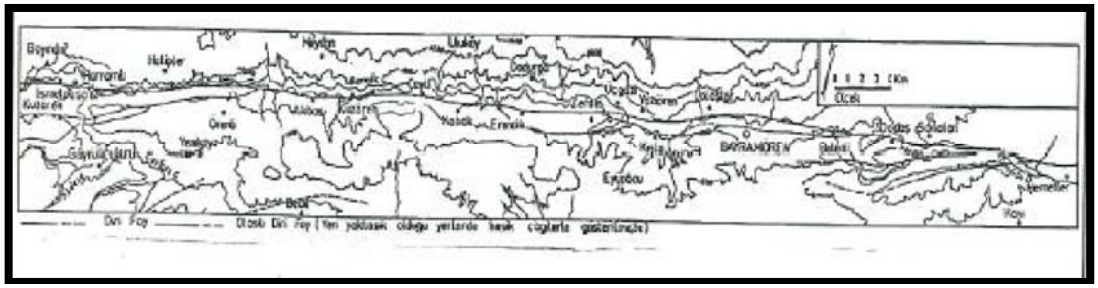

Figure 2.2 The NAF between the Ismetpaşa and the Ilgaz (Şaroğlu et al., 1987)

2.1.2 Ismetpaşa – Yeniçağa Segment

The Ismetpaşa – Yeniçağa Segment is about 47 km long, and its strike is N80E. The fault trace is morphologically apparent in addition to geological features (Figure 2.3), therefore the area between Yeniçağa and Ismetpaşa is one of the best places to study cracks of NAF even 100 years after the earthquakes.

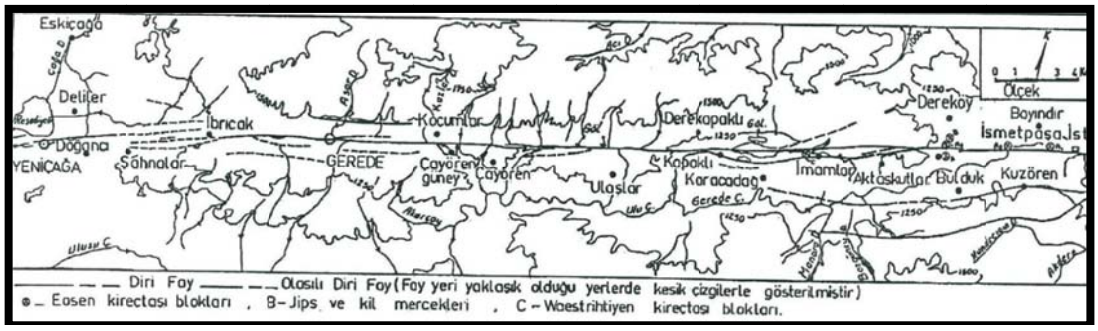

Figure 2.3 NAF segment between the Yeniçağa and the Ismetpaşa (Şaroğlu et al., 1987)

The NAF in this field has right lateral strike slip fault characteristics that gathers different kinds of rocks units. Therefore, two different stratigraphic sequences are found in both South and North of the NAF. In the North of this region, Devonien aged Yumaktepe Quarsite, the Beykoy Granite, the Cankurtaran limestone and the Capak Formation which contains sediments at the bottom exists. The Mesozoic aged units which observed in this segment starts with flish characterized, early Cretase aged Ulus formation at the bottom and continues with Arkotdağ group at the top. The upper Cretase Gücük formation is represented by red limestone and clayed limestone. The sediments which formed in Upper Cretase-Paleocene, Limestone resifs, sandstone, and sandy limestones are named as the Eskipazar formation, the Yazıkavak formation, the Kızıkyayla formation and the Safranbolu formation, respectively. Eocene Taşlık formation which is represented by sediments and the Akçagil formation with volcanites are considered as two different formations on the map (Figure 2.4). The Pazarbasi Formation which forms the units at the bottom is composed of gravelstones, the Budaklar formation is comprised of lake limestone and the Meydan formation includes basalts and agglomerates. Quaternary travertine and alluviums are big enough to be drawn on the map.

In the south of this region, Upper Jura rock units can be seen at the bottom. The Enseliler formation, the Kayabaşı formation and the Akbaş formation are volcanic, which cut the Kadak formation, limestone and sediments at the upper. The Örenli formation which is characterized as flishes is in the age of Santonien-Kampanien-Meastrihtiene. The middle Eocene Taşlık formation and the Akcagil formation overlap lower units with an angular unconformity. Late Miocene and Early Pliocene are separated into some transitive formations which are closely related to one another. The Akçaşehir formation which has gravelstones is at the bottom. Limestone as the Kayabaşı formation, red mudstones as the Tazaklar formation is shown on the map (Figure 2.4). Volcanic agglomerates as andesites and basalts are named as the Mangallar formation, the Ortadag formation, and the Karakuz formation. Plioquaternary units, which are in the south of the NAF, are separated into the Selkoğlu Formation and the Kavaklar formation. Also, Quaternary travertine sediments exist in the field. Stratigraphy of the area indicates that the last unconformity is among the Pinarbaşi formation in the North, the Akçaşehir formation in the South and older units. As a result, the units above the unconformity are closely related to the evolution of NAF.

The formation types seen in Ismetpaşa – Yeniçağa area are:

a) **The Pazarbaşı Formation:** The unit which has red gravelstones with claystones, siltstones and mudstones is really common on the center of the region. The formation has very large scaled outcrops on south of Eskipazar. Volcanic products are amalgamated with gravelstones around the Yıprak Village. This unit is composed of gravelstones, grey blue mudstones with siltstones and sandstones at the bottom. Grains are loose, un-layered and nearly horizontal. None of the deformations can be interpreted as a fault or as a fold. The Pazarbaşı formation covers all older units with an angular unconformity. Its age is Early Pliocene according to collected fossils. Generally, the unit represents continental conditions, and having mudstones and

limestone show that it is relevant to lacustrine facieses. The average thickness of this formation is about 250-300 meters.

b) **The Bahçepınar Formation:** This approximately 150 meters thick formation which expands in the middle of the region is represented by limestone and travertines. It is represented by lacustrine limestone which is thick or thin layered in some regions. Its porous levels are unfilled by travertines. Layers are horizontal, and important structural units cannot be seen on the surface. Its age is probably Early Pliocene according to the Pazarbaşı formation.

c) **The Meydan Formation:** The unit settled in a large area from the Eskipazar-Gerede way to the East. It includes basalts and basaltic agglomerates. Tuff and agglomerates are seen together with coaled sediments in the west of Meydan Village and North of Yıpracık Village. The age of volcanic activity in the region is Pliocene.

d) **Unnamed Units:** Quaternary travertines are not named even though they are drawn on the map (Figure 2.4). Vertebrate animal fossils which are denoted as Quaternary Sediments on the map (Figure 2.4) were found along the Gerede-Cerkes Road. Their age is Steinhenien (400,000 years old) to today.

e) **The Akçaşehir Formation:** The Akçaşehir formation is generally composed of red gravelstones which expand toward the south of area (Figure 2.4). There are some parts of tuff, tuffites and lacustrine limestone at the upper part of unit. The Kayabasi and the Tozaklar, which are big enough to be mapped, are mapped seperately as lacustrine limestone (Figure 2.4). The thickness of Akçaşehir formation is about 250 meters and its age is interpreted as Lower Pliocene according to fossils in clayed limestone. This unit is a product of continental facieses, and it is comprised of fans with lacustrine sediments.

f) **The Limestone Member:** Lacustrine limestone that exists in the Akcaşehir Formation is mapped as a distinctive member in Figure 2.4. Its bedding is obvious and similar structures to pysolites are seen in the lower parts of the layer. Its clayed levels have gastropods and plant fossils. The Kayabaşı formation covers other layers discontinuously. It is about 50 meters thick, and its age is Early Pliocene. The limestone is created in lacustrine facieses.

g) **The Tozaklar Member:** Red clays and mudstones in the Akçaşehir formation are drawn on the map as a seperate unit (Figure 2.4). It is composed of red or brown claystones, siltstones and mudstones. Borders of this layer are generally not clear. The Tozaklar member is mainy sedimented in laguner conditions and it is likely to cause landslides. There are many fossils seen in limestone, mudstone at the lower levels which has 80 meters thickness. From the fossil samples, its age is Early Pliocene.

h) **The Mangallar Agglomerates:**Tertiary volcanites, expanding mainly from the East to the West in south block of the NAF, have these agglomerates. Its matrix is well attached ash, so it has many landslides. Besides, it has a little tuff and gravelstone which participated to the unit by basalt and andesitic lava flaws. Its layers are not clear. Silicate infillings exist in some joints. Its thickness is about 500 meters and its age is Pliocene due to its relationships with the Akçaşehir formation, but its lower levels may be Upper Miocene.

i) **The Ortadag Andesites:** They are Tertiary andesites in south of the study area. The Ortadağ andesites are mostly settled down like lava flows in atmospheric

conditions and doms. These lava flows' centers are distributed on the area rather than a single point. The main outflow center is near the Ortadağ.

j) **The Karakuz Basalts:** They are the third group of Tertiary volcanism which expands through large areas. Basalts' color is determined as dark grey or black and light minerals cannot be observed. Its age is approximately Upper Miocene- Pliocene. They came over the Akçaşehir formation in Early Pliocene by cutting some areas; hence, the age of lavas- Pliocene- is certain.

k) **The Ilgaz Formation:** Limited outcrops of this continental facieses in the south east path of study area are sequences of sandstones, siltstones and gravelstone. East part of this layer is Pliocene. It is reasonable to think that the formation is sedimented like a meandrous river, and then it turns to lacustrine conditions.

l) **The Selkeoglu Alluvium Fans:** These alluvium fans, whose geometrical shapes are still preserved, are mapped as a different unit in the middle of study area (Figure 2.4). This unit has an importance about both age and slip of the NAF. It is well compacted with the elements of sandstones, gravelstones and siltstones. Thus, it causes many landslides in the region. The main color is grey and dirty brown, gravels are not well rounded. The recharge area is not clear because the tectonic activity in the area distributed geometrical shapes of fans. It covers all units with angular unconformity. Its average thickness is about 100 meters, and its age is Late Pliocene-Quaternary

m) **The Kavaklar Alluvium Fan:** This layer expands from the edge of NAF zone to Gerede. Its typical sections are not able to be determined because it is not well compacted, and it could easily be altered. The main color of this layer is red and can only be seen along the Ankara-Istanbul way. This fan which has gravelstone, siltstone and sandstone material preserves its original shape. It is aged as Plioquaternary, and its thickness is about 50 meters.

n) **The Unseparated Quaternary Sediments:** There are a lot of sediment stocks which are related to today's sedimentary system on a large area between the Yeniçağa and the Çerkeş. They are fans, which are developed along the fault valley, are transitional to lacustrine sediments. Only travertines in south west of the Yeniçağa Lake among these sediment stocks are mapped (Figure 2.4). Its thickness is about 100 meters.

o) **The Asagikuldan Travertines:** The travertines in the south east part of the Yeniçağa are mapped with this geographical name (Figure 2.4). These rarely massive light colored travertines are about 50 meters thick. Quaternary travertines are still produced by outflows of mineral water on today.

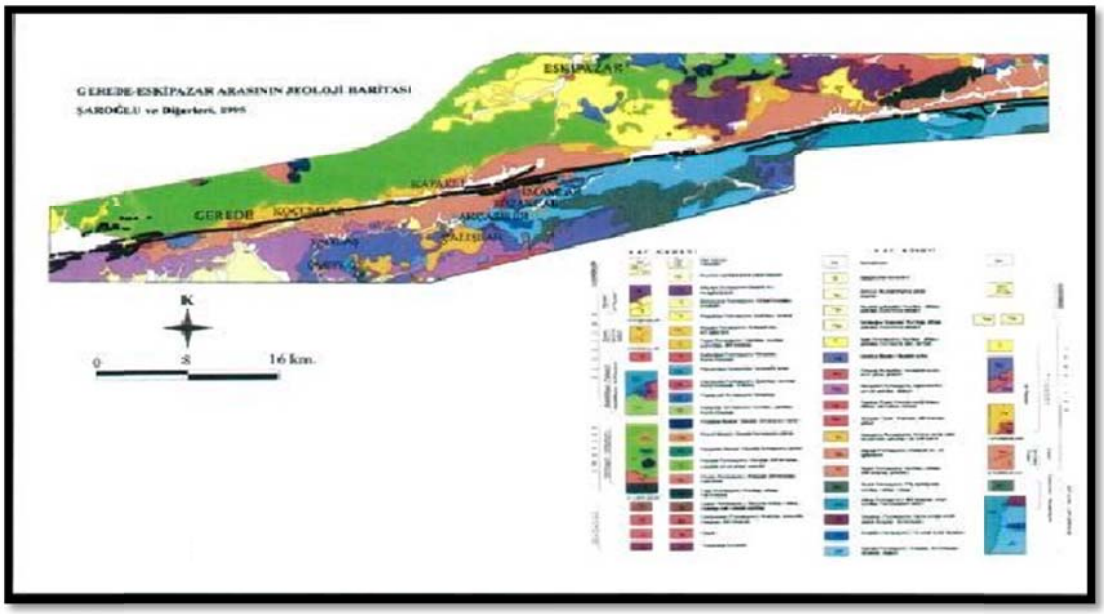

Figure 2.4 Geological Map between Gerede and Eskipazar (Şaroğlu et al, 1995)

2.1.3 Yeniçağa – Abant Segment

The Yeniçağa – Abant segment lies between the Yeniçağa and Guney Mahallesi in south of the Abant for 75 km. Its strike is generally N75E. The fault trace has linear borders in the Bolu Plain from the South (Figure 2.5). It cuts the Pliocene sediments consisting of gravelstones, sandstones and claystone sequences near the Uctepeler. Another fault trace whose strike is N40E exists 15 km long before it connects to the NAF main branch in the North of the Dereceören Village. Large scaled landslides can be seen along the fault zone in east of the Yeniçağa. The Yeniçağa Lake is a fault set lake whose drainage is closed by the fault. The fault trace appears in a stone pit (a quarry) where the fault intersects with the highway in south of the Kırka Village. There is a 30 meters width limestone in the squashed zone. The travertines (Figure 2.6b) along the fault line in east of the Kandıra Village are shifted 200 meters to the right by the fault (Aktimur and others 1983). Travertines are also common along the fault between the Koy-Yenice Road and the Mudurnusuyu (Figure 2.6a). Cracks, convergent ridged and opening joints are formed by the earthquake in 1957, but they are still obvious. While the fault's morphology may be observed by air photographs, it is not evident on the field.

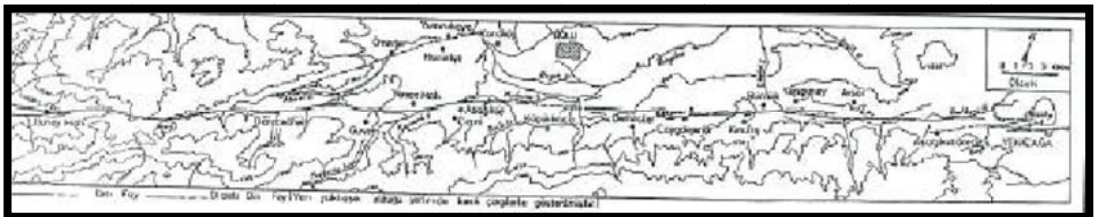

Figure 2.5 NAF segment between Yeniçağa and Abant (Şaroğlu et al., 1987)

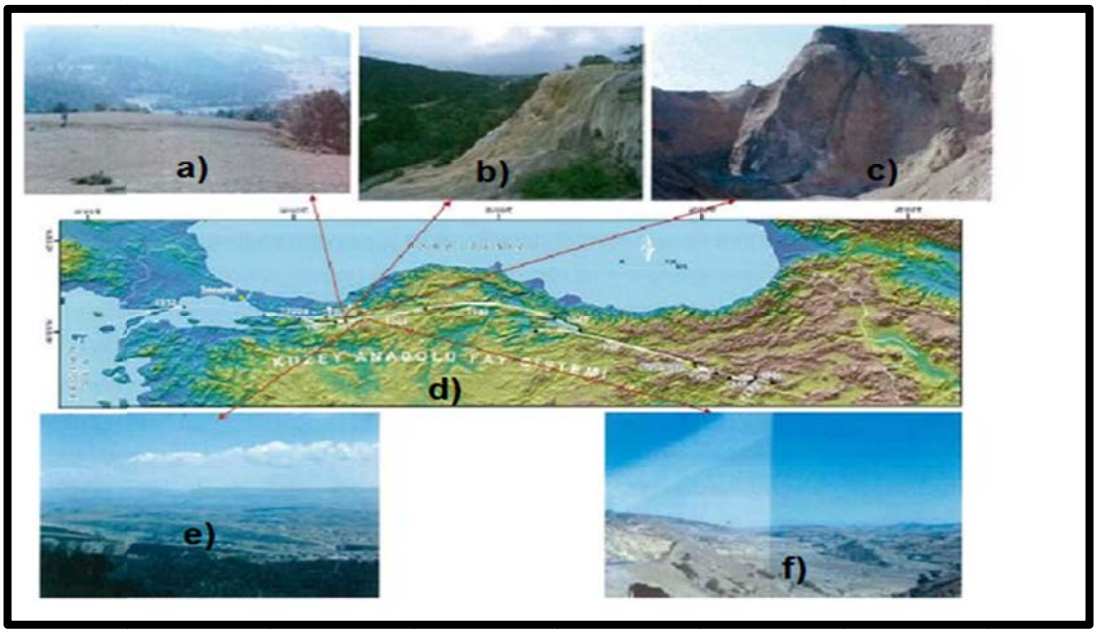

Figure 2.6 General features of the NAF Segment between Gerede and Ismetpaşa (Photos taken from Şaroğlu, TPAO Seminar, 2010)

2.2 Seismo-tectonics of NAF Bolu-Ilgaz Segment

The 1944 Bolu-Gerede earthquake rupture zone divides the study area into two parts from East to West. Its general strike is N172E. It has all special features of typical strike slip fault zone, and it is still active as seen from earthquakes occurred in the last century. NAF Bolu-Yeniçağa Segment may also be described by geologic, geomorphologic and seismic investigations indicating that fault zone is generally linear, but it has a 4-5 km long disintegration zone with breccias. There are some geologically unrelated blocks to the local geology, and their all contacts are faulted.

The geological features of the area between Ismetpaşa-Yeniçağa are interpreted to determine the age and activity of the NAF. There are different structural units formed from Paleozoic to Quaternary in the Yenicağa and the Çerkeş. Not with standing new events differentiated the historical background, there are some hints to make some structural interpretations. There are four structural units if local slips and lateral transitions are ignored. The first one is composed of Paleozoic rock units with little folded cracked metamorphic. The second unit consists of different sedimentary units ranged from Mesozoic deep sea sediments to carbonate rocks (platform).The third one is Eocene volcano sedimentary units. The last unit started in Miocene – Pliocene, and it still continues today. Neotectonic processes cover all these units by low angles. Mezoscopic structures, fault breccias, milonites and the best appeared landslide surfaces are from the West the East along the Yeniçağa-Gerede highway (Figure 2.6c). The fault in this part has a 4 km width zone. It deforms into Plioquaternary claystones and mudstones. All contacts in the area are deformed, and nearly all parts are shifted.

The second most obvious place to see the fault zone is on the ridge in west of the Derekapaklı Village. Sediments of Pliocene and Quaternary are deformed in this area and some secondary structures are developed on them. Slices of the faults are concave to the North and the South. The relationships between different kinds of rocks on the fault zone are not able to be deciphered. Sequenced parts of outcrops may be followed on a single line from the Deresopran to the East. There are a lot of springs on them. The NAF takes the Gerede formation against to the Mangallar formation. It shifted these units laterally in the right direction near the Taşlık and Akçagil formations. It, also, creates a border line between

the Akçagil formation and the Kandak formation in the East. The Taşlik and Akçagil formations are the youngest ones among units which are developed independently and NAF did not affect them. It is likely to verbalize that the Akçaşehir formation and its coeval rock units are deformed by a new tectonic process instead of the NAF according to expanding areas of these units, sediments and outflow centers of volcanic sequences. Plioquaternary fans and sediments are consistent on expanding area, sediments and deformations which are controlled by the NAF.

All special morphological features related with typical strike slip faults are developed in areas where the linear surface trace of NAF can be observed. There are fault valleys, ridges at the beginning of the NAF. The most typical fault valley settles from east of the Gerede to the Akçabey Village. A similar one is about 10 km from south west of the Derekapaklı to the East. Ridges and erosions on the fault are obvious along the Gerede Stream to the East. The fault splays from the Gerede Stream to the South along the last 25 km in the East as shaping a new valley.

Many stress points are observed where the fault pieces formed jumps and curves along the NAF zone. The Yeniçağa Lake is an example to these areas, and there are secondary faults with acute angles to the main faults, which are concave to the North. They do not have any normal component. It is possible to propose that the north of Yeniçağa Collapse is an old valley shaped by erosions, and the south part of it is a fault lake formed by a set shifted by the NAF. A rising stress area was observed between Gerede and east of the Yeniçağa Lake by Şaroğlu, 2010 (Figure 2.7). Typical fault lakes and ridges with sediments are parallel to the fault in this area. A sample of a fault valley has a drainage system, and fans shifted by the fault which is a single line in this area. Geometrical shapes of fans and drainage prove an existence of a right lateral strike slip fault (Figures 2.6f and 2.6e). The fault has a zonal structure besides to the forming a fault valley in east of the Derekapaklı Road. Slices of it are concaved to the North, and the ridges in south of the Derekapaklı are parallel to the fault. The Keçi, Koç and Suluk Lakes are examples of fault set lakes. Faults are getting younger from the North to the South in this area according to the fans and their movements during the last earthquake.

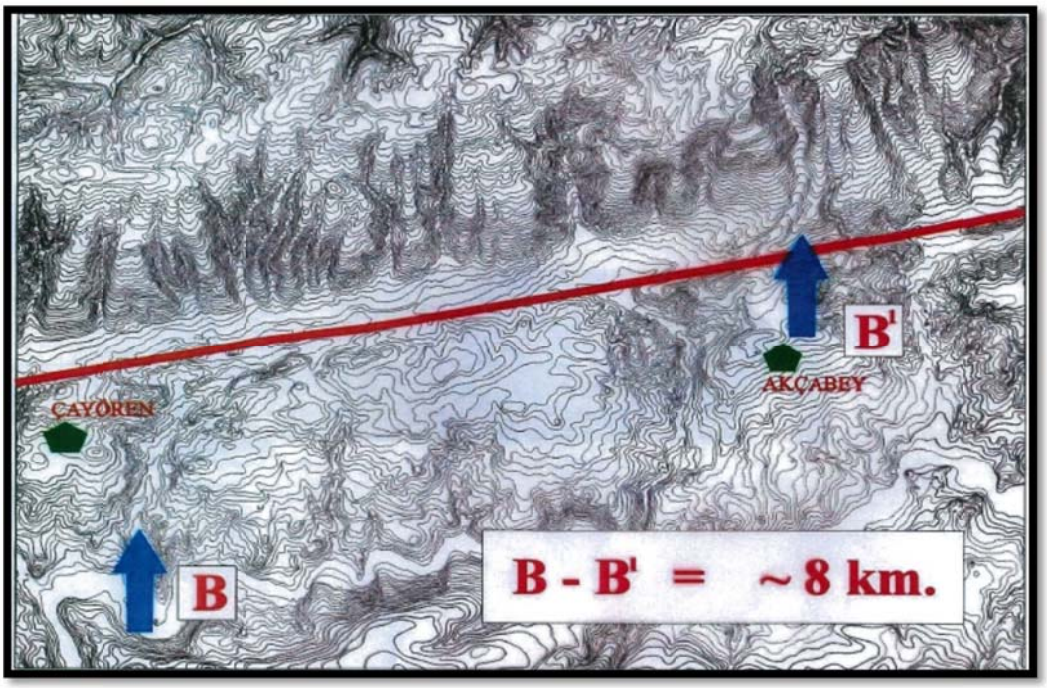

Figure 2.7 The geomorphologic shapes which was formed by the NAF at east of the Gerede (Şaroğlu, 2010)

The fault has a compression effect between the Imamlar and the Gerede Stream, the rocks in the area are mostly deformed. This field is higher than its west and its east. The fault is linear in the East. There are ridges, fault lakes and landslides. It is suggested that the south block of it is higher than its north because it spreads to the far eastern from the Gerede Stream, and it shaped a new valley. There are a lot of right lateral slips on morphological features along the fault as long as a range from a meter to a kilometer.

Two large scaled earthquakes occurred in the area in 1944 and 1953, measuring 7.4 and 6.0 on the Richter scale. A 2 meters long a right-lateral strike slip as related to the fault near the Bolu and a 2 meters long right-lateral strike slip near east of the Gerede were observed as a result of the earthquake in 1944. The creep measurements on the wall of the Ismetpaşa General Directorate of Highways Treatment Station show that the movement of the fault is still going on. These observations show that sedimentation of the Akçaşehir formation has a new active tectonic regime. This tectonic age started in the Middle and Upper Miocene before Early Pliocene.

2.3 General Geomorphologic Features of the NAF Bolu-Ilgaz Segment

The geomorphological structures of the area are governed by NAF zone. The age and slip rate of the NAF can be inferred by the distinctive ground shapes that are formed by erosions and sedimentation of shifted river beds. The length of NAF between the Yeniçağa and the Kabak Villages in the North of Cerkes is about 85 km as cutting through the area, which improves morphological structures (Figure 2.6). The area may be evaluated as two different sections; Gerede-Bayındır and the Bayındır-Kabak, due to their distinctive geomorphologic structures. While the north block of fault is morphologically lower in east of the area, the north block of it between the Gerede and the Bayındır is higher than the other in the South. This reversal structure is generally a product of the right strike slip fault, or the NAF, and it is closely related to contacts of different units each other.

Upper Pliocene can be identified by geomorphologic erosion units in the area. In this epoch, erosion features were shaped apparently upon Lower Pliocene sediments and volcanic features. This activity eroded old structural features in the area. Upper Pliocene erosion surfaces along the Bayındır-Eskipazar-Dağlacık in the north block of NAF, along the Gerede and the Gerede Stream in the south block may clearly be seen on 1000-1300 meters altitudes. These erosion surfaces are really interesting along the NAF zone. The south border of plains, which Upper Pliocene erosion features shaped between the east part of the Bayındır-Eskipazar and the north block of NAF, is determined by the NAF. This border is about 1500-1600 meters long in the south part of it. The north border of these erosion surfaces between the Ismetpaşa and the Gerede ends up along the NAF zone. There are discordances between the Upper Pliocene drainage which shaped erosion surfaces and the Quaternary drainage which has been affected by the NAF. Erosion surfaces in the south block may be seen between the Ismetpaşa and the Gerede like they are in the north block.

These observations indicate that the NAF does not have any effect on geomorphologic activities in the Upper Pliocene; Erosion plains in east of the Bayındır were formed in the same facieses; the drainage was shaped from the South to the North. The NAF shifted these erosion surfaces about 20 km along the right lateral, and it carried them against high morphologies. The upper Pliocene drainage is deformed along the NAF zone shows that the onset of NAF is the end of Upper Pliocene, or the beginning of Quaternary Age. Quaternary morphology of the NAF has apparently most of morphological features of the active right lateral strike slip fault. The forms of units, the width of the fault zone, organizations of cracks forming the fault zone and drainage-fault relationships may differ. Travertines may be seen besides many springs along the fault 6 km away from the east Hamamlı. Many right lateral offsets, which the most obvious one is in the Kabak valley, are formed along additional valleys combining to the Gerede Stream. The Akdere Valley is shifted to the right lateral about 1 km by the NAF. Some sediments of landslides in the east part of the Hamamlı are shifted laterally in right direction. Convergent ridges and sag ponds which were shaped by

the earthquake in 1944 are still obvious. The NAF between the Ismetpaşa and the Gerede has geomorphologic features about right lateral strike slip. The NAF zone is about 25 km in east of the Gerede, and it looks like a dry valley because it does not have any drainage area. This channel, which is formed how valleys from the North are blocked in the south block of the fault, has many fault-set basins. It has some lakes created by this activity. This morphological channel along the NAF zone is filled with sediments of Quaternary alluvium fans. As the older fans were deformed by the NAF, younger fans are able to preserve their morphologies. Parallel ridges to the fault are really apparent in the fault zone between the Kapaklı and the Deresaplan. Right lateral separations may be observed on the streams which are perpendicular to the fault's strike. The most obvious one is near Imanlar. The Akdere Valley is shifted about 1.5 km in right lateral. The south block of the fault is morphologically higher between the Kapaklı and Gerede. Units in the north generally consist of alluvium fans. Many cut and shifted ridges are in the south of the fault. The most spectacular examples of these ridges is upon the plains formed by alluviums in west of the Kapaklı. A recently shaped very young hill may be observed in north-east of the ridge which the fault cut. The slope of east parts the stream valleys which are perpendicular to the fault in east of the Gerede is much more than the west part of it. This information shows that Quaternary drainage along the NAF is formed by the effect of a right lateral strike slip fault. The Yeniçaga Lake basin is bordered by the NAF in the South.

All deformations of geomorphologic units of geomorphologic units and inversions on slopes of units show that the NAF is really active in Quaternary, and they have been formed for a long time. The morphological features shaped by the earthquake in 1944 prove this differentiation. Its micromorphology can be easily determined because of the terrains used for agricultural aims.

2.4 Discussion and Conclusion

The geology, tectonics, geomorphology and seismicity of the study area is investigated and the results of previous field investigations are summarized in terms of the age, length, slip rate and fault mechanism of NAF. The NAF is younger than the Akçasehir formation since it cuts the formation. The age of the NAF is relatively Late Pliocene. The amount of its slip is determined by comparing the same rock units on both sides of the fault each other. The most obvious slip of it is about 28 km on the contact of the Akçagil formation. The Pazarbaşi formation in north of the fault and the Akçasehir formation in south of it seems like the shifted parts of the same unit. The average slip from both sides of the fault is about 25 km. It is about 29 km if the Kavaklar formation in the South and the Cretase Ulus formation are accepted as the same unit. There is coeval erosion plain in the South, which cuts the Akçasehir formation. The slip is approximately 25 km in this field (Figure 2.8). Following interpretations can be made:

- The age of the NAF is about 3 million years.
- Total offset according to Eosen formation, pliosen Akçasehir formation, erosional surfaces, and drainage systems with en error of ±30 km.
- The average annual movement is 30 km/ 3 million years (1 cm / year). (This value is due to long time measurements, for the critical 100 years periods the value will change).

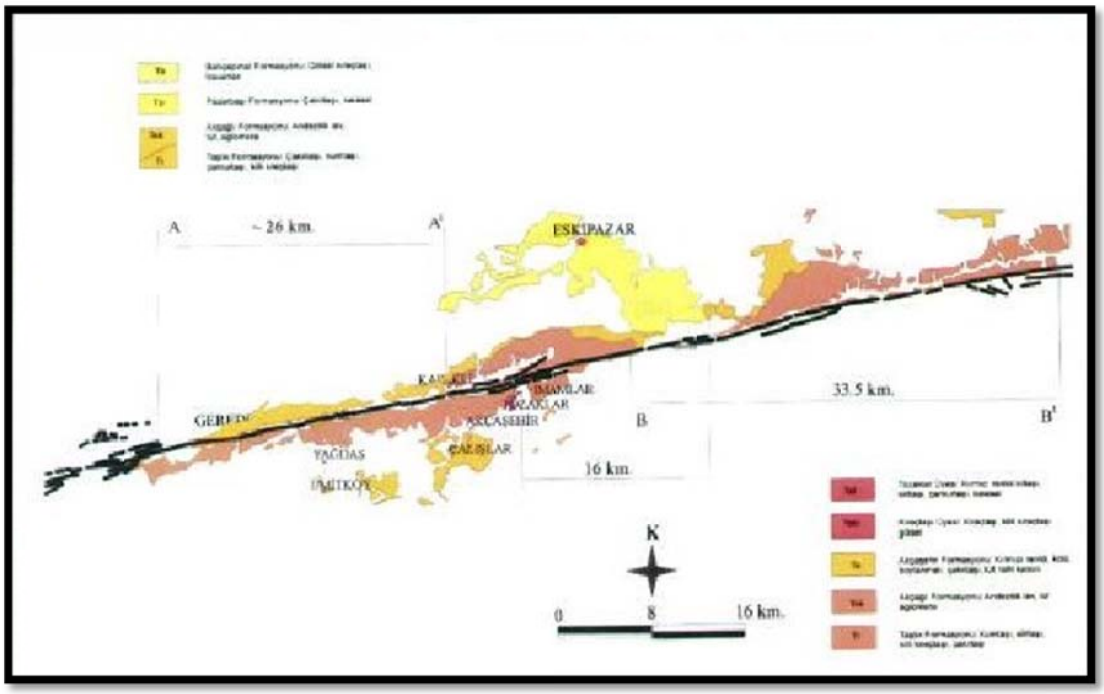

Figure 2.8 Geological map and total offsets in study area (Şaroğlu, 2010)

2.4.1 Rock Classification

Detailed in-situ geotechnical tests are definitely required to make a compherensive site classification. However, using the geology, tectonics and geomorphology of the study area, an empirical rock classification model is constructed by dividing the study area into two parts; hard rock (denoted by A in Figure 2.9) and soft rock (denoted by B in Figure 2.9). The base map provided in Figure 2.9 is taken from Zonguldak and Sinop cities' geological maps published by General Directorate of Mineral Research and Explorations. Since, no site specific measurements are available the rocks are classified with respect to their neotectonic period or paleotectonic period. The rocks from the neotectonic period are assumed as units that did not face enough diyasine and classified as soft rock on the map. On the contrary, the rocks from the paleotectonic period assumed as units that faced enough diyasine and classified as hard rock on the map.

However, a few exceptions can be considered on the proposed general rock definitions. Some basalts can be classified as hard rocks even they were formed in neotectonic period. For some landslide areas, highly altered areas and regions with high water table can be classified as soft rocks. It should be noted with great importance, that Figure 2.9 is given only to give a general idea to the reader about site classification of the study area. The real site specific characteristics should be determined by the help of in-situ geotechnical tests.

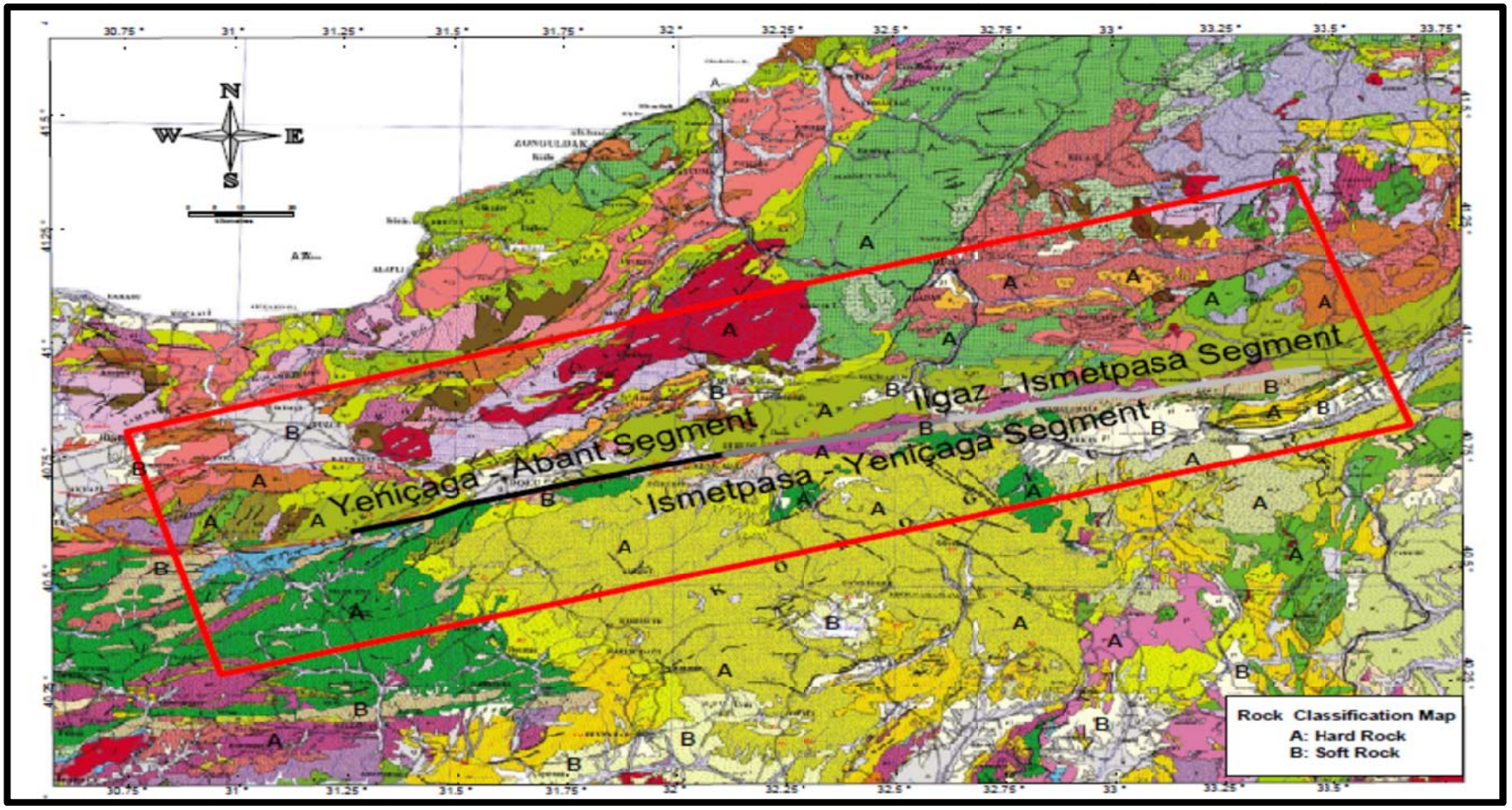

Figure 2.9 Rock classification map of the study area

CHAPTER 3

SEISMIC SOURCE CHARACTERIZATION OF ILGAZ-ISMETPAŞA SEGMENTS (1944 RUPTURE) OF NORTH ANATOLIAN FAULT

Probabilistic Seismic Hazard Assessment (PSHA) described as a procedure of four steps: i) identification of the seismic sources and source geometry, ii) characterizing the seismic sources in terms of magnitude recurrence models, iii) estimation of ground motion intensity measures and its variability for each scenario, iv) constructing the hazard curve. The first two steps in the PSHA framework includes; the definition of the source geometry in terms of length, width, dip and strike angles of the fault plane, identification of the segmentation point locations, and modeling the earthquake recurrence relations of the source with the help of historic seismicity and available geological information. This is a critical part of PSHA since the estimated magnitudes of the future earthquake scenarios depend on this information (Reiter, 1990).

Since speciality on structural geology, tectonics and seismology is a necessity to achieve an accurate and proper modeling of the seismic sources as an input to PSHA, expert evaluation of Dr. Şaroğlu for the fault geometry and source-epicenter matching for 1944 rupture zone is adopted for this study. General geological and tectonic features of the NAF system in the study area was presented in Chapter 2, however, contribution of this information to building the source model is summarized in this chapter. Furthermore, activity rates estimation and the reoccurrence relations are also included in this chapter whereas the use of seismic source models in probabilistic seismic hazard assessment will be discussed in details at Chapter 4.

3.1 Source Geometry of 1944 Bolu Earthquake Rupture Zone

On 1 February 1944, a destructive earthquake occurred in the Bolu and Gerede regions along the west-central portion of the NAF. The magnitude of this earthquake was recalculated as Ms=7.3 (Dewey, 1976) using seismogram records and as Mw=7.4 based on an empirical magnitude-slip relation and the assumed mean slip (Barka, 1996). Rupture trace of the earthquake was first examined by Taşman (1944) who reported the length of rupture as 180 km, the right-lateral strike-slip as 3.5 m, and vertical displacements as 0.4–1.0 m. Later on, various aspects of the 1944 Bolu-Gerede earthquake were reexamined by several other authors (Ketin 1948, 1969; Ambraseys 1970; Lienkaemper 1984; Ozturk et al. 1984; Wells and Coppersmith 1994; Barka 1996; Ambraseys and Jackson 1998; Demirtaş 2000; Herece 2005; Kondo et al. 2005). The rupture zone extended from north of Kurşunlu (Bayramören) to the Abant Lake (Ketin, 1969; Ambraseys, 1970; Ozturk et al., 1984) for 165 kilometers. The epicenter was located near the eastern end of the rupture zone (Dewey, 1976) and depth of the 1944 Bolu-Gerede earthquake was estimated to be 21.6 km by Jackson & McKenzie (1988). The thicknesses of the seismogenic layer and the crust in this area were reported to be 17 km (Ozalaybey et al. 2002) and 31 ± 2 km (Zor et al. 2006), respectively. It was also suggested that the locking depth is between 15 and 21 km along the ruptured section of the Gerede fault zone (Nakiboğlu et al. 1998; Meade et al. 2002; Kocyiğit et al. 2006; Reilinger et al. 2006).

Kondo et al. (2005) characterized the source geometry of 1944 Bolu-Gerede earthquake rupture zone using geomorphologic and geological investigations and eyewitness interviews. Stereoscopic interpretation of air photos was examined, tectonic landforms were identified and offsets were measured to characterize the source geometry efficiently. Kondo et al. (2005) proposed a 5-segment model for the 1944 Bolu-Gerede Earthquake rupture zone: Bolu, Yeniçağa, Gerede, İsmetpaşa, Bayramören segments from west to east as shown in Figure 3.1. Length of the segments ranges between 21 and 46 km with a total rupture length of 180 km as given in Table 3.1. Moreover, maximum and average slips were examined by 47 different offset measurements and the average slip due to 1944 Bolu-Gerede earthquake was determined as 3.4 m. The size and average slip of each segment are comparable to those of the well examined segments of the 1999 Kocaeli Earthquake rupture even through the jogs are relatively smaller than the 1999 Izmit rupture (Kondo et al., 2005).

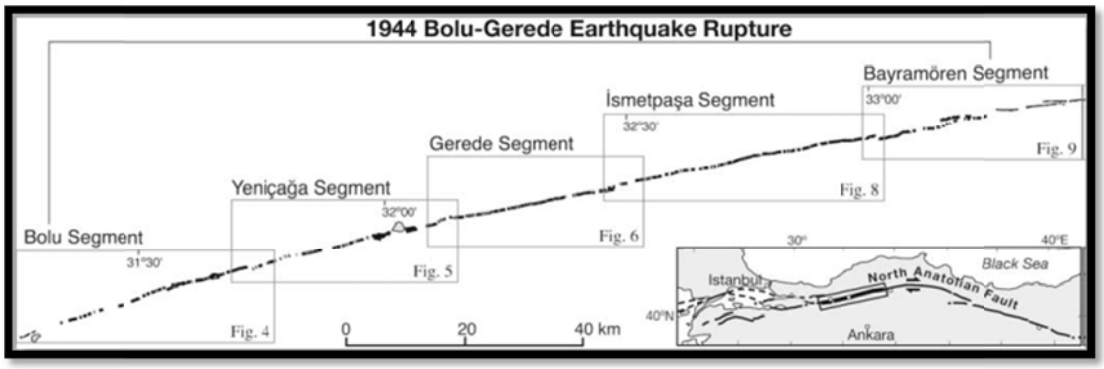

Figure 3.1 Fault segmentation of 1944 Bolu-Gerede Earthquake Rupture (After Kondo et al., 2005)

Table 3.1 Segment Geometry of 1944 Bolu-Gerede earthquake proposed by Kondo et al. (2005)

Sizes of Segments and Jogs									
Segment					**Jog**				
		Slip (m)				**Size**			
Segment	**Length (km)**	**Maximum**	**Average**	**Data Points**	**Type**	**Length (km)**	**Width (km)**	**L*W (km^2)**	**Bend (deg)**
1967					Rst. Bend	4.0?	0.6?	2.4?	-
Bolu	28	3.8	2.8 ± 0.8	4	Rst step-over/bend	2	0.2	0.4	6
Yeniçağa	40	3.8	2.7 ± 0.9	6	Rst. Double bend	4	0.9	3.6	12 >
Gerede	27	6.3	4.9 ± 1.1	10	Rst step over	1.4	1	1.4	12>
İsmetpaşa	43	5.1	4.2 ± 0.7	8	Rls step over	0.9	0.5	0.5	-
Bayramören (1943)	19	1.9	1.9 ± 0.1	3	Rst step over	1.9	0.9	1.7	8
Only slip data points of good quality were used in the calculation. Abbreviations: L*W, length by width; Rst., restraining; Rls., releasing									

Kondo et al. (2005) compared the proposed segmentation model with historical earthquakes, the extent of rupture and the damage intensity associated with the historical earthquakes of 967, 1035 and 1050 is found to be consistent with the segmentation model. When compared to historical earthquakes, 1944 Bolu-Gerede rupture activated with a different multi-segment pattern. Bolu and Yeniçağa segments ruptured during the 967 earthquake and Bayramören segment ruptured during the 1035 earthquake. Therefore, the authors concluded that the historical data and the segmentation data found in the study indicates that the 1944 Bolu-Gerede rupture resulted in earthquakes with distinct rupture length through recent earthquake cycles.

Koçyiğit and Ayhan (2009) also examined the source geometry of 1944 Bolu-Gerede earthquake and stated that serious uncertainties are involved in the source model; epicenter location, magnitude, ground rupture and its geometry, co-seismic offset along the ground rupture zone, total geologic offset, slip rates and the return period of large earthquakes. The authors proposed a 3-segment model for the source as shown in Figure 3.2. Total length of the rupture is found as 191km and width of the fault is estimated as 16 km. Rupture surface is located between Lake Abant in the west and Osmangöl (Bayramören) in the east, dips northward and southward 85°± 5°. Its right-lateral strike slip and normal dip-slip components, geodetic scalar moment and moment magnitude are found as 4.40 ± 0.11 m., 1.02 ± 0.17 m., $M_0 = 4.02 \times 10^{20}$ Nm, and $M_w = 7.74$, respectively, using triangulation, GPS and geologic offset measurements and geodetic data.

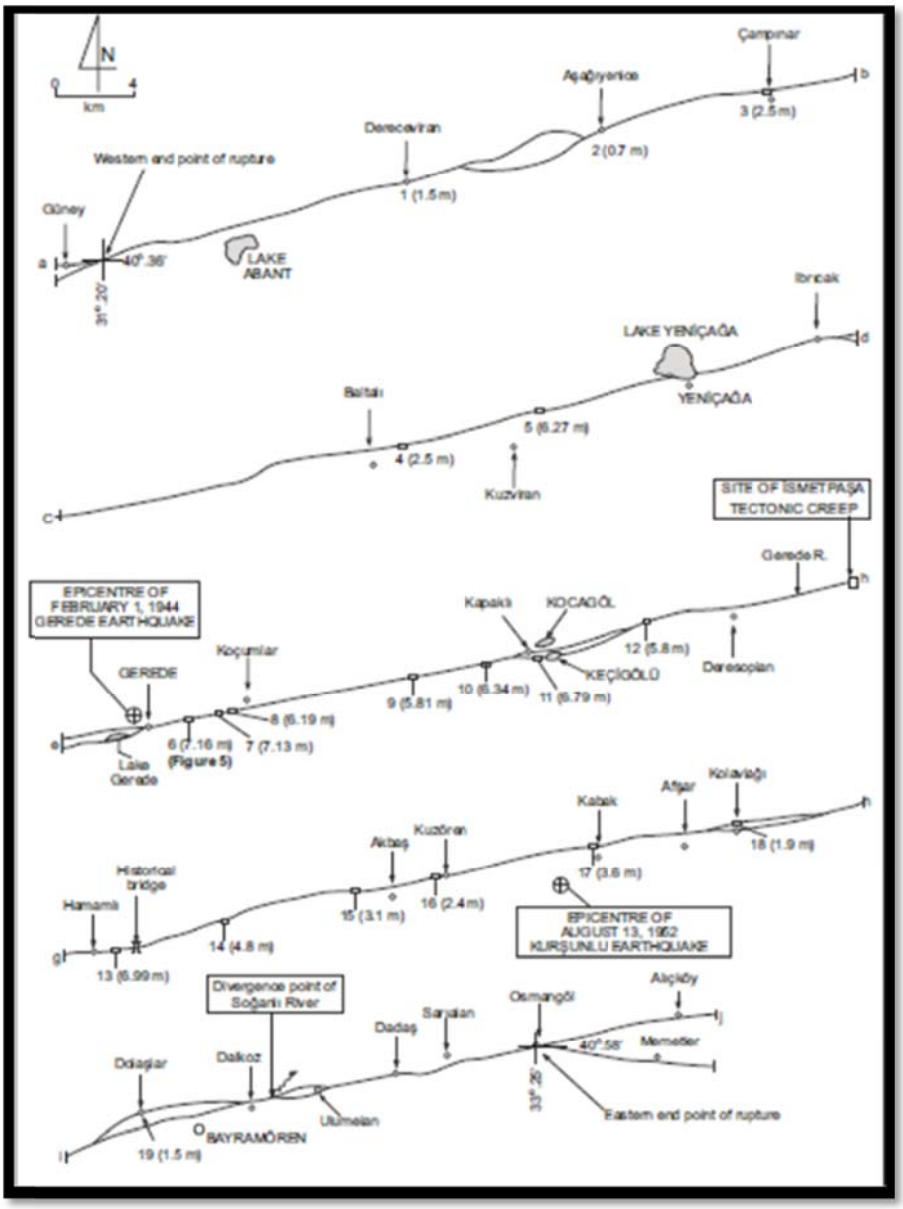

Figure 3.2 Rupture trace of 1944 Bolu-Gerede earthquake and various right-lateral offsets measured on it (After Koçyiğit and Ayhan, 2009)

Koçyiğit and Ayhan (2009) obtained the geologic and geodetic peak offsets as 7.16 m. and 7.41 m., which are higher than the values proposed by Kondo et al. (2005). The authors proposed the geodetic recurrence interval as 232 ± 25 yr. which agrees with the proposed geologic recurrence interval of 266 ± 35 yr. for characteristic earthquakes from this fault zone.

Considering the fault segmentation models defined by Koçyiğit and Ayhan (2009) and Kondo et al. (2005), 1944 Bolu-Gerede earthquake rupture zone is divided into 3 segments as shown in Figure 3.3. According to Figure 3.3, from west to east the three primary fault segments in the area are; Ilgaz -İsmetpaşa Segment (Segment - 1), İsmetpaşa-Yeniçağa Segment (Segment - 2), and Yeniçağa - Abant Segment (Segment - 3). In equation 3.1 by using the Wells and Coppersmith (1994), area-magnitude relations the width of the fault zone are calculated as 16 km.

$$\mathrm{Mchar} = 3.98 + 1.02\log(\mathrm{RA}) \ (\pm 0.23) \qquad 3.1$$

where RA is the rupture area. Barka et al. (2002) calculated the width of 1999 Kocaeli Earthquake as 17 km and Koçyiğit and Ayhan (2009) estimated the width of this segment as 16 km. Therefore, the width value used in this study is logical when compared with these two studies. The segments, rupture length and width values for each segment, slip rates and characteristic magnitude values used in this study are listed in Table 3.2.

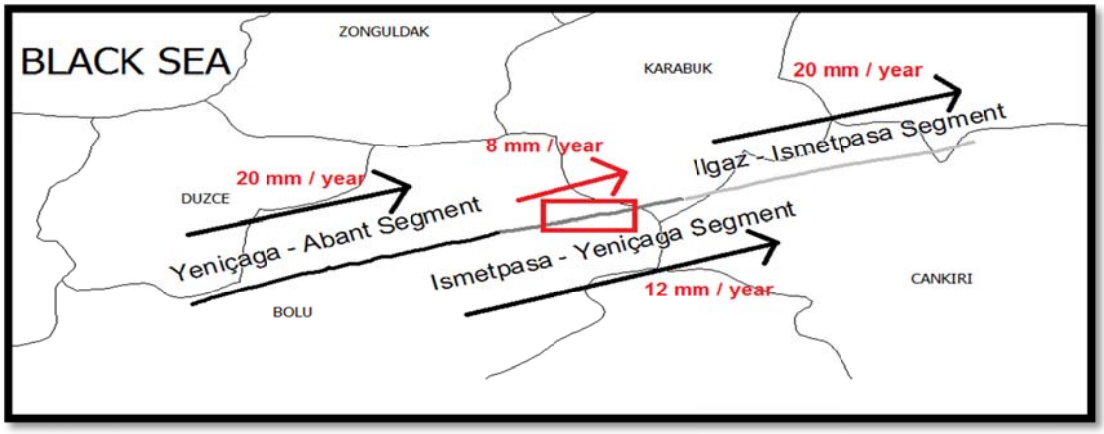

Figure 3.3 The general layout of the fault segments and the slip rates assigned to each source

Table 3.2 Segment geometry, assigned slip rate and characteristic magnitude for each segment

	Segment Name	Length (km)	Width (km)	Slip Rate (mm/yr)	Characteristic Earthquake (M_{char})
1	Ilgaz - İsmetpaşa	69	16	20	7.08
2	İsmetpaşa - Yeniçağa	47	16	12	6.91
3	Yeniçağa – Abant Lake	75	16	20	7.12

Using geological, seismological and paleo-magnetic methods, Barka and Kadinsky-Cade, 1988; Kasapoğlu and Toksöz, 1983; Kiratzi and Papazachos, 1999; Kozacı et al., 2007; Pınar et al., 1996; Piper et al., 1997; Tatar et al., 1995; and Taymaz et al., 1991 measured the long-term slip rate of NAF between 10 mm/year and 20.5 mm/year. The geodetic measurements along the central and the western segments of the NAFZ are used for the calculation of short-term geological slip rate. Straub (1996) proposed a larger slip rate than the long-term measurements within a range of 24 mm/year to 28 mm/year. McClusky et al. (2000) used the Euler pole estimation and mentioned the long-term slip rate as a range of 22 mm/year to 24 mm/year. Reilinger et al. (2006) used the block modeling and found the slip rate as 25 mm/year. Yavaşoğlu et al. (2011) used a local GPS network between Ladik and Ilgaz. The GPS network observations along five years estimated the slip rate as ranging between 18.7 ± 1.6 mm/year and 21.5 ± 2.1 mm/year. The distribution of the slip vectors along NAF is generally shown in Figure 3.4. In this study, the slip rate of the fault segment is taken as 20 mm/year except for the Ismetpaşa – Yeniçağa segment.

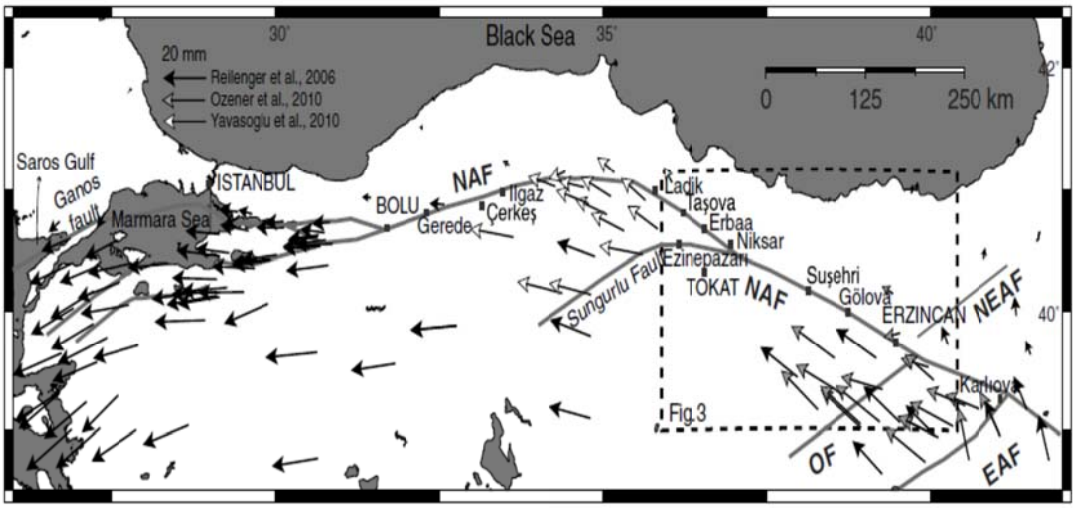

Figure 3.4 Slip rate vectors along NAFZ by Tatar et al (2011)

Apart from the studies on the measurement of general slip rate of NAFZ, there are studies showing that there is a creeping fault around Ismetpaşa fault segment in the region of 1944 Bolu-Gerede earthquake. Kondo et al. (2005) and Çakır et al. (2005) stated that Ismetpaşa fault segment was probably re-ruptured during the 1951 earthquake. After the slip of 1944 Bolu-Gerede Earthquake, the slip of the 1951 Kurşunlu Earthquake and remotely triggered surficial slips by recent large earthquakes are the main explanations of Ismetpaşa creep (Doğan et al., 2003; Çakır et al., 2005). Barka (1996) showed that the 1944 Bolu-Gerede earthquake has a restraining bend (creep) at the East of Ismetpaşa (Figure 3.5). In Figure 3.5; open circles indicate measurements done by Allen (1969) and Öztürk et al. (1985). Open triangles show measurements reported soon after the 1944 Bolu-Gerede earthquake by Taşman (1944), Ketin (1948, 1969) and Ambraseys (1970). In order to estimate the creep rate of Ismetpaşa-Yeniçağa segment, creep amount, time period, and measurement errors proposed in the previous studies for the region are collected and a catalog of creep rates from 1957 to 2010 prepared as given in Table 3.3 and Figure 3.6.

Table 3.3 The reference studies of the calculation of Ismetpaşa Creep Rate

Ismetpasa Creep Rate Reference Studies				
Time Period	Creep Rate (mm/year)	Error	Measurement Type	By
1957-1969	20	0.6	by measurements on the wall of the train station	Ambraseys, 1970
1969-1978	11	0.4	geodetic network by triangulation	Aytun, 1982
1972-1982	10	0.1	geodetic network by trilateration	Uğur, 1974
1982-1992	9	0.1	geodetic network by trilateration	Deniz et al., 1994
1992-2002	7	0.1	geodetic network by GPS	Kutoglu and Akcın, 2006
2002-2007	12	0.1	geodetic network by GPS	Kutoglu et al., 2008
1992-2000	8	0.3	InSAR	Cakır et al., 2005
2010	9,1-1,01	0.4	LIDAR	Karabacak et al., 2011

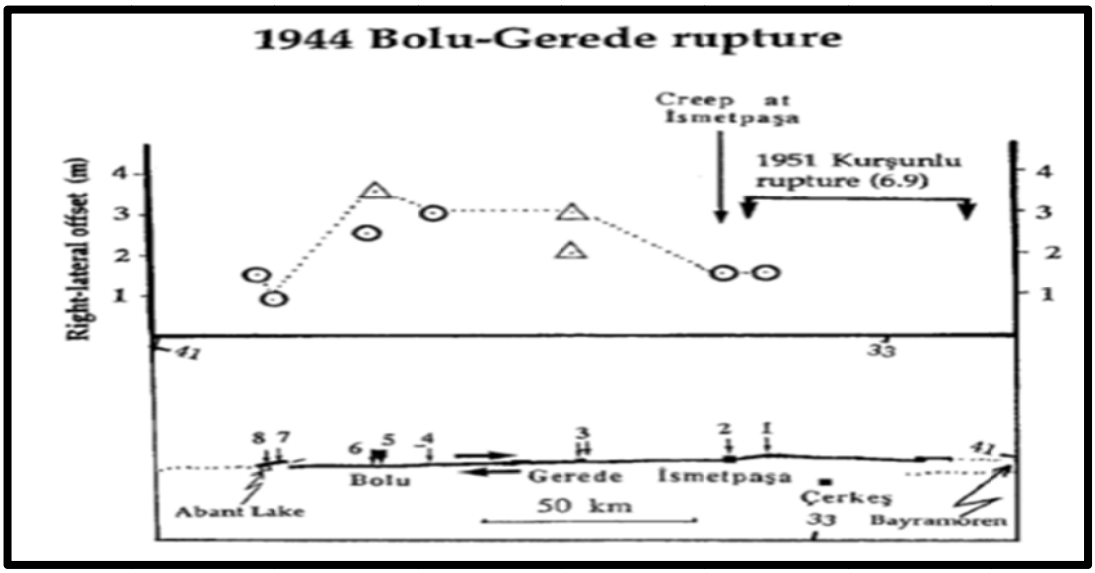

Figure 3.5 Slip Distribution along the rupture zone of the 1944 Bolu-Gerede earthquake (After Barka, 1996)

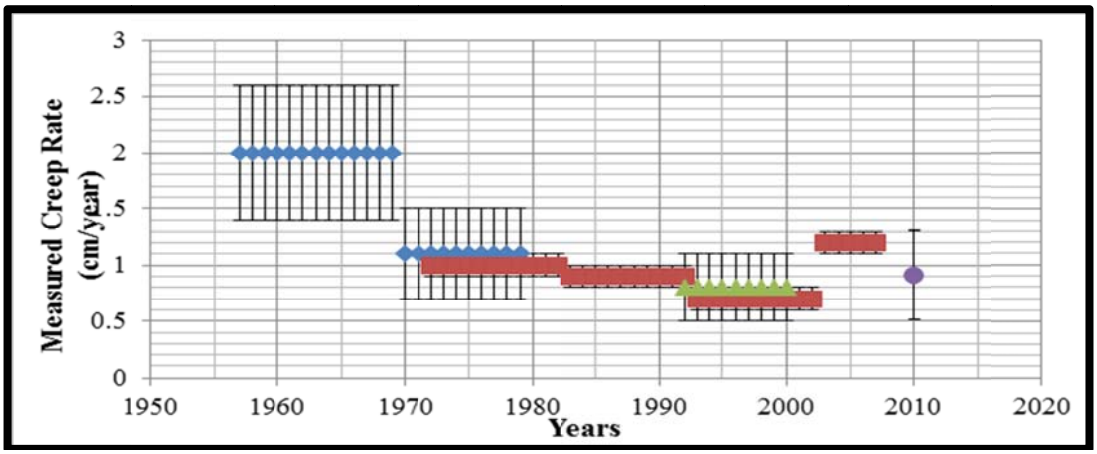

Figure 3.6 Measurements for Ismetpaşa creep rate given in Table 3.3.

Figure 3.6 indicates that the average creep rate measured by recent studies is approximately 8 mm/year. The slip rate assigned to the fault segment is reduced by this value for Ismetpaşa-Yeniçağa Segment and a total slip rate of 12 mm/year is assigned to that segment as shown in Figure 3.3.

3.2 Source-Epicenter Matching and Magnitude Distribution Models

A range of earthquake magnitudes will occur by a seismic source. The relative number of different magnitude earthquakes which occur on the seismic source is described by the magnitude distributions. Typical magnitude distributions used in PSHA are;

1. Truncated Exponential Model
2. Truncated Normal Model (Characteristic Model)
3. Composite Model (Youngs and Coppersmith, 1985)

The basic magnitude recurrence relation proposed by Gutenberg – Richter (G-R) (1944) is;

$$\mathrm{LogN(M)} = \mathrm{a} - \mathrm{bM} \qquad 3.2$$

In equation 3.2, the constants “a” and “b” represent the rate and relative frequency of earthquakes and the cumulative number of earthquakes greater than M is represented by N (M). Since there is a maximum magnitude for the source and a minimum magnitude for engineering interest, the G – R (1944) distribution is typically truncated at both ends and renormalized so that it integrates to unity. The truncated exponential model is limited at the minimum and maximum magnitude values and equation 3.3 shows that the distribution function is normalized to set the total probability value to unity.

$$fm(Mw) = \frac{\beta \exp\left(-\beta\ (\mathrm{Mw} - \mathrm{Mmin})\right)}{1 - \exp\left(-\beta\ (\mathrm{Mmax} - \mathrm{Mmin})\right)} \qquad 3.3$$

Where β is ln(10) times the b value.

Youngs and Coppersmith (1985) proposed that the truncated exponential distribution is suitable for large regions or regions with multiple faults but in most cases does not work well for fault zones. Recent earthquakes and advances in understanding of earthquake generation process have indicated that EQ recurrence on individual faults may not conform to the exponential model developed from regional historical observations (Ocak, 2011).

Instead, individual faults or fault segments may tend to rupture in what have been termed “characteristic” size events at or near. The characteristic magnitude distribution model in which the faults tend to generate only characteristic (or maximum) size events depends on the fault geometry. The general form of the fully characteristic model is represented by truncated normal distribution (Schwartz and Coppersmith, 1984). Truncation is done according to the standard deviation in magnitude – rupture area relation as shown in Figure 3.7 (Ocak, 2011)

Composite models combine the truncated exponential model and the characteristic model. The earthquakes whose sizes are small represented with the truncated exponential model whereas the earthquakes whose sizes are large represented with characteristic model in Composite Model. Equations 3.4 and 3.5 shows that 94% of seismic moment is released by the characteristic earthquakes whereas the rest of the total seismic moment is released by the smaller size earthquakes due to the constraints of the distribution equation.

$$fm(Mw) = \begin{cases} \dfrac{\beta \exp\left(-\beta(\mathrm{Mw}-\mathrm{Mmin})\right)}{1-\exp\left(-\beta(\mathrm{Mmax}-\Delta\mathrm{M}_2-\mathrm{Mmin})\right)} \mathrm{x}\, \dfrac{1}{1+\mathrm{c}}, & Mw \le Mmax - 0.5\Delta M2 \\ \dfrac{\beta \exp\left(-\beta\,(\mathrm{Mmax}-\Delta\mathrm{M}_1-\Delta\mathrm{M}_2-\mathrm{Mmin})\right)}{1-\exp\left(-\beta\,(\mathrm{Mmax}-\Delta\mathrm{M}_2-\mathrm{Mmin})\right)} \mathrm{x}\, \dfrac{1}{1+\mathrm{c}}, & Mw > Mmax - 0.5\Delta M2 \end{cases} \quad 3.4$$

In these equations;

$$c = \frac{\beta \exp\left(-\beta\,(\mathrm{Mmax}-\Delta\mathrm{M}_1-\Delta\mathrm{M}_2-\mathrm{Mmin})\right)}{1-\exp\left(-\beta\,(\mathrm{Mmax}-\Delta\mathrm{M}_2-\mathrm{Mmin})\right)} \mathrm{x}\, \Delta\mathrm{M}_2 \quad 3.5$$

$$\Delta\mathrm{M}_1 = 1.0, \qquad \Delta\mathrm{M}_2 = 0.5$$

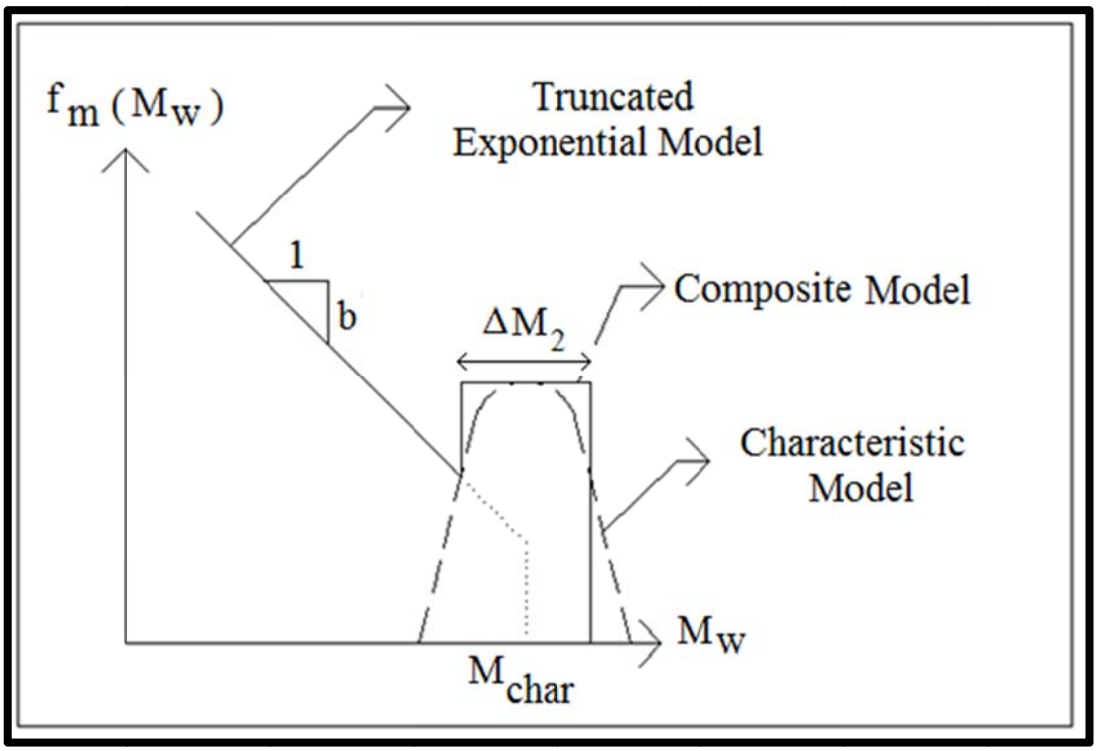

Figure 3.7 Magnitude distribution functions used in PSHA, truncated exponential, truncated normal (characteristic) and composite models (Y&C (1985) (Ocak, 2011)

This study selects composite model to represent the relative rates of different size magnitude events for 1944 Bolu-Gerede Earthquake Rupture Zone. Application of either truncated exponential or composite model requires specification of a b-value in order to define the frequency of smaller magnitude events. In the absence of fault specific data, the b-value obtained from analysis of the regional seismicity is usually used (Ocak, 2011). However, when the regional b-value is used for fault specific recurrence models, the predicted regional recurrence rate obtained by combining recurrence estimates for all the sources will have a somewhat different b-value due to varying maximum magnitudes of different sources. To recover the observed regional b-value, a somewhat smaller b-value should be used on a

fault specific basis with truncated exponential model and a somewhat larger b-value should be used with the characteristic model.

To calculate the b-value for the region, using of the earthquake catalog is a necessity. After filtration of the foreshocks, aftershocks and explosions to represent the seismicity of the whole Turkey, the Integrated Homogeneous Turkey Earthquake Catalog provided by Kandilli Observatory and Earthquake Research Center (Boğaziçi University) is prepared by Kalafat (2010). Kalafat (2010) searched the time period of 1900-2010 (110 years) and calculated the b-value is as 1.00 – 1.25 for different regions of Turkey. In this study, the b-value is calculated specifically for the study area. The remaining database after declustering by Kalafat (2010) is composed of 166 events with moment magnitudes between 4.0 and 7.5 as given in Table 3.4. Spatial distribution of the events in Table 3.4 is presented in Figure 3.8.

Table 3.4 Distribution of magnitudes of the earthquakes within the catalog in the study area

MAGNITUDE BIN	# OF EARTHQUAKES
≥ 4 - < 4.5	78
≥ 4.5 - < 5.0	46
≥ 5.0 - < 5.5	26
≥ 5.5 - < 6.0	10
≥ 6.0 - < 6.5	2
≥ 6.5 - < 7.0	2
≥ 7.0	2
TOTAL	**166**

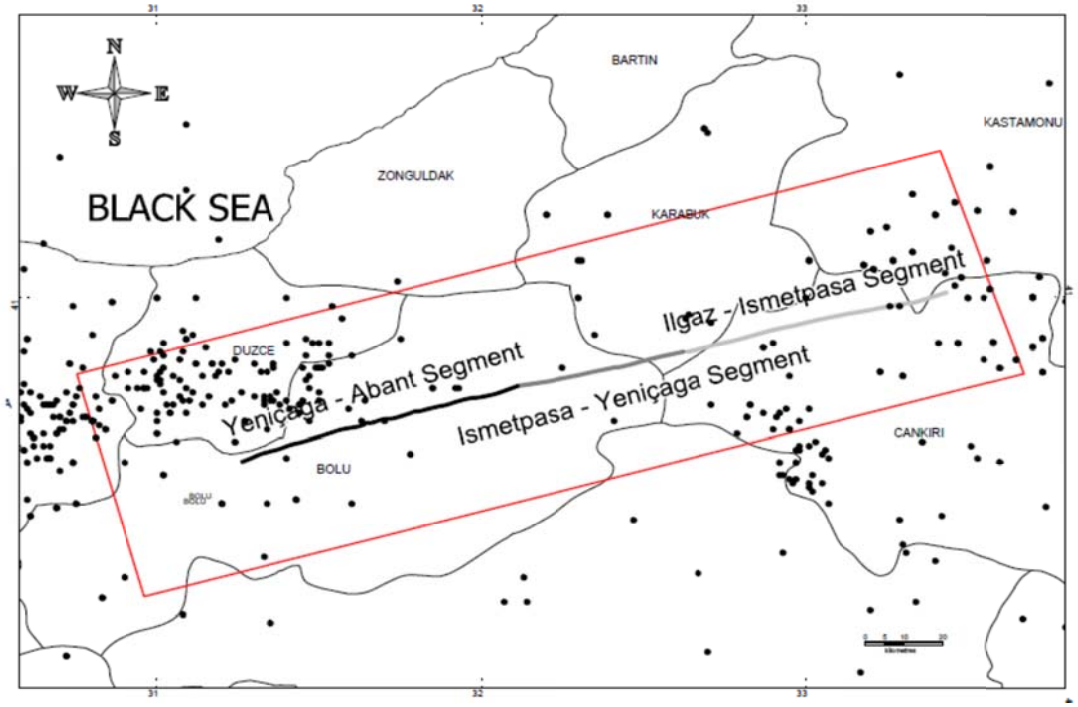

Figure 3.8 Spatial distribution of the earthquakes in the study area.

Aki (1965) proposed the basic maximum likelihood method to estimate the b-value, which is given in equation 3.6:

$$\frac{1}{\beta} = \bar{M} - M_o \qquad 3.6$$

Where $\bar{M}$ is the average magnitude and M_o is the lowest magnitude at which the catalog is complete. In this study, the modified maximum likelihood method which takes into account the variability of the completeness in the catalog for the different magnitude bins is used (Weichert, 1980). The average magnitude ($\bar{M}$) is found by considering the rates for the magnitude bins:

$$\bar{M} = \frac{\Sigma M_i R_i}{\Sigma R_i} \qquad 3.7$$

$$R_i = \frac{N_i}{T_i} \qquad 3.8$$

In these equations, the average magnitude of each magnitude bin (eg. 4-4.5, 4.5–5.0 …) is represented by M_i, rate for each interval is represented by R_i, the number of events within each magnitude bin is represented N_i and the time interval for each magnitude bin is represented by T_i which the catalogue is assumed to be complete. Table 3.5 shows summarizing of the results of the maximum likelihood method analysis in a tabular form. According to this study, β parameter equals to 1.38 leading to b parameter, which is the value of the recurrence parameter, calculated as 0.60. The b-value used by the previous studies in the literature are in consistent with the value estimated in this study, the b-value used by Erdik et al., 2004, Kalkan et al., 2009, and Crowley and Bommer (2006) for eastern Marmara were 0.80, 0.72, and 0.69, respectively.

Table 3.5 Maximum likelihood estimation of the recurrence parameter b

M1	M2	M_i	N_i	Time Interval	R_i	$M_i * R_i$
4.0	4.5	4.25	78	110	0.71	3.0
4.5	5.0	4.75	46	110	0.42	2.0
5.0	5.5	5.25	26	110	0.24	1.2
5.5	6.0	5.75	10	110	0.09	0.5
6	6.5	6.25	2	110	0.02	0.1
6.5	7.0	6.75	2	110	0.02	0.1
7.0	7.5	7.25	2	110	0.02	0.1
SUM =					**1.5**	**7.1**
$\bar{M}$ **=**					**4.7**	
M_o **=**					**4.0**	

In order to evaluate the contribution of the variability in the b value for composite magnitude recurrence model, a sensitivity analysis is performed by arbitrarily chosing the b value as 0.5, 0.6, 0.7, 0.8, 0.9, 1.0. PSHA are conducted for Bolu City Centre (located in the near vicinity of Yeniçağa-Abant Segment), and hazard curves are compared in Figure 3.9. Figure 3.9 indicates that the hazard results are insensitive to the changes in b value especially for high hazard levels. Youngs and Coppersmith (1985) explains the changes in b value as

follows; “The changes in the b-value have an insignificant effect on the recurrence relation but the function is more sensitive to the changes in upper bound magnitude”. The magnitude distribution function for each source is bounded with a minimum magnitude considering the engineering interest. The minimum magnitude is set to magnitude 4.5 for all sources considering the historical seismicity of the source. The upper bound for the magnitude distribution functions is calculated by adding 0.25 to the characteristic magnitude for each source (Youngs and Coppersmith, 1985).

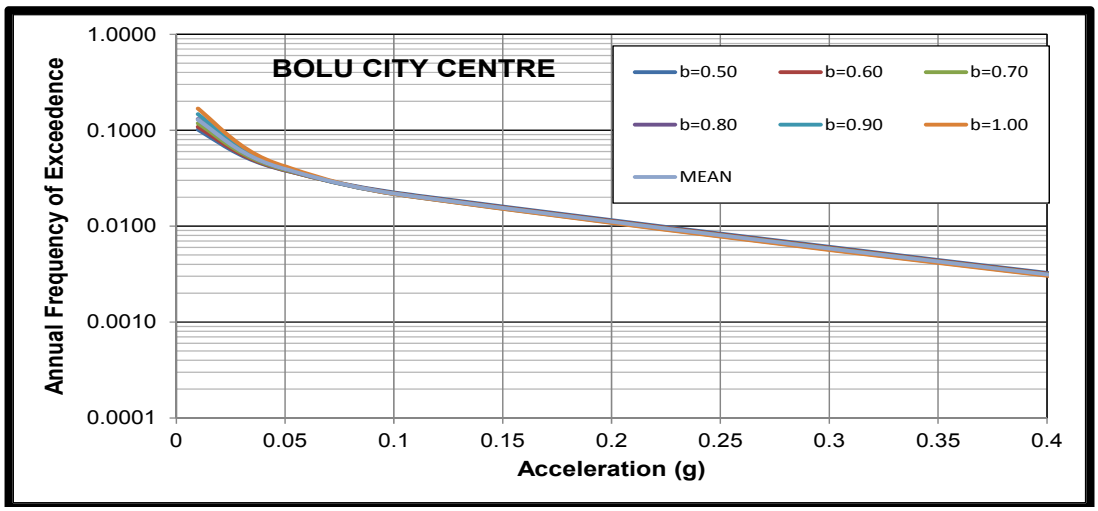

Figure 3.9 Hazard Curves for Bolu City Centre for different b values

3.3 Fault Rupture Model

Two types of sources can be defined in PSHA; areal sources and linear sources. Areal sources are based on the historical seismicity and these type of sources are used commonly in regions with unknown faults. Linear and multi-planar fault sources can be defined in the regions where trustable tectonic information on the fault geometry is available. Within the contents of this study, the definitions of USGS Working Group for Earthquake Probabilities (2003) (USGS_WG (2003)) are adopted for the first time for 1944 Bolu-Gerede earthquake rupture zone.

The shortest fault capable of rupture to produce large earthquakes repeatedly defined as a **segment** by USGS_WG (2003). Three non-overlapping segments are defined above for 1944 Bolu-Gerede earthquake rupture zone. Furthermore, fault segment or a combination of multiple adjacent fault segments that are possible to rupture and produce an earthquake in the future defined as **source** by USGS_WG (2003). These three segments are combined into six different rupture sources such as;

a. Fault segments rupturing individually (Source 1,2 and 3 in Figure 3.10b),
b. Combined rupture of two adjacent segments (Source 4 and 5 in Figure 3.10b)
c. Combined rupture of three adjacent segments (Source 6 in Figure 3.10b).

A **scenario** is defined as any possible combination of sources that describes a possible failure mode. Rupture scenario covers the decision of assigning either a single or a set of faults to be involved in rupture. Six rupture sources creates four rupture scenarios as:

1) Rupture of the three segments individually (Segment-1, Segment-2, Segment-3) (Figure 3.10c)
2) Rupture of the first two segments together and the third segment separately (Segment 1+2, Segment-3) (Figure 3.10c)
3) Rupture of the last two segments together with the first segment separately (Segment-1, Segment 2+3) (Figure 3.10c)
4) Rupture of the three segments together (Segment 1+2+3)(Figure 3.10c)

The weighted combination of all possible scenarios produced from the seismic source defined as a **rupture model.** Precise knowledge on the historical seismic activity of the source is vital to assign the weights to each scenario. The seismic sources and rupture scenarios generated for 1944 Bolu-Gerede earthquake rupture zone is presented in Table 3.6. The sources that ruptured in a particular rupture scenario is denoted by 1 and the sources that did not rupture are denoted by 0 in Table 3.6.

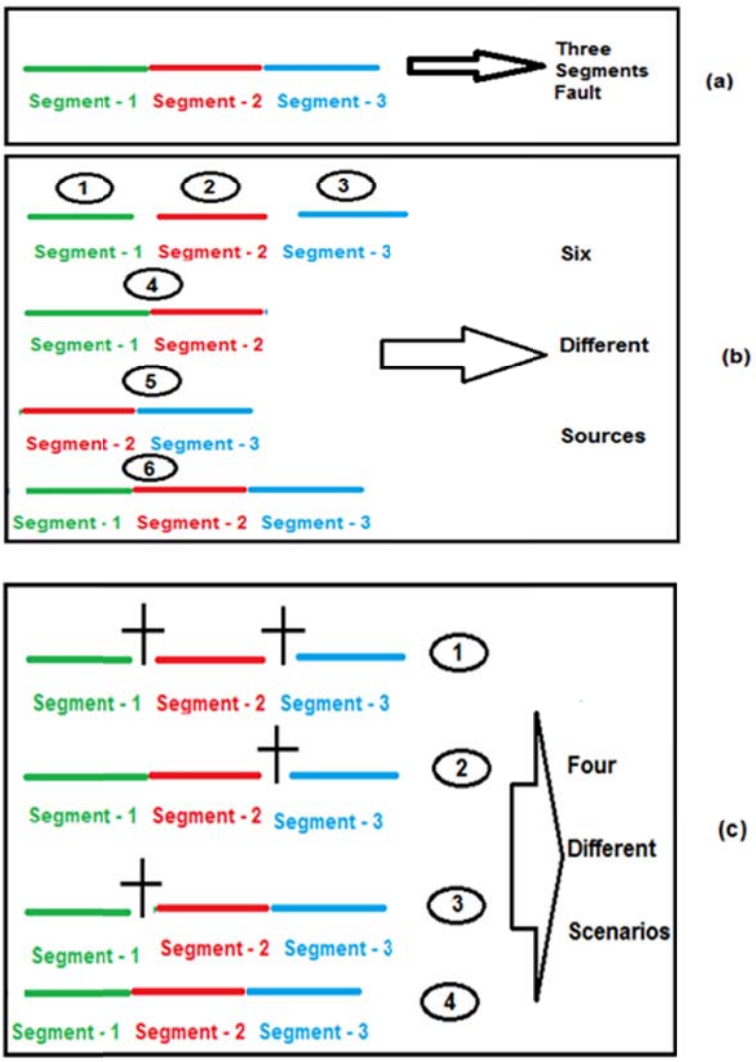

Figure 3.10 Illustration of the segment, source and scenario concepts

Table 3.6 Seismic Sources and Rupture Scenarios considered for study area

Seismic Sources → / Rupture Scenarios ↓	S1	S2	S3	S(1+2)	S(2+3)	S(1+2+3)
S1, S2, S3	1	1	1	0	0	0
S(1+2), S3	0	0	1	1	0	0
S1, S(2+3)	1	0	0	0	1	0
S(1+2+3)	0	0	0	0	0	1
S1 = Ilgaz - İsmetpaşa Segment (Segment-1)						
S2 = İsmetpaşa - Yeniçağa Segment (Segment-2)						
S3= Yeniçağa - Abant Lake Segment (Segment-3)						

3.4 Activity Rates and Recurrence Relations

In addition to the magnitude distribution model, estimation of activity rate is required for determining the magnitude reoccurrence relation of a seismic source. The definition of activity rate of a source can be given as the rate of earthquakes above the minimum magnitude and denoted by N_{min}. Abrahamson, (2000) proposed that the historical seismicity or the geological information about the fault can be used for the estimation of the the activity rate. The geological (or geodetic) information is to be used to estimate N_{min} and then it is required that balancing of the accumulation of the seismic moment by the release of the seismic moment in earthquakes. The total accumulated seismic moment (Mo) on a source is given by;

$$\mathrm{Mo} = \mu \,.\, \mathrm{A} \,.\, \mathrm{D} \qquad 3.9$$

Where, μ is the rigidity of the crust (~3 x 10^{11} dyne / cm²), A is the fault area (km²) and D is the average displacement.

By taking the time derivative the annual accumulating seismic moment is found as;

$$\frac{\partial \mathrm{Mo}}{\partial \mathrm{t}} = \mu \,.\, \mathrm{A} \,.\, \mathrm{s} \qquad 3.10$$

Where, s is the slip rate (cm/year). Seismic moment release during an earthquake is given by Equation 3.10.

$$\mathrm{Mr} = 10^{1.5\,\mathrm{M}+16.05} \qquad 3.11$$

Therefore the activity rate N_{min} is calculated by integrating the moment release per earthquake times the relative frequency of earthquakes as given in Equation 3.11

$$\mathrm{N(Mmin)} = \frac{\mu \,.\, \mathrm{A} \,.\, \mathrm{s}}{\int_{\mathrm{Mmin}}^{\mathrm{Mmax}} fm(Mw)\, 10^{1.5\,\mathrm{Mw}+16.05}\,\mathrm{dm}} \qquad 3.12$$

The activity rate N_{min} is combined with the magnitude distribution function to develop the recurrence model N_{min} for the source:

$$N(M) = N(Mmin) \int_{Mmin}^{Mmax} fm(Mw) \quad 3.13$$

The cumulative rates of earthquakes for each scenario is calculated and plotted in Figure 3.11 along with the cumulative rate of the events attributed to this 1944 Bolu-Gerede earthquake rupture zone. Uncertainty in the rates is represented by the error bars calculated by Weichert (1980) equations. Weichert (1980) developed empirical models explaining the uncertainty in the rates and suggested that the estimation of recurrence parameters of Gutenberg-Richter relation should always employ a maximum likelihood method. The method presented by Weichert (1980) gives the necessary extension of known results to the important case of unequal periods of observation.

A weight is assigned to each rupture scenario presented in Table 3.6 and the weighted average of these scenarios (red line in Figure 3.11). To establish the best fit between the cumulative rates of historic earthquakes and weighted average lines, the weights of individual scenarios are modified.

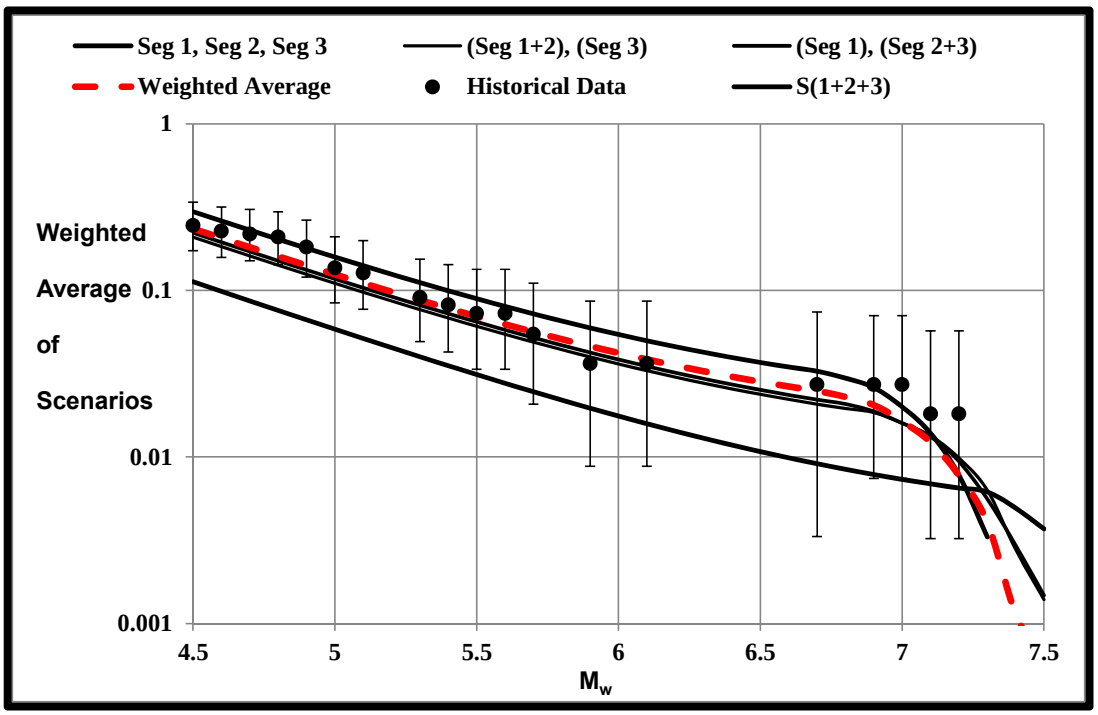

Figure 3.11 Comparison of rupture scenarios and weighted average scenario including Weichert (1980) error bars

In order to evaluate the contribution of the weights for rupture scenarios, a sensitivity analysis is performed by arbitrarily changing the weights of rupture scenarios. Totally 223 different rupture scenario weights are considered and PSHA are conducted for Bolu City Centre (located in the near vicinity of Yeniçağa-Abant Segment) for T=1 sec spectral period. Then, the median and the standard deviation of the total hazard is calculated for 223 different weighted average scenarios. The median and 86th percentile hazard curves are presented in Figure 3.12. In Figure 3.12, the red line represents the median value, the

dashed lines are median ± 1 σ values and the gray line is the selected weighted average ratio combination in this study. According to Figure 3.12, the selected weighted average ratio combination is slightly above the median but lies between ± 1 δ range.

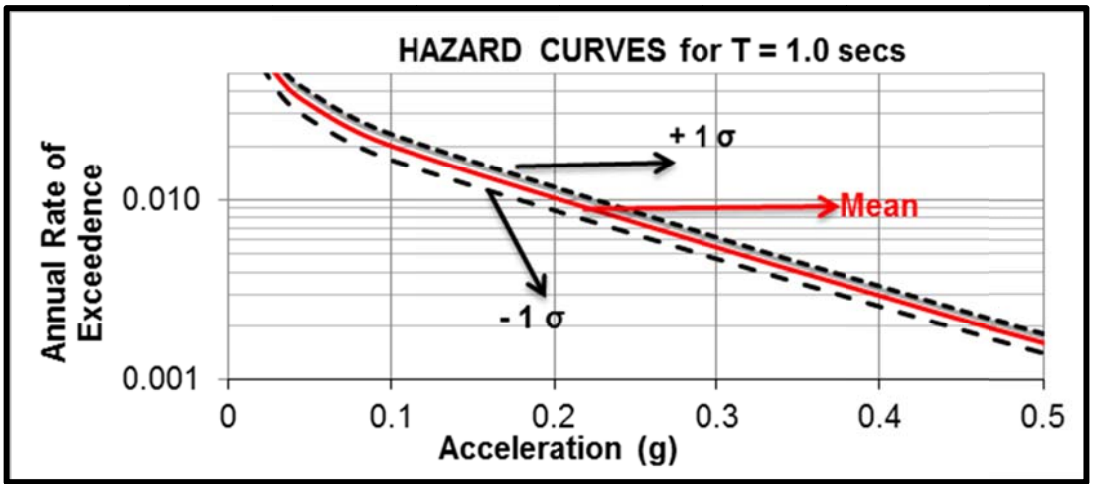

Figure 3.12 The sensitivity analysis results for selected weighted average ratio combinations (Bolu City Centre, T=1.0 sec)

CHAPTER 4

PROBABILISTIC SEISMIC HAZARD ASSESSMENT METHODOLOGY AND RESULTS

The seismic source models to be used in probabilistic seismic hazard assessment (PSHA) were developed for the fault zones in study area and presented in Chapter 3. The activity rates, magnitude distribution functions, reoccurrence models and activity rates from the seismic source models were connected in hazard assessment analyses. Within the contents of this chapter, the probabilistic seismic hazard assessment methodology used for this study is summarized in terms of the hazard integral and its main ingredients. The selected ground motion prediction models and the evaluated hazard code are explained. The hazard curves, deaggregation of the hazard and uniform hazard spectrum for four selected sites in the region are offered. Acceptable hazard levels in Turkish Earthquake Code (TEC-2007) are presented and the uniform hazard spectra for selected four sites at rock and soil site conditions are compared to the TEC-2007 requirements. Hazard maps developed for rock and soil site conditions for PGA, T=0.2 and T=1 second spectral accelerations are offered. The rock classification map proposed in Chapter 2 is interconnected with the PSHA results and a site specific hazard map is given for future reference. The results provided in this chapter are discussed sufficiently in Chapter 5**.**

4.1 Probabilistic Seismic Hazard Assessment Methodology

The basic methodology of probabilistic seismic hazard analysis (PHSA) (Cornell 1968 and McGuire 2004 approach) requires the computation of how often a specific level of ground motion will be exceeded at the site. In other words, in a PSHA, the annual rate of events that produce a ground motion intensity measure, IM that exceeds a specified level, L, at the site is computed. This annual rate, ν, is also called the "annual rate of exceedence". Traditionally, the equation for a seismic hazard analysis due to a single source has been given by:

$$\nu(IM > L) = N_{\min} \cdot \int_M \int_R f_M(M) f_R(M,R) P(IM > L | M,R) \times dM \times dR \qquad 4.1$$

where the distance from the source to site is the R, earthquake magnitude M is the; the annual rate of earthquakes with magnitude bigger than or equal to the minimum magnitude is the N_{min}, the probability density functions for the magnitude and distance are $f_M(M)$ and $f_R(M,R)$ and the probability of beholding a ground motion greater than L for a given earthquake magnitude and distance is the P(IM>L | M,R).

Gülerce and Abrahamson (2010) explained that the probabilistic seismic hazard analysis comprises of identifying a set of earthquake scenarios, forecasting the range of ground motions for each earthquake scenario, and calculating the rate of each combination of earthquake scenario and ground motion. Each scenario is identified by the size of the earthquake (magnitude, M) and the location which defines the distance, R, from the site. The ground motion variability is contained in the P(IM>L | M,R) term such as:

$$P(IM > L | M,R) = \int_\varepsilon f_\varepsilon(\varepsilon) \times P(IM > L | M,R,\varepsilon) \times d\varepsilon \qquad 4.2$$

where the number of standard deviations above or below the median is ε, the probability density function for the epsilon (given by a standard normal distribution) is the $f_\varepsilon(\varepsilon)$ and $P(IM>L \mid M,R,\varepsilon)$ is either 0 or 1. Bommer and Abrahamson (2006) said about this formulation that $P(IM>L \mid M,R,\varepsilon)$ chooses those scenarios and ground motion combinations that cause ground motions greater than the test level L. The final form of the hazard integral is given in Equation 4.3:

$$\nu(IM>L) = N_{\min} \cdot \iiint_{M\,R\,\varepsilon} f_M(M)\, f_R(M,R)\, f_\varepsilon(\varepsilon) P(IM>L|M,R,\varepsilon) \times dM \times dR \times d\varepsilon \qquad 4.3$$

For multiple seismic sources, the sum of the annual rate of events from the individual sources (assuming that the sources are detached) is the total annual rate of events with ground motions that exceed L at the site is given in Equation 4.4:

$$\nu(IM>L) = \sum_{i}^{Sources} \nu_i(IM>L) \qquad 4.4$$

Seismic source characterization involves the definition of the location and geometry of seismic sources, assigning of the characteristic magnitude and activity rate for each seismic source, and selection of the suitable magnitude distribution function along with the reoccurrence relation. The probability density functions f(M) and f(M,R) in Equation 4.3, and the activity rates (denoted by N_{min} in Equation 4.3) for the seismic sources in the study area were explained in Chapter 3. The hazard integral were combined to the ground motion and ground motion variability denoted by $P(IM>L \mid M,R,\varepsilon)$ and $f_\varepsilon(\varepsilon)$ by the selected ground motion prediction models.

Gülerce et al. (2013) explained that Next Generation Attenuation (NGA-W1) models are renewed and improved in terms of supplement prediction parameters (such as depth of the source, basin effects, magnitude dependent standard deviations, etc.), statistical approach, and a well constrained global database. The feasibility of the NGA-W1 models developed for California (US) is an argumentative topic for PSHA studies handled in other tectonic environments. Gülerce et al. (2013) modified and used the recently developed Turkish Strong Motion Database (TSMD, Akkar et al., 2010) to check the compatibility of the magnitude, distance, and site amplification scaling of NGA-W1 horizontal prediction models with the ground motions recorded in Turkey and adjusted necessary coefficients of these models to reflect the regional characteristics for the PSHA applications in Turkey. The Turkey-Adjusted NGA-W1 prediction models are employed by to represent the ground motion variability for the first time on NAF system.

A sensitivity analysis is performed to evaluate the effect of weights assigned to different TR Adjusted NGA-W1 models. The hazard curves for PGA for Bolu City Centre with rock site conditions that are developed using TR Adjusted NGA-W1 models individually are provided in Figure 4.1. A less than 0.02g difference in the hazard for small annual probability of exceedance levels (0.03 or less) caused by using different attenuation models. However, as the level annual probability of exceedance getting smaller, the effect of ground motion prediction model getting larger. The hazard curves obtained using TR Adjusted BA 2008 and TR Adjusted CB 2008 models are quite similar since only magnitude adjustment was applied to these models (Gülerce et al., 2013). In addition to the magnitude adjustment, the site amplification and large distance terms of AS 2008 and CY 2008 models were also modified. Therefore, these two models result in lower hazard curves for rock site conditions. To fully represent the ground motion variability, equal weights are assigned to each model for this step.

To check for the effects of regionalized ground motion prediction models to the final hazard output, the analysis were repeated for the same site with two sets of ground motion models. In the first set, equal weights are assigned to the original NGA-W1 models (denoted by the red line in Figure 4.2) and in the second set, equal weights are assigned to the TR-Adjusted NGA-W1 models (denoted by the blue line in Figure 4.2) in the hazard run. Figure 4.2 indicates that the TR-Adjusted models leads to smaller hazard estimates for small return periods. This result is expected since all of these models were over-predicting the ground motions from small-to-moderate magnitude events, and modified to smaller estimates of ground motions in TR-Adjusted versions. For higher hazard levels, hazard curves from both sets of ground motions are in good agreement since, large magnitude scaling of the NGA-W1 models were not modified to preserve the statistical stability of well-constrained NGA-W1 database.

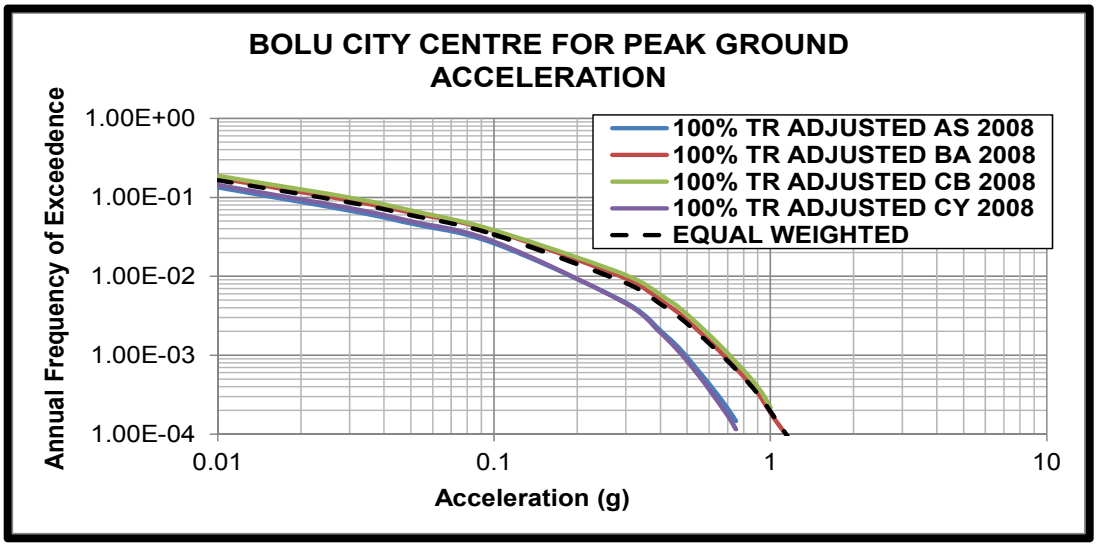

Figure 4.1 The hazard curves for PGA developed using TR Adjusted NGA-W1 models individually for Bolu City Centre with rock site conditions.

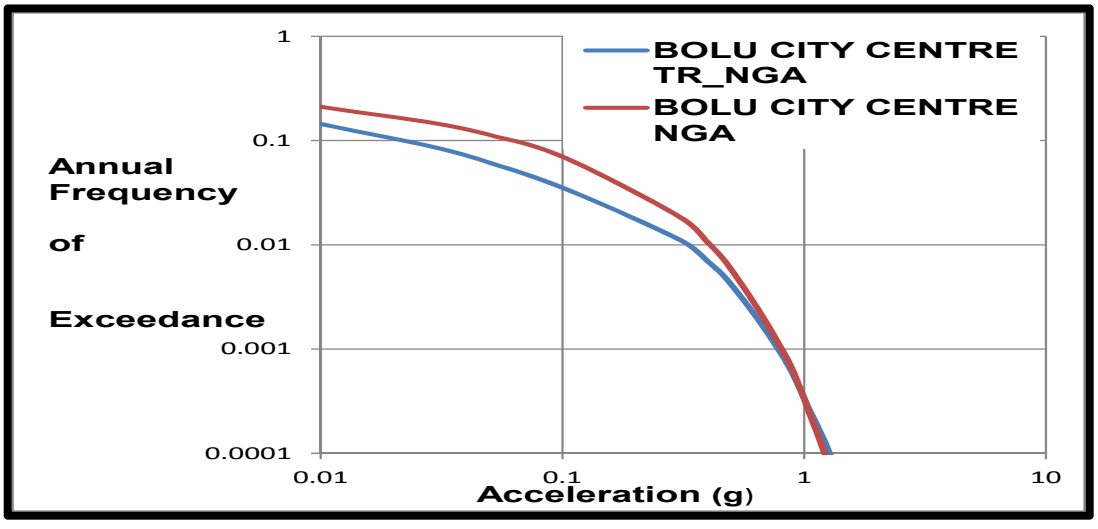

Figure 4.2 Comparison of the results of TR Adjusted NGA-W1 and NGA models hazard curves for PGA for Bolu City Centre

To make the comparison of the hazard results to the defined hazard levels in the Turkish Earthquake Code (TEC, 2007) possible, Poisson process is used:

$$\nu(IM > L) = \frac{-\ln(1 - P(IM > L|T))}{T} \quad 4.5$$

where the number of years is T and the chance of being exceeded is the P(IM>L | T). The return period is theinverse of this rate. The different design codes around the world have acceptable hazard levels similar to the TEC-2007. Table 4.1 shows the different design codes including TEC-2007 with their acceptable hazard levels which were converted to the probability of exceedance and return periods:

Table 4.1 Acceptable hazard levels in TEC-2007 and other design codes

Code	Time	Prob. of Exceedance	Return Period	ν
TEC 2007	50 years	2%	2475 years	0.0004
	50 years	10%	475 years	0.0021
	50 years	50%	72 years	0.0139
NEHRP (FEMA - 273)	50 years	2%	2475 years	0.0004
	50 years	10%	475 years	0.0021
Eurocode	50 years	10%	475 years	0.0021
	10 years	10%	95 years	0.0105

4.2 PSHA Results for Example Sites in the Study Area

The numerical integration of the PSHA integral is performed by the computer code HAZ43 (developed by N. Abrahamson). The numerical integration of the hazard interval for this study is performed by HAZ39 (developed by N. Abrahamson, HGE, 2010). However, the code is modified to implement Turkey adjusted NGA-W1 models. HAZ 39 treats epistemic uncertainties in the source characterization and the GMPEs through the use of logic trees. For each source, all combinations of the logic tree are evaluated and combined to develop fractals on the total hazard. The results of the study are provided as hazard curves, deaggregation of the hazard, and uniform hazard spectrum for 4 sites in study area; Bolu City Centre, Bolu Mountain Tunnel, Hasanlar Dam, Sarıyar Dam (denoted by red stars in Figure 4.3). The effect of all possible combinations of magnitude and distance on the probability of exceeding a selected ground motion level is illustrated in hazard curves (Abrahamson, 2006).

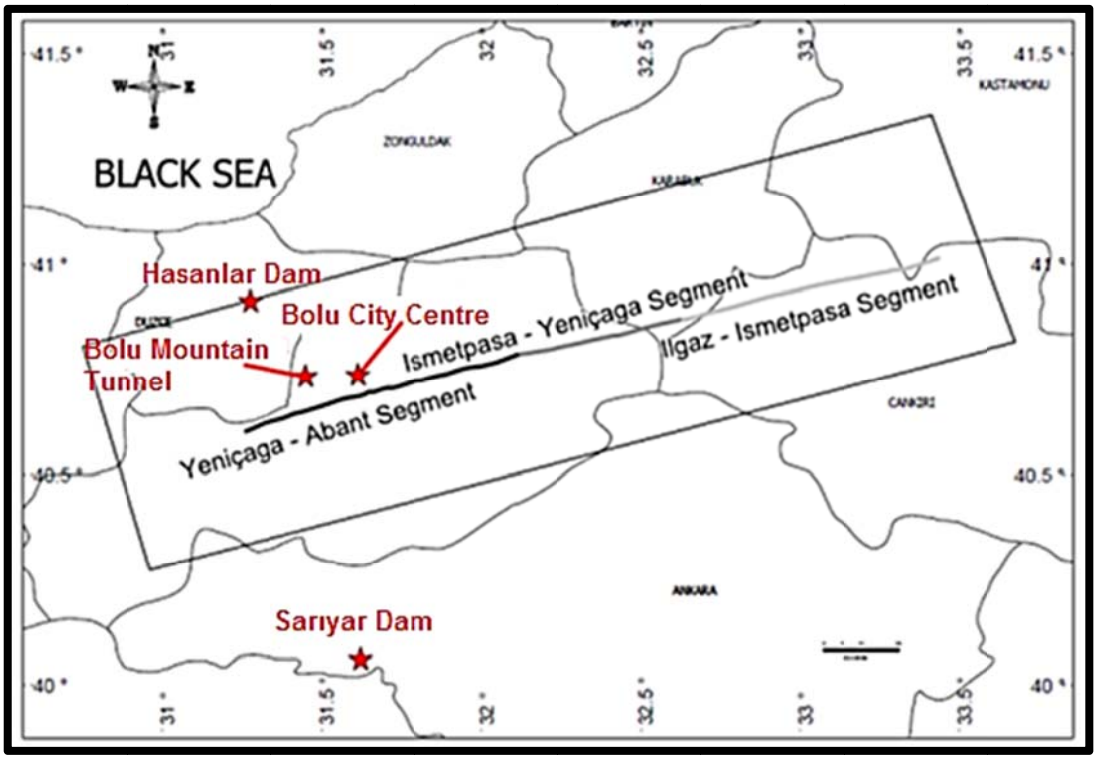

Figure 4.3 The four locations where the analysis are performed

The analyses are performed for PGA and 22 spectral periods (T=0.01, T=0.03, T=0.05, T=0.075, T=0.1, T=0.2, T=0.5, T=1, T=1.5, T=2, T=2.5, T=3, T=3.5, T=4, T=4.5, T=5, T=5.5, T=6, T=6.5, T=7, T=7.5, and T=10 seconds) and hazard curves at four selected sites at chosen spectral periods assuming rock site conditions (V_{s30} = 760 m/s) and soil conditions (V_{s30} = 270 m/s) are presented in Figure 4.4 to Figure 4.21.

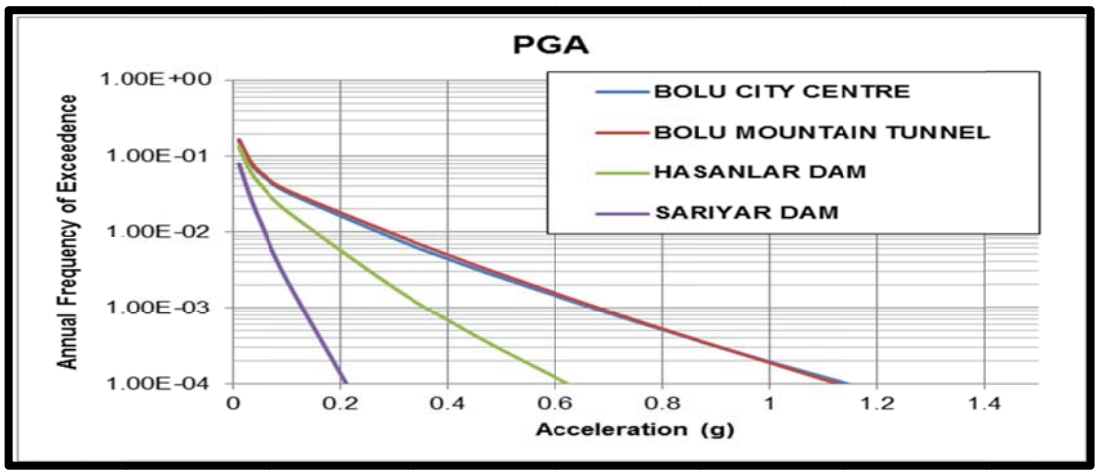

Figure 4.4 Hazard Curves for T = 0 second, (V_{s30} = 760 m/s)

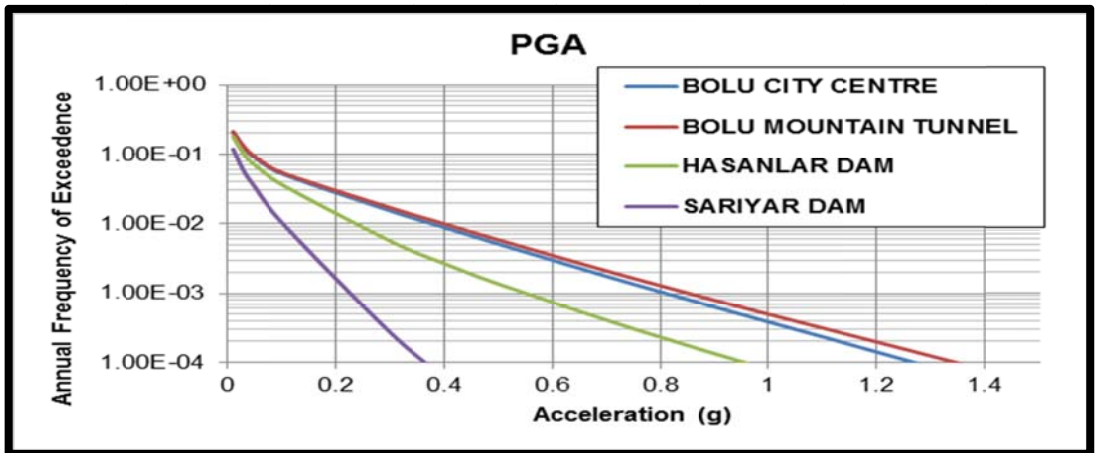

Figure 4.5 Hazard Curves for T = 0 second, (Vs30 = 270 m/s)

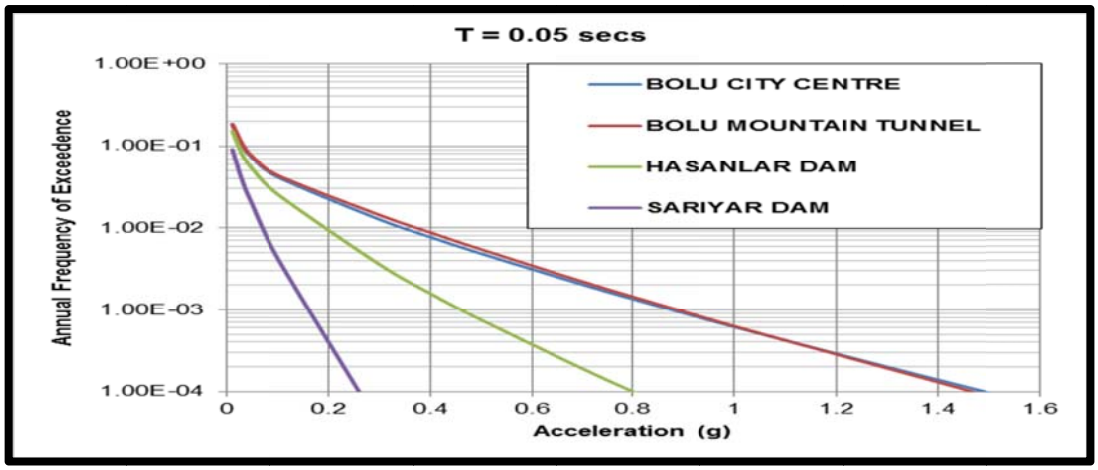

Figure 4.6 Hazard Curves for T = 0.05 second, (V_{s30} = 760 m/s)

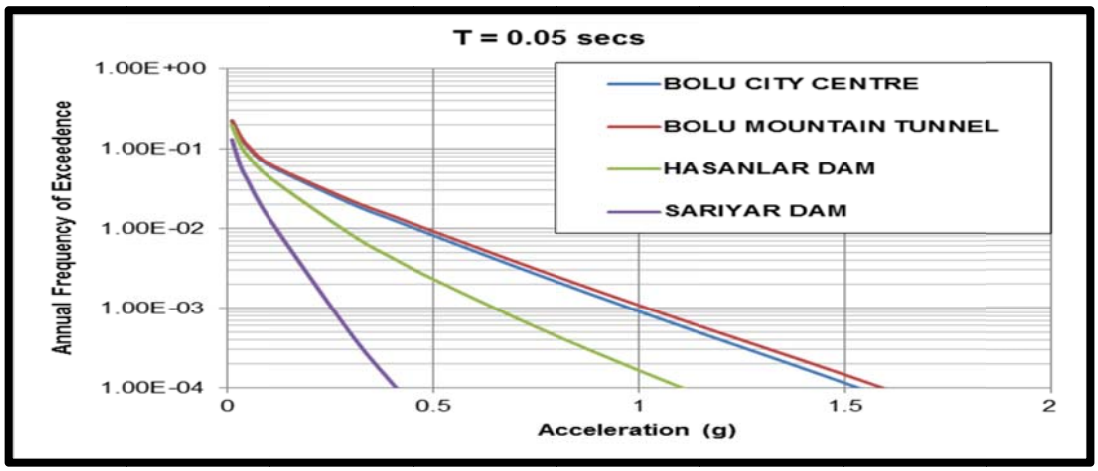

Figure 4.7 Hazard Curves for T = 0.05 second, (V_{s30} = 270 m/s)

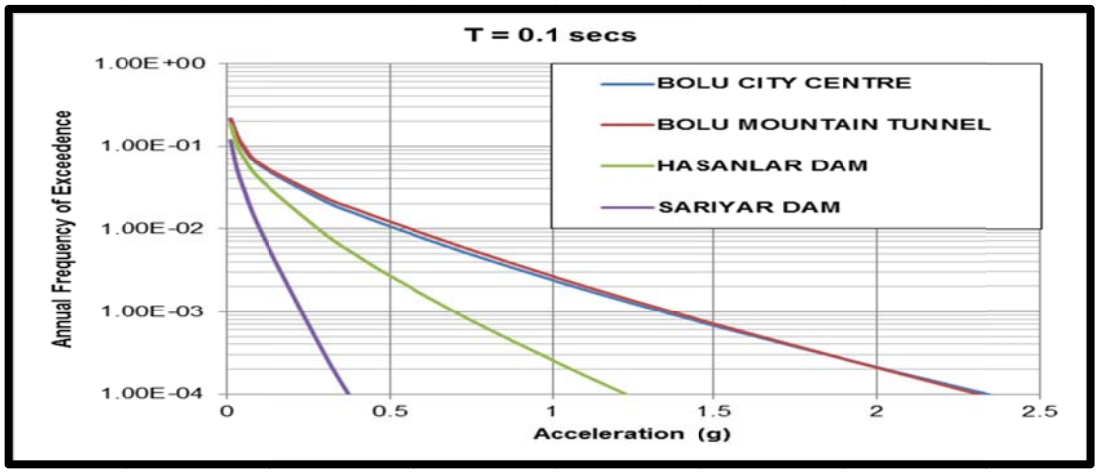

Figure 4.8 Hazard Curves for T = 0.10 second, (V_{s30} = 760 m/s)

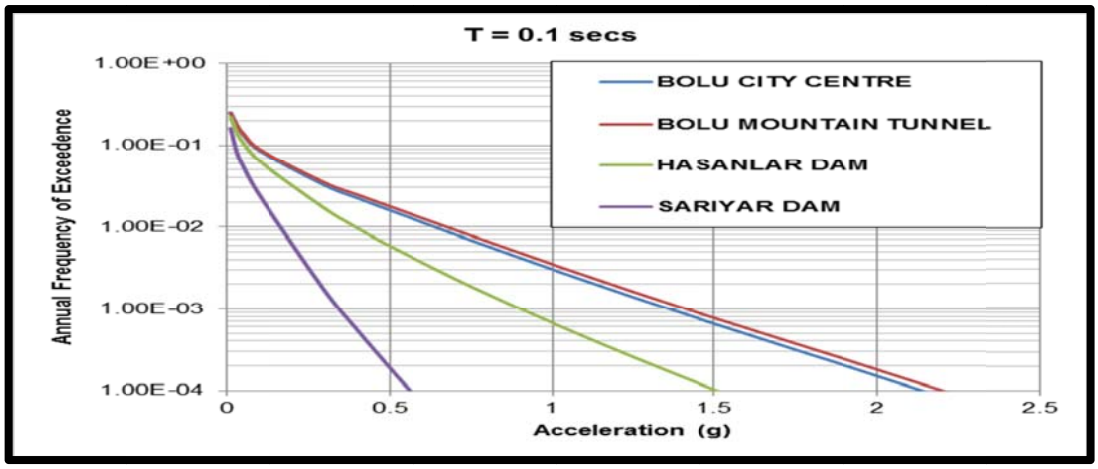

Figure 4.9 Hazard Curves for T = 0.10 second, (V_{s30} = 270 m/s)

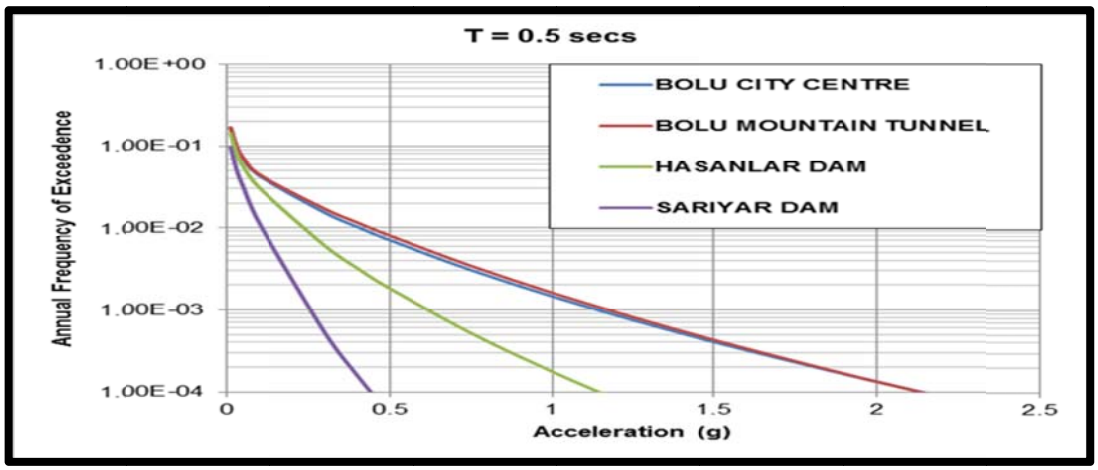

Figure 4.10 Hazard Curves for T = 0.50 second, (V_{s30} = 760 m/s)

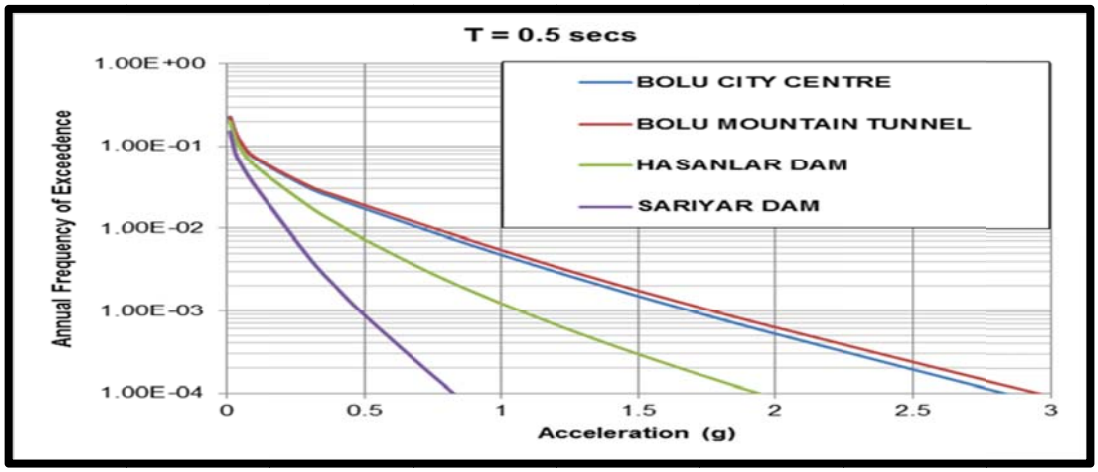

Figure 4.11 Hazard Curves for T = 0.50 second, (V_{s30} = 270 m/s)

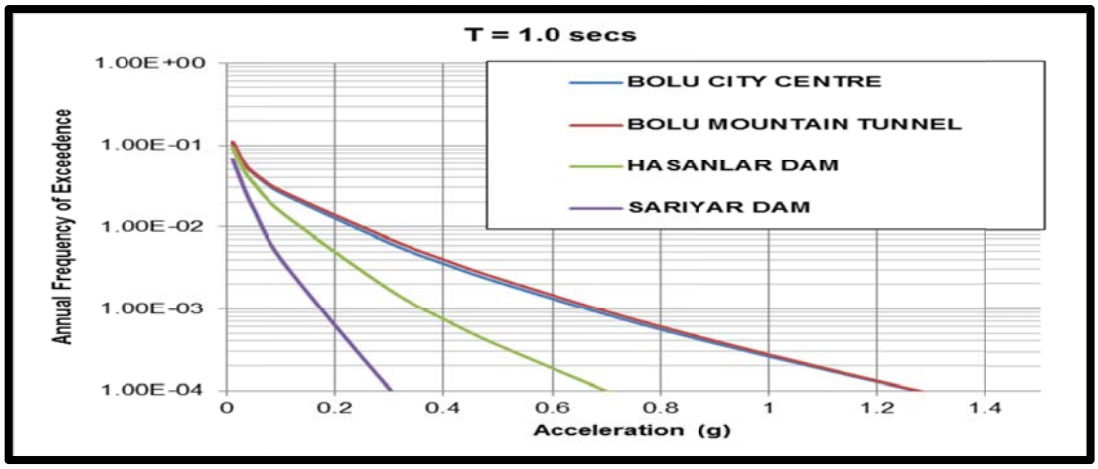

Figure 4.12 Hazard Curves for T = 1.00 second, (Vs30 = 760 m/s)

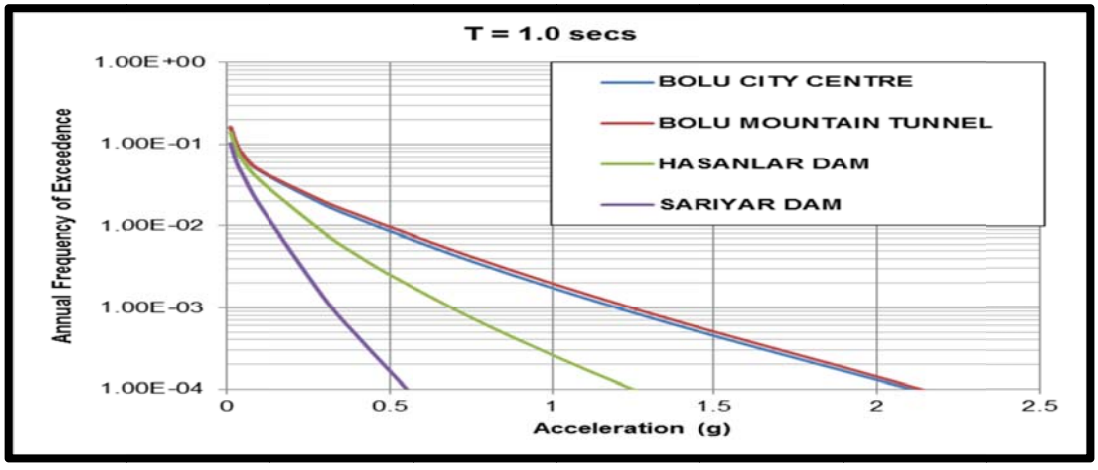

Figure 4.13 Hazard Curves for T = 1.00 second, (Vs30 = 270 m/s)

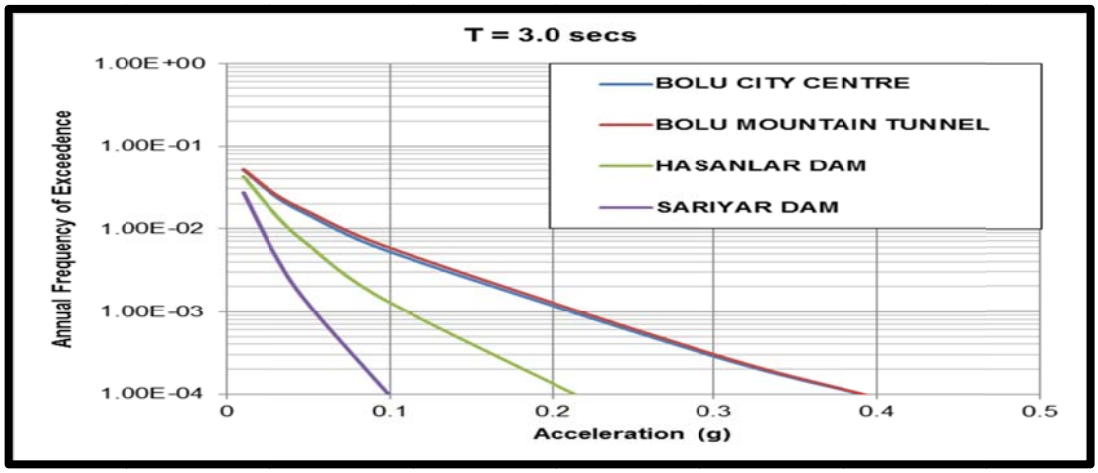

Figure 4.14 Hazard Curves for T = 3.00 second, (Vs30 = 760 m/s)

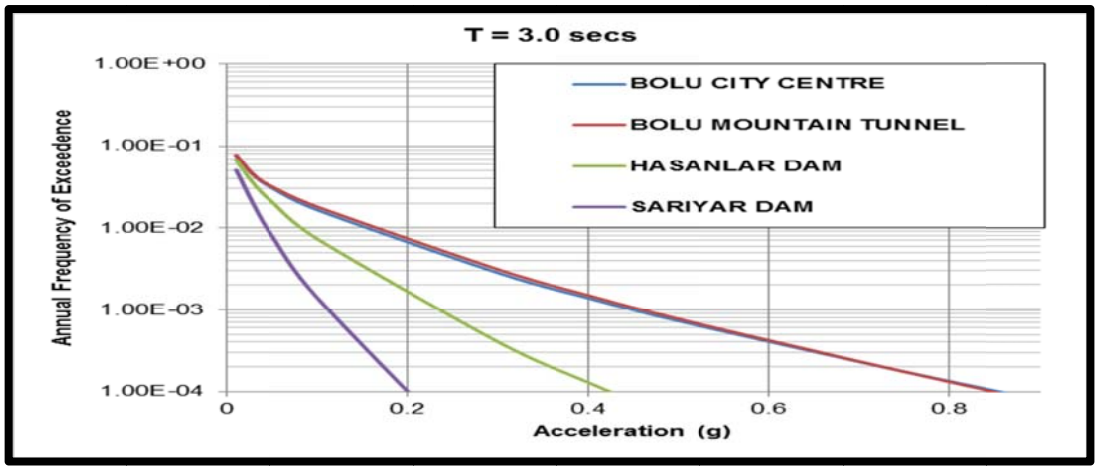

Figure 4.15 Hazard Curves for T = 3.00 second, (Vs30 = 270 m/s)

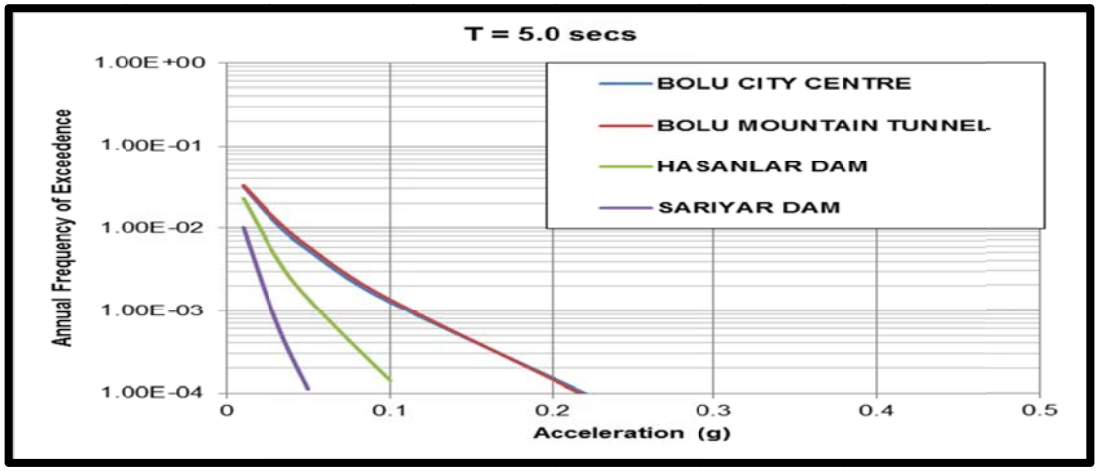

Figure 4.16 Hazard Curves for T = 5.00 second, (Vs30 = 760 m/s)

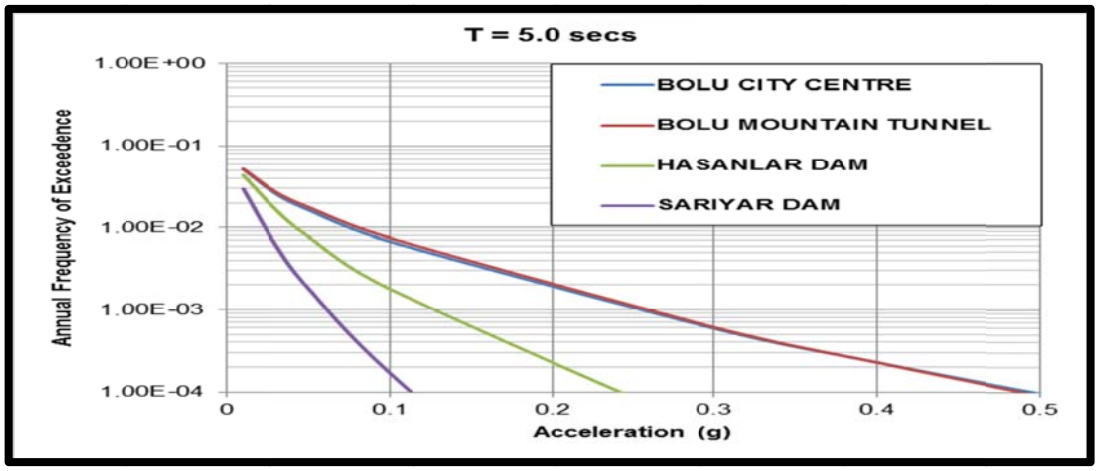

Figure 4.17 Hazard Curves for T = 5.00 second, (Vs30 = 270 m/s)

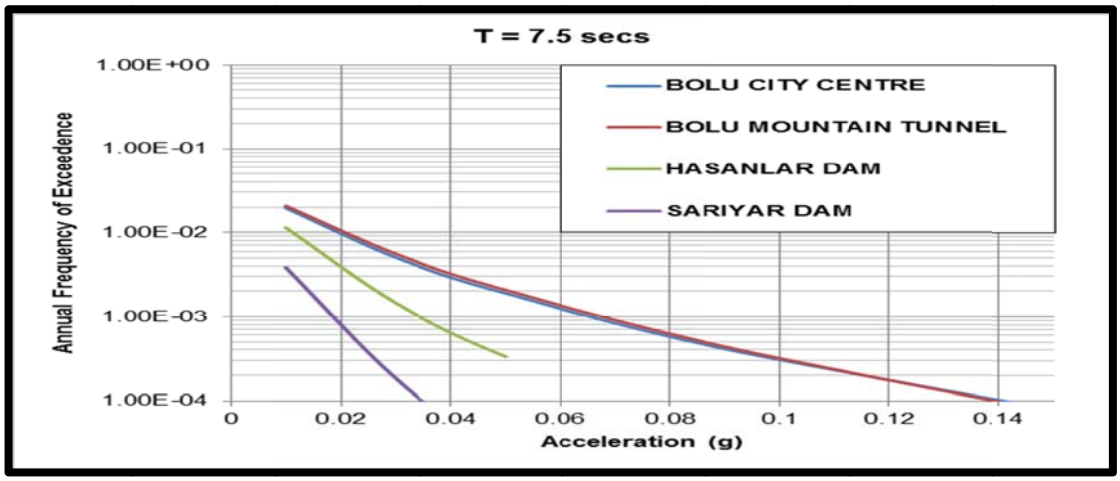

Figure 4.18 Hazard Curves for T = 7.5 second, (Vs30 = 760 m/s)

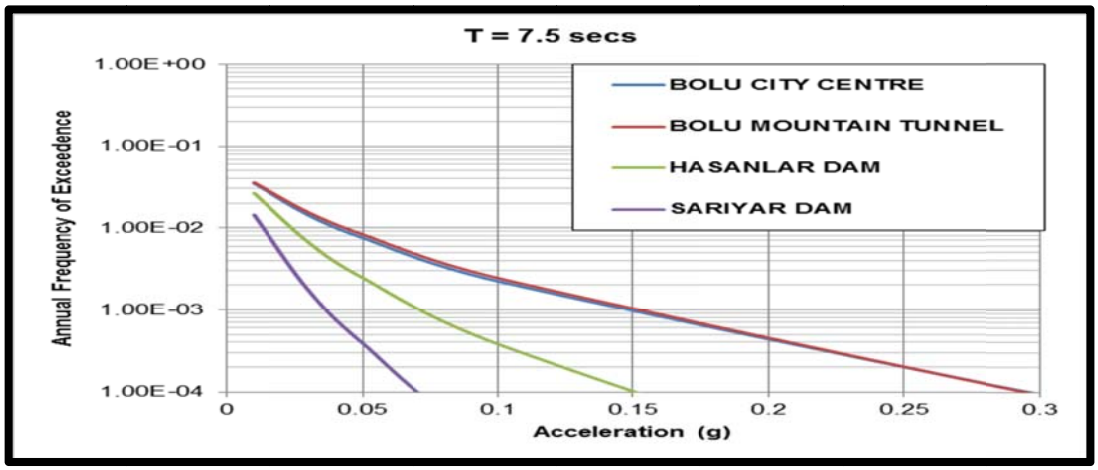

Figure 4.19 Hazard Curves for T = 7.5 second, (Vs30 = 270 m/s)

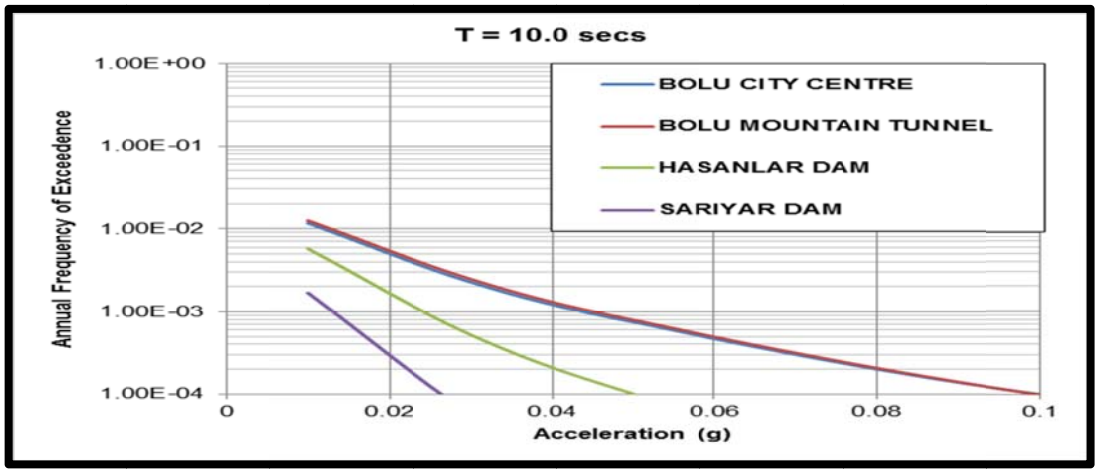

Figure 4.20 Hazard Curves for T = 10.0 second, (Vs30 = 760 m/s)

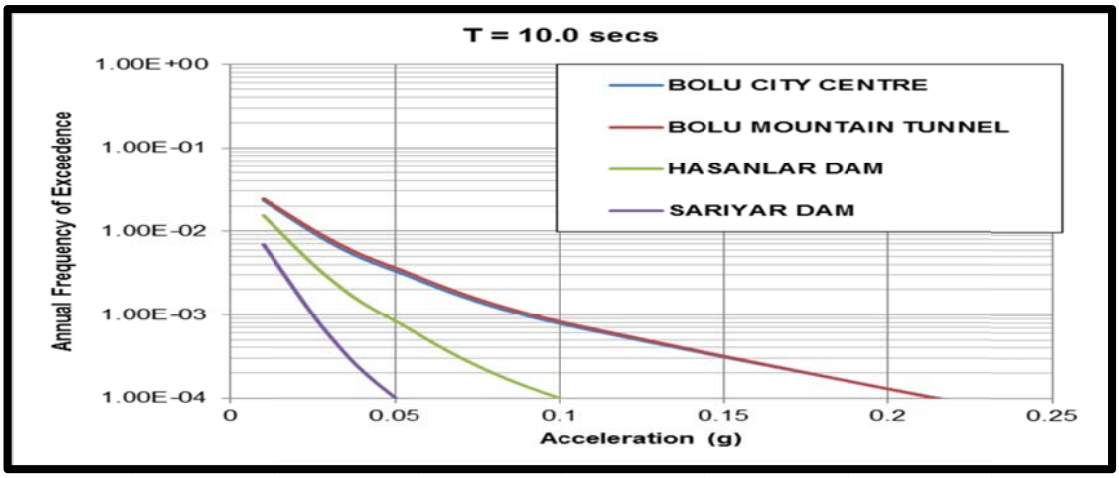

Figure 4.21 Hazard Curves for T = 10.0 second, (Vs30 = 270 m/s)

Bolu Mountain Tunnel and Bolu City Centre have the highest level of seismic hazard for all spectral periods as expected, since these sites are closer than the other sites to 1944 Bolu-Gerede earthquake rupture zone. Hazard at Sarıyar Dam is significantly lower than the other sites due to the fact that the location is outside of the study area and far away from the fault zone when compared to the other analysis locations. The hazard curves for the soil site conditions are higher than the rock site conditions for all spectral periods due to the site amplification model incorporated in GMPEs. The highest hazard levels are observed in the median frequency band, as the spectral period increases the annual frequency of exceedance decreases.

The peak ground accelerations for 2%, 10% and 50% probability of exceedance levels in 50 years at the selected sites for rock site conditions (Vs30 = 760 m/sec) are presented in Table 4.2 and and for soil site conditions (Vs30 = 270 m/sec) are presented in Table 4.3. The study area is located in first seismic zone according to TEC 2007 and 475 years return period design peak ground acceleration is 0.4g for regular buildings. The analysis results are higher than the TEC 2007 requirements at Bolu City Centre, Bolu Mountain Tunnel, Hasanlar Dam due to the close proximity of selected sites to the fault system. Lower PGA values should be expected for sites at distances bigger than 30 kilometers such as Sarıyar Dam.

Table 4.2 PGA for different exceedance levels at four locations at rock site conditions

Hazard Level	Bolu City Centre	Bolu Mountain Tunnel	Hasanlar Dam	Sarıyar Dam
2% in 50 years	0.850	0.850	0.450	0.160
10% in 50 years	0.550	0.600	0.270	0.100
50% in 50 years	0.225	0.250	0.110	0.050

Table 4.3 PGA for different exceedance levels at four locations at soil site conditions

Hazard Level	Bolu City Centre	Bolu Mountain Tunnel	Hasanlar Dam	Sarıyar Dam
2% in 50 years	1.000	1.000	0.700	0.260
10% in 50 years	0.675	0.700	0.450	0.200
50% in 50 years	0.300	0.310	0.200	0.075

Gülerce and Abrahamson (2010) said that the merged effect of all magnitudes and distances on the probability of exceeding the specified ground motion level is given by the hazard curve. It is hard to realize what is controlling the hazard from the hazard curve by itself because all of the sources, magnitudes, and distances are combined together. Bazzurro and Cornell (1999) brake down the hazard curve into its contributions from different earthquake scenarios to obtain a sense into which events are most critical for the hazard at a given ground motion level. They called this operation as deaggregation. Figure 4.22 to Figure 4.33 shows the deaggregation plots for 2%, 10%, 50% probability of exceedance levels in 50 years at the selected four sites for rock site conditions at PGA.

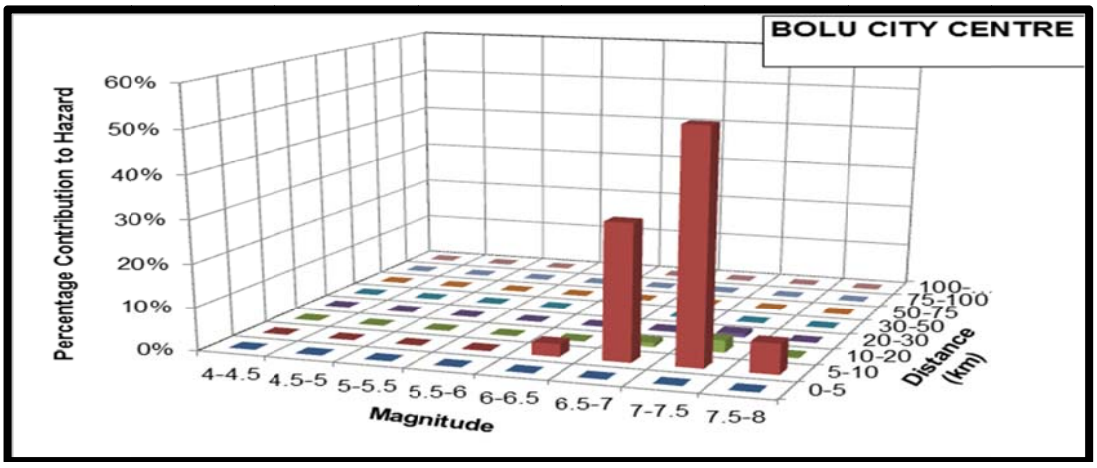

Figure 4.22 Deaggregation for Bolu City Centre for 2% of exceedance in 50 years (Vs30 = 760 m/sec, PGA)

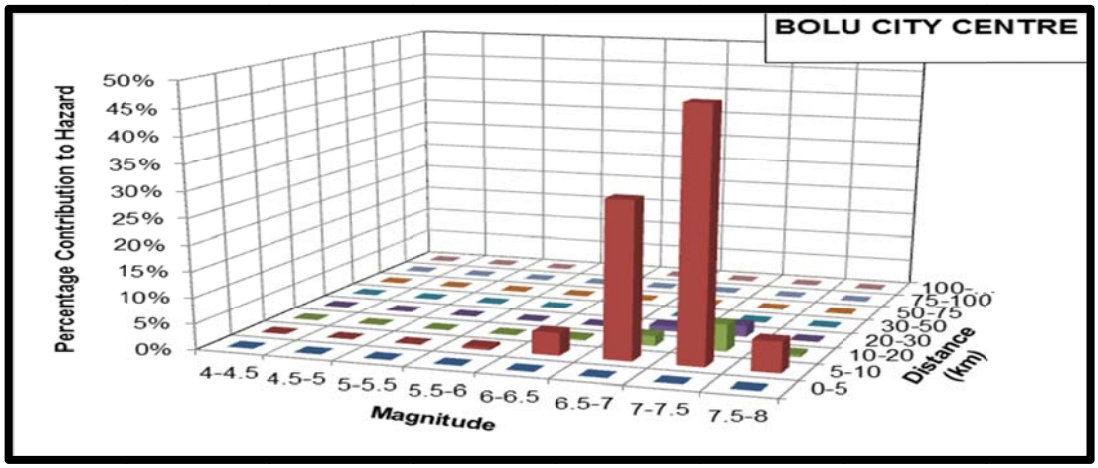

Figure 4.23 Deaggregation for Bolu City Centre for 10% probability of exceedance in 50 years hazard level (Vs30 = 760 m/sec, PGA)

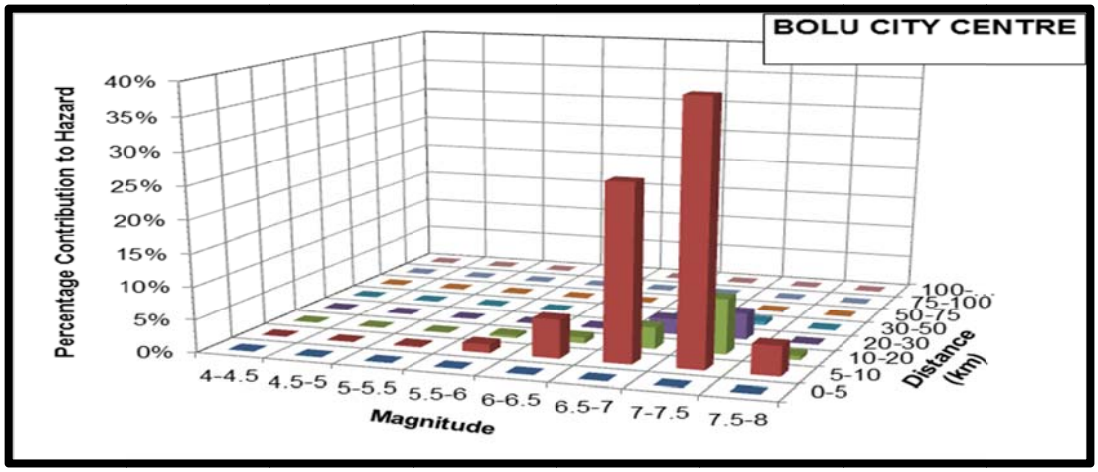

Figure 4.24 Deaggregation for Bolu City Centre for 50% probability of exceedance in 50 years hazard level (Vs30 = 760 m/sec, PGA)

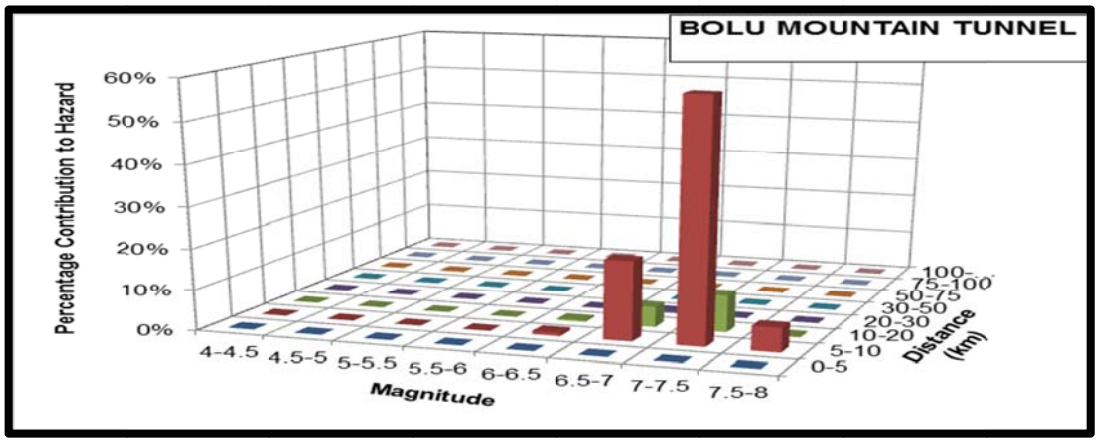

Figure 4.25 Deaggregation for Bolu Mountain Tunnel for 2% probability of exceedance in 50 years hazard level (Vs30 = 760 m/sec, PGA)

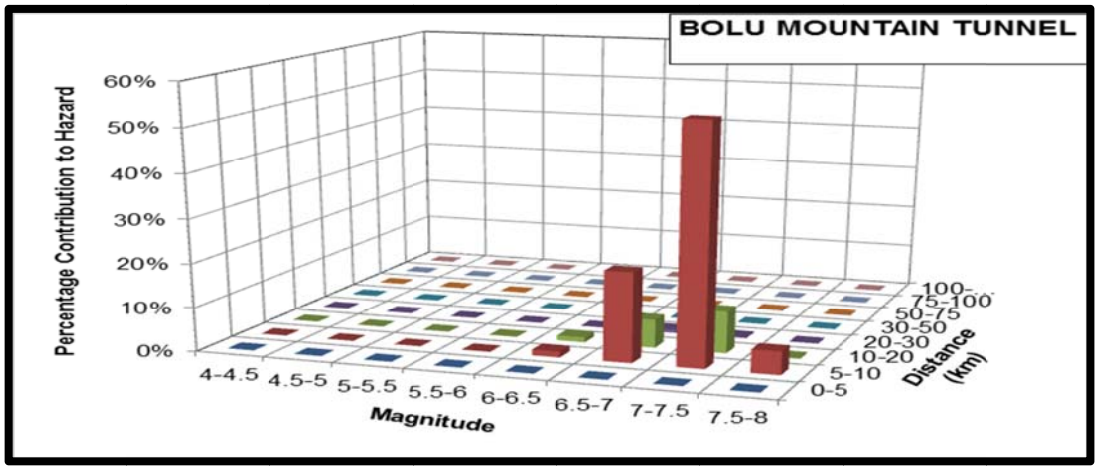

Figure 4.26 Deaggregation for Bolu Mountain Tunnel for 10% probability of exceedance in 50 years hazard level (Vs30 = 760 m/sec, PGA)

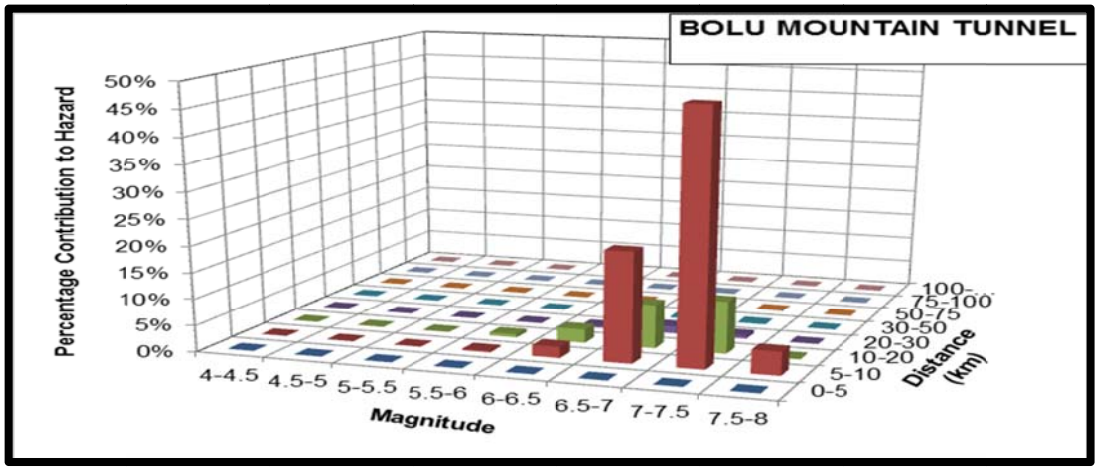

Figure 4.27 Deaggregation for Bolu Mountain Tunnel for 50% probability of exceedance in 50 years hazard level (Vs30 = 760 m/sec, PGA)

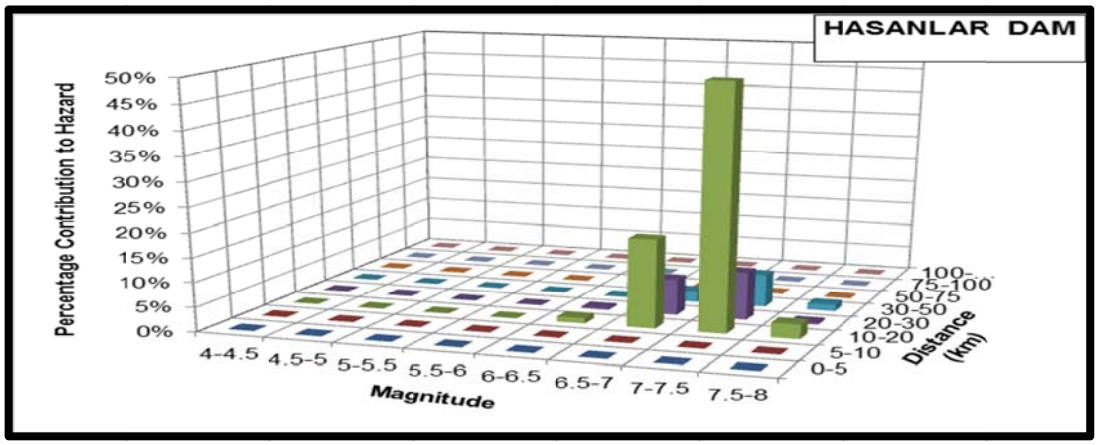

Figure 4.28 Deaggregation for Hasanlar Dam for 2% probability of exceedance in 50 years hazard level (Vs30 = 760 m/sec, PGA)

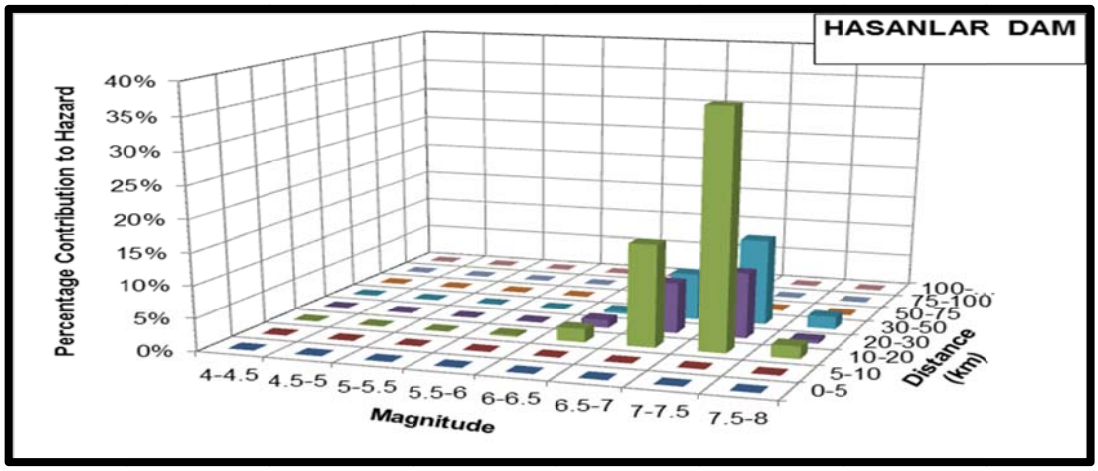

Figure 4.29 Deaggregation for Hasanlar Dam for 10% probability of exceedance in 50 years hazard level (Vs30 = 760 m/sec, PGA)

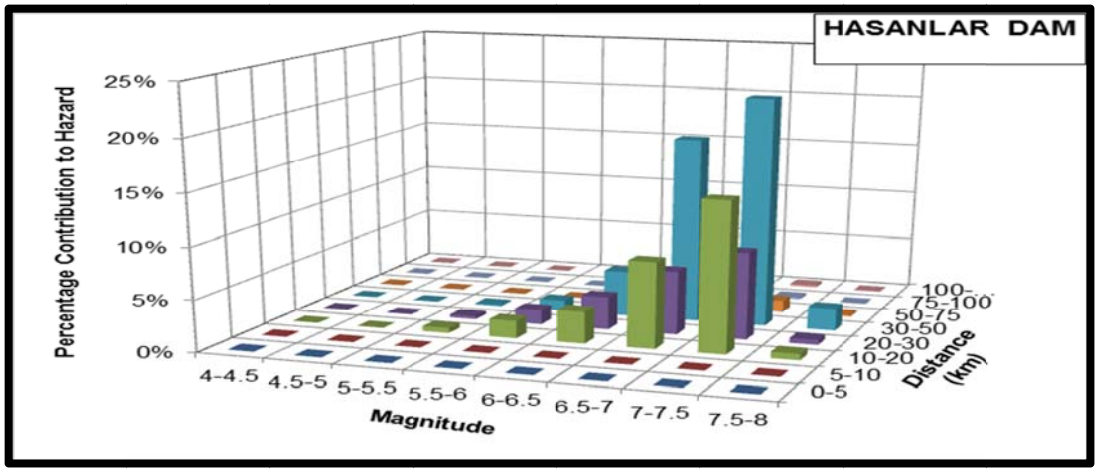

Figure 4.30 Deaggregation for Hasanlar Dam for 50% probability of exceedance in 50 years hazard level (Vs30 = 760 m/sec, PGA)

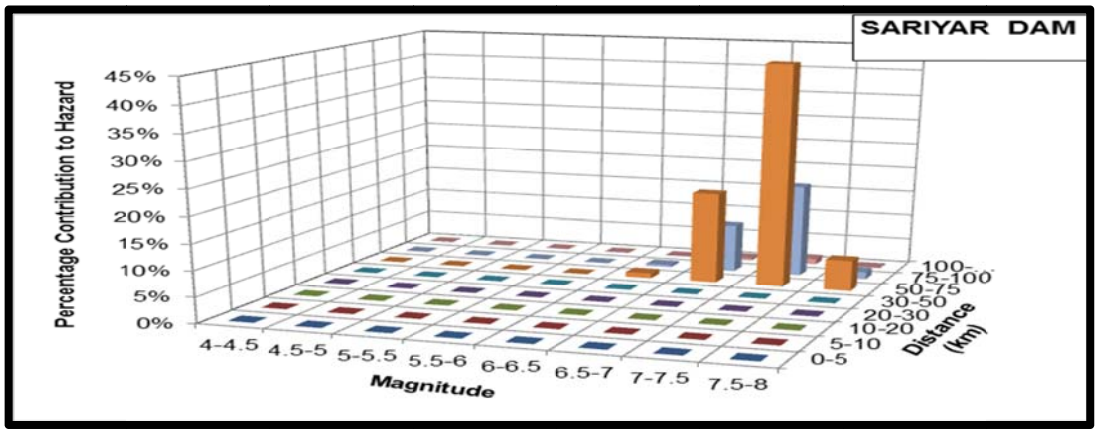

Figure 4.31 Deaggregation for Sarıyar Dam for 2% probability of exceedance in 50 years hazard level (Vs30 = 760 m/sec, PGA)

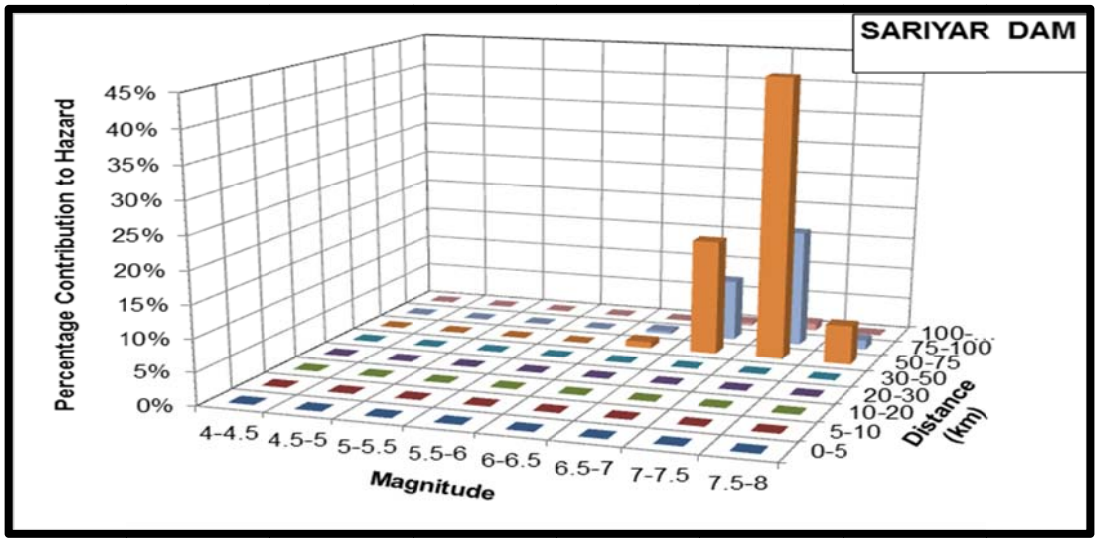

Figure 4.32 Deaggregation for Sarıyar Dam for 10% probability of exceedance in 50 years hazard level (Vs30 = 760 m/sec, PGA)

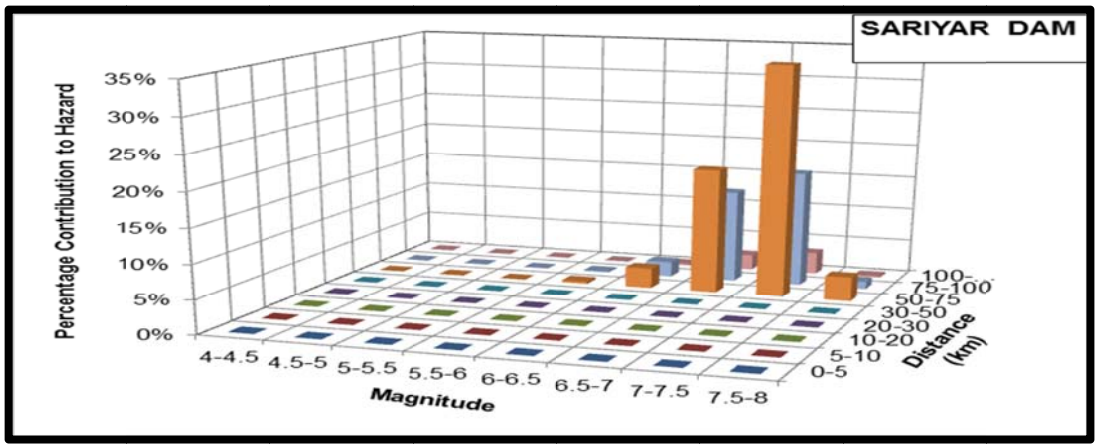

Figure 4.33 Deaggregation for Sarıyar Dam for 50% probability of exceedance in 50 years hazard level (Vs30 = 760 m/sec, PGA)

For sites close to the Yeniçağa-Abant segment (Bolu City Centre and Bolu Mountain Tunnel), the hazard is dominated by this source as shown in Figure 4.22 to Figure 4.27. For both of these sites, the dominating scenario has the magnitude between 6.5-7.5 at 5-10 km. distance. When the hazard level increases (as shown in Figure 4.22, 4.24, 4.25, 4.27) , the magnitude of the dominating scenario shifts to magnitude 6.5 – 7 band but the distance band does not change.

For Hasanlar Dam, the dominating source is again the Yeniçağa-Abant segment as shown in Figure 4.28 to Figure 4.30. The dominating scenario has the magnitude between 6.5-7.5 similar to the Bolu City Centre and Bolu Mountain Tunnel. However, the distance of dominating scenario increases to 10-20 kilometers for this site. The large contribution of magnitude 7-7.5 distance 30-50 km. scenario is due to the effect of Ilgaz-Ismetpaşa segment. The contribution of Ismetpaşa-Yeniçağa segment is smaller than Ilgaz-Ismetpaşa even if it is closer to the site, since the slip rate of this segment is lower than the others. Unlike Bolu City Centre and Bolu Mountain Tunnel, the dominating scenario changes when the hazard level increases. For 2% and 10% of probability exceedance in 50 years hazard

levels, the dominating source is the Ilgaz-Ismetpaşa segment.. For 50% of probability of exceedance, the dominating scenario has magnitude 6.5-7.5 at the distance 30-50 kilometers (Figure 4.30).

For Sarıyar Dam, the dominating scenario again has the magnitude of 6.5-7.5 similar to the other sites (Figure 4.31 to Figure 4.33). For this site, the distance range of dominating scenario is 50-75 kilometers because of being far away from the seismic sources. When the hazard level increases, the percentage contribution of the dominating scenario to the total hazard decreases. However, the dominating scenario is always the same for different hazard levels.

4.3 Uniform Hazard Spectrum and TEC 2007 Comparison

The usage of Uniform Hazard Spectrum (UHS) is a general method for enhancing design spectra due to the probabilistic approach. The UHS is formed by calculating the hazard independently at a group of spectral periods and then calculating the ground motion for a determined probability level at each spectral period. Since the spectral acceleration value at each period has an equal opportunity of being exceeded, the term “uniform hazard spectrum” is used (Gülerce and Abrahamson, 2011).

Figure 4.34 to Figure 4.36 show the uniform hazard spectra of the selected sites (Bolu City Centre, Bolu mountain Tunnel, Hasanlar Dam and Sarıyar Dam) at 2%, 10% and 50% probability of exceedance hazard levels for rock site conditions (V_{s30}=760 m/s). Similarly, Figure 4.37 to Figure 4.39 show the uniform hazard spectra of the selected sites at the same probability of exceedance hazard levels for soil site conditions (V_{s30}=270 m/s). In order to compare the results with the TEC-2007 design specifications, the UHS plots include also the TEC-2007 design spectrum for rock or soil site conditions. According to TEC 2007 specifications, for plotting the TEC 2007 design spectrum, Z1 type soil class is assigned to represent rock site conditions (V_{s30} = 760 m/s) and Z3 type is assigned to represent the soil site conditions (V_{s30} = 270 m/s).

For rock site conditions of Bolu City Centre and Bolu Mountain Tunnel the UHS developed is significantly higher than TEC-2007 design spectrum for all spectral periods at the hazard level levels of 2% and 10% probability of exceedance. For 50% probability of exceedance hazard level, Bolu City Centre UHS is smaller than the TEC-2007 design spectrum after 0.25 second spectral period. Again for 50% probability of exceedance hazard level, the Bolu Mountain Tunnel UHS is smaller than the TEC-2007 design spectrum after 1 second spectral period. For the soil site conditions, the UHS developed is significantly higher than TEC-2007 design spectrum at all of the hazard levels.

For rock site conditions of Hasanlar Dam, the UHS developed is significantly lower than TEC-2007 design spectrum for all spectral periods and all of the hazard levels. However, for soil site conditions of Hasanlar dam, at 2% probability of exceedance hazard level, the UHS is higher than the TEC-2007 design spectrum up to 0.3 second spectral periods. For 10% probability of exceedance hazard level, the UHS level is approximately same as the TEC-2007 design spectrum until 0.075 second spectral period. UHS is significantly lower than the TEC-2007 design spectrum for 50% probability of exceedance hazard level.

For both rock and soil site conditions of Sarıyar Dam, the UHS developed is significantly lower than TEC-2007 design spectrum for all spectral periods and all of the different hazard levels.

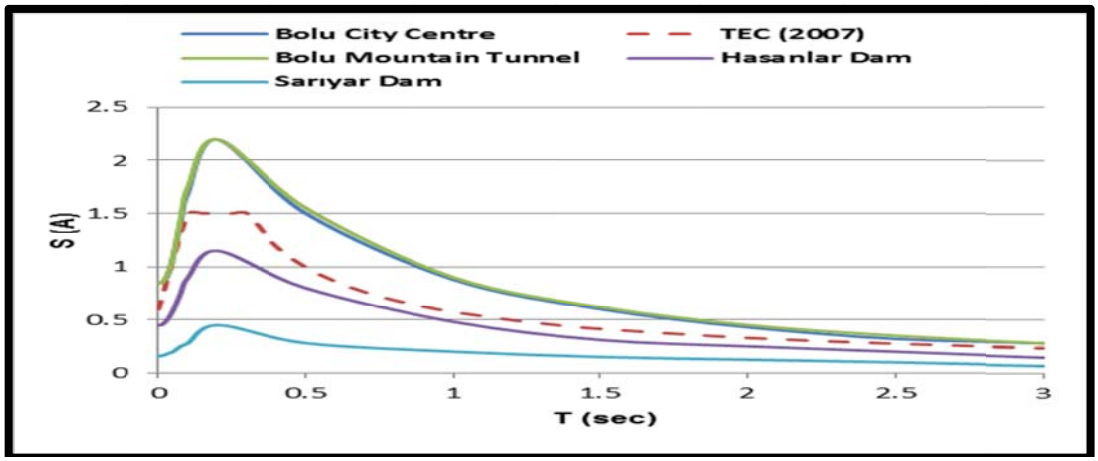

Figure 4.34 Uniform Hazard Spectra for 4 critical location, 2% probability of exceedance hazard level, Vs30 = 760 m/sec

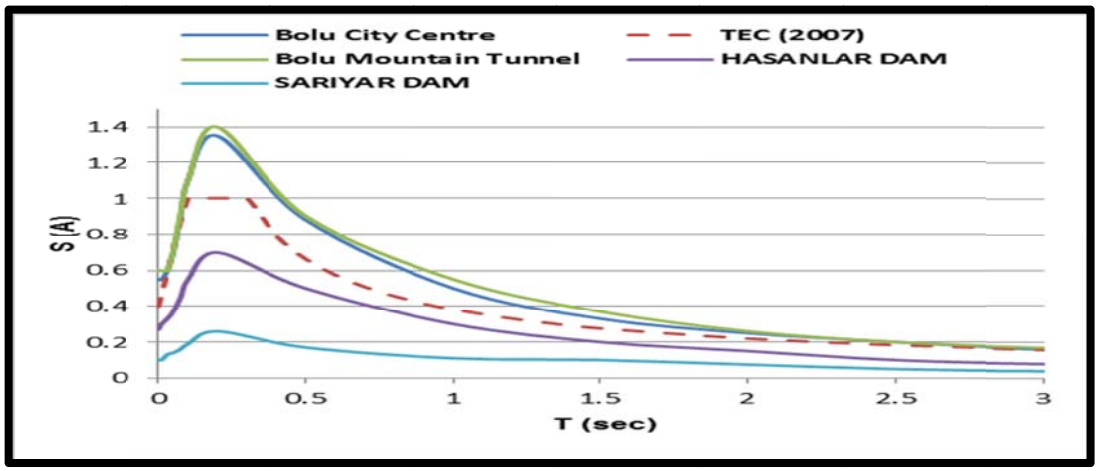

Figure 4.35 Uniform Hazard Spectra for 4 critical location, 10% probability of exceedance hazard level, Vs30 = 760 m/sec

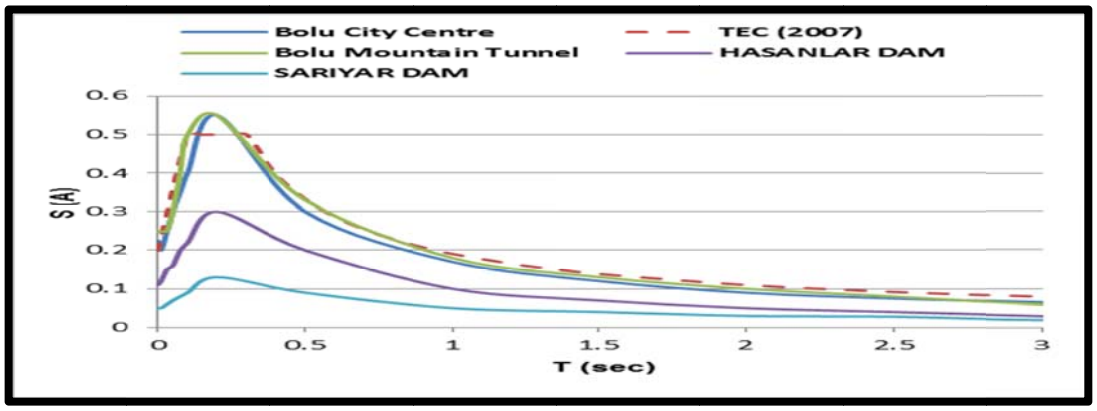

Figure 4.36 Uniform Hazard Spectra for 4 critical location, 50% probability of exceedance hazard level, Vs30 = 760 m/sec

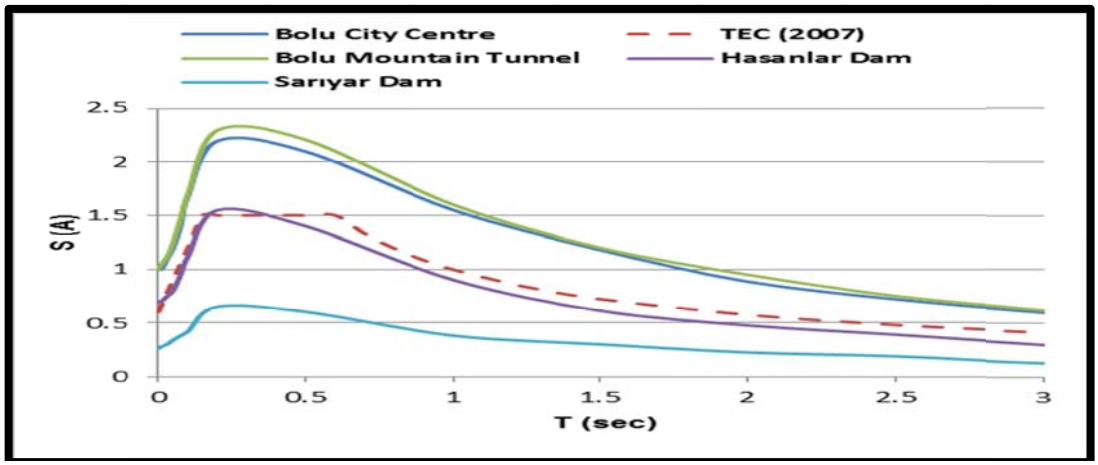

Figure 4.37 Uniform Hazard Spectra for 4 critical location, 2% probability of exceedance hazard level, Vs30 = 270 m/sec

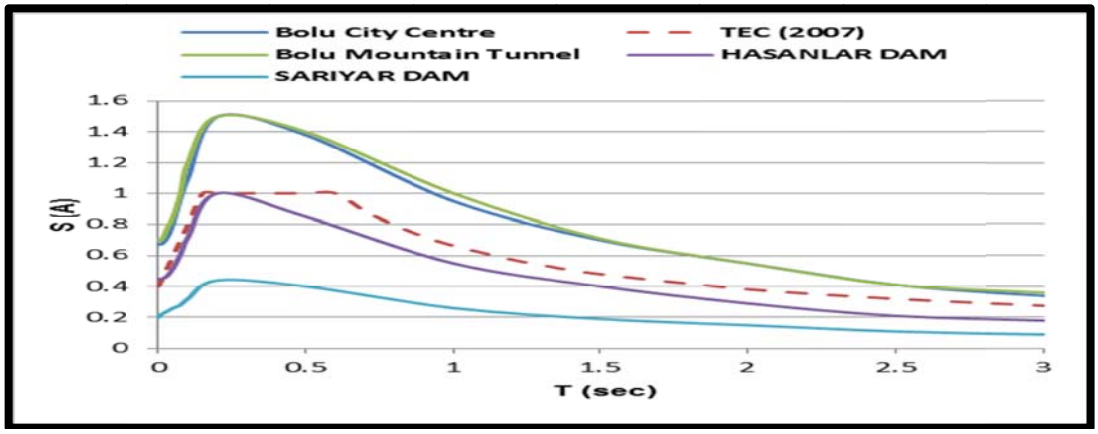

Figure 4.38 Uniform Hazard Spectra for 4 critical location, 10% probability of exceedance hazard level, Vs30 = 270 m/sec

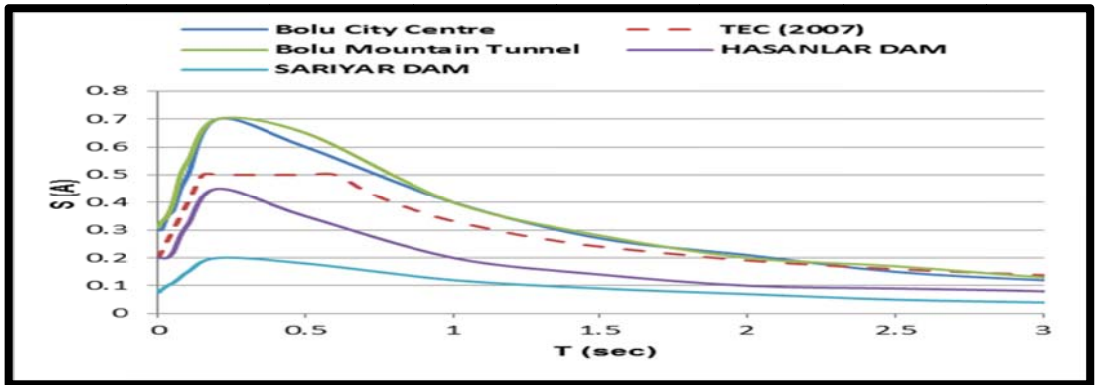

Figure 4.39 Uniform Hazard Spectra for 4 critical location, 50% probability of exceedance hazard level, Vs30 = 270 m/sec

4.4 Hazard Maps for Study Area

The hazard maps for the region for the rock site and soil site conditions at the applicable hazard levels in Turkish Earthquake Code (2007) are built for PGA, T=0.2 second and T=1 second spectral periods. For this purpose, 108 grid nodes were defined in the study area as shown in Figure 4.40 and PSHA was performed at each grid node. In addition to 1944 Bolu-Gerede earthquake rupture zone, two more seismic sources close to the study area are adopted from (Gülerce and Ocak, 2013) and included in the PSHA analysis. These sources are presented in Figure 4.40 by a blue line for Mudurnu Abant Segments (North Anatolian Fault Southern Straned) (Source-2) and a red line Düzce Fault (source-3) in Figure 4.40.

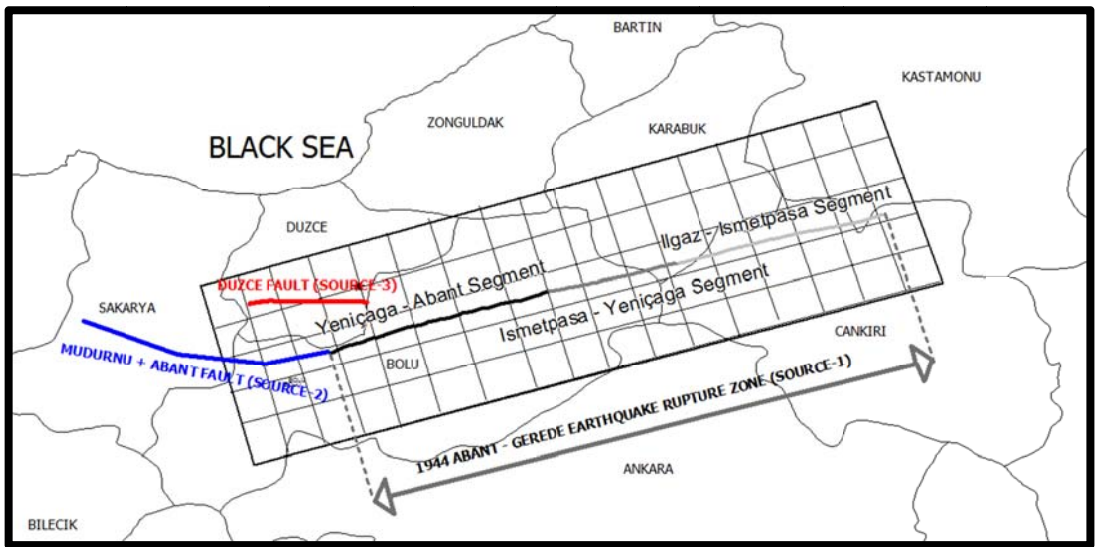

Figure 4.40 Grids and sources assigned to region

Figure 4.41 to figure 4.58 represents the seismic hazard maps for rock site conditions (Vs30 = 760 m/s) and soil site conditions for PGA at 2%, 10% and 50% probability of exceedance in 50 years hazard levels. Generally, the fault lines followed by the contours of the maps as expected. The assigned segmentation locations on the sources and the overlap locations of the seismic sources are the locations where hazard level increase. Following interpretations are made from the hazard maps:

- For rock site conditions, the highest value of PGA is around 0.77g at 2% probability of exceedence hazard level, 0.49g at 10% probability of exceedence hazard level and 0.21g at 50% probability of exceedence hazard level.

- For soil site conditions, the highest value of PGA is around 0.95g at 2% probability of exceedence hazard level, 0.62g at 10% probability of exceedance hazard level and 0.29g at 50% probability of exceedence hazard level.

- The seismic hazard maps for T=0.2 second for rock site conditions (Vs30 = 760 m/s) and soil site conditions at 2%, 10% and 50% level of probability of exceedance at 50 years are provided in Figure 4.51 to Figure 4.56. Generally, the contours of the maps follow the fault lines as expected. The assigned segmentation locations on the sources and the overlap locations of the seismic sources are the locations where hazard level increase.

- For rock site conditions, the highest value of T=0.2 second is around 1.77g at 2% probability of exceedence hazard level, 1.22g at 10% probability of exceedance hazard level and 0.45g at 50% probability of exceedance hazard level.

- For soil site conditions, the highest value of T=0.2 second is around 2.09g at 2% probability of exceedence hazard level, 1.38g at 10% probability of exceedance hazard level and 0.65g at 50% probability of exceedance hazard level.

- The seismic hazard maps for T=1.0 second for rock site conditions (Vs30 = 760 m/s) and soil site conditions at 2%, 10% and 50% level of probability of exceedance at 50 years are provided in Figure 4.57 to Figure 4.62. Generally, the fault lines followed by the contours of the maps as expected. The assigned segmentation locations on the sources and the overlap locations of the seismic sources are the locations where hazard level increase.

- For rock site conditions, the highest value of T=1.0 second is around 0.81g at 2% probability of exceedence hazard level, 0.47g at 10% probability of exceedance hazard level and 0.17g at 50% probability of exceedance hazard level.

- For soil site conditions, the highest value of T=1.0 second is around 1.42g at 2% probability of exceedence hazard level, 0.86g 10% probability of exceedance hazard level and 0.35g at 50% probability of exceedance hazard level.

- For both rock and soil conditions and all of the different hazard levels, smaller hazard levels are observed in the regions close to segment-2. The slip rate of segment-2 is smaller than the other segments due to the creep observed in Ismetpaşa.

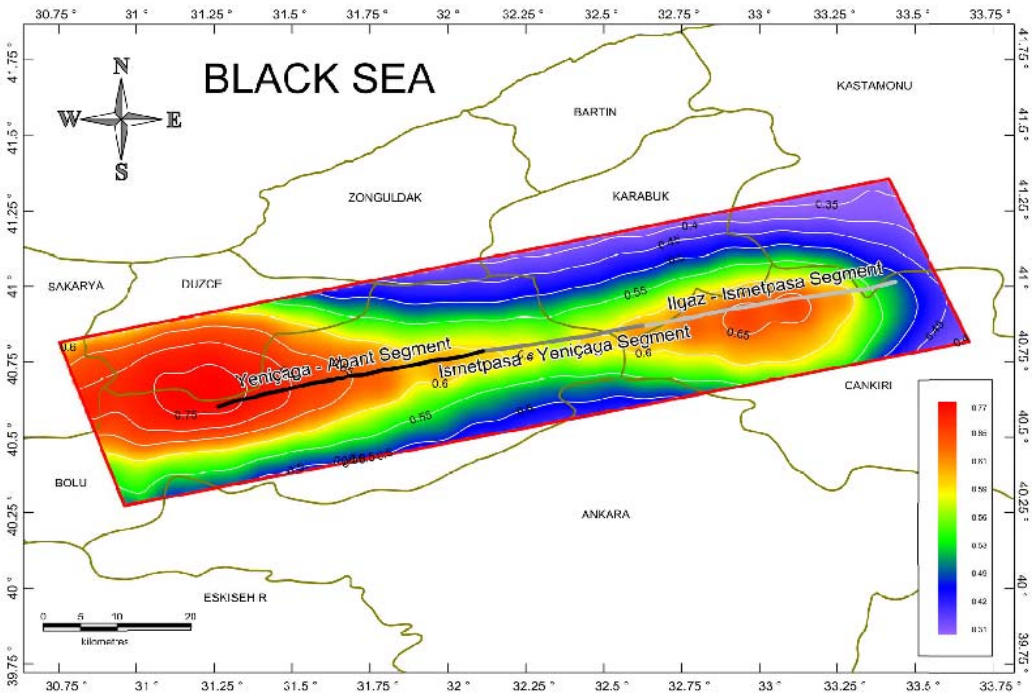

Figure 4.41 Hazard Map for PGA and Vs30 = 760 m/sec at 2% probability of exceedence hazard level

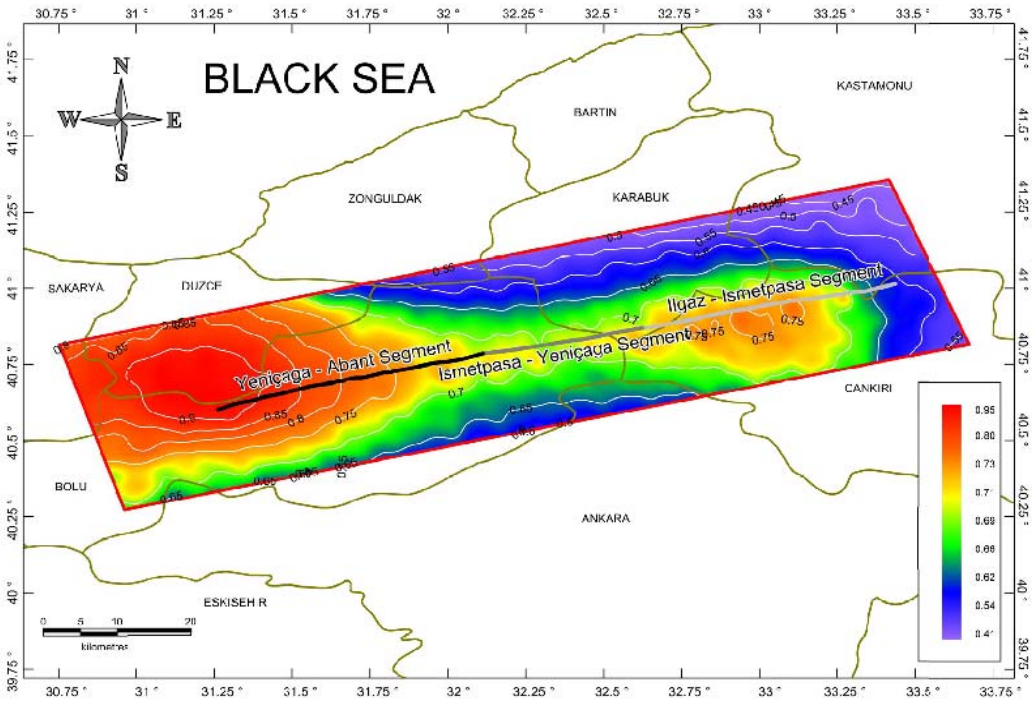

Figure 4.42 Hazard Map for PGA and Vs30 = 270 m/sec at 2% probability of exceedence hazard level

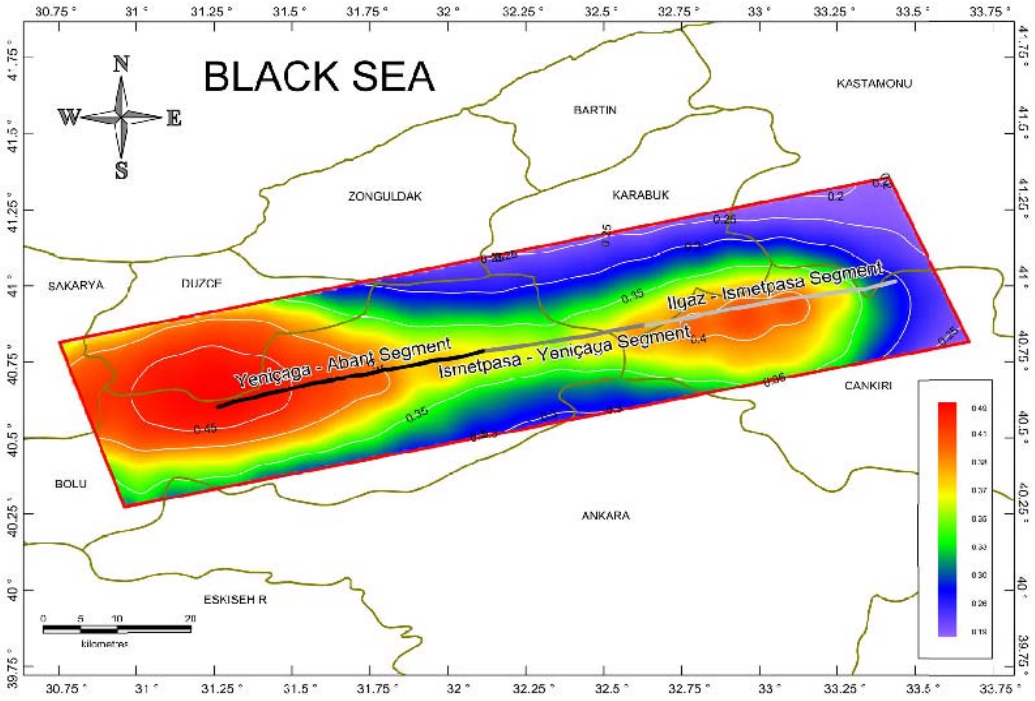

Figure 4.43 Hazard Map for PGA and Vs30 = 760 m/sec at 10% probability of exceedence hazard level

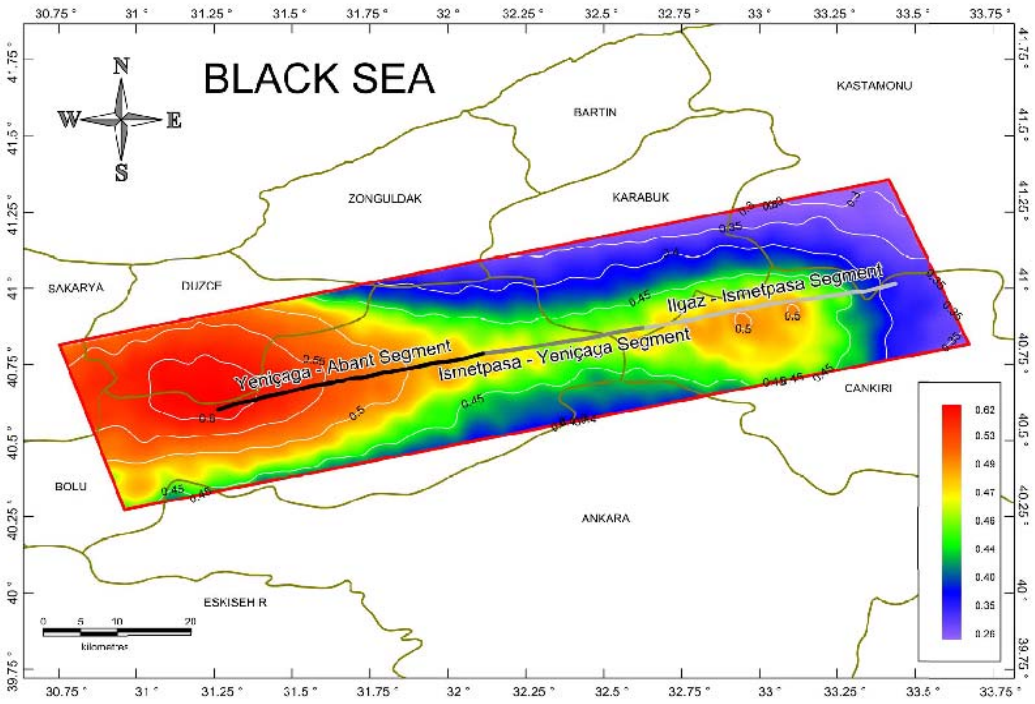

Figure 4.44 Hazard Map for PGA and Vs30 = 270 m/sec at 10% probability of exceedence hazard level

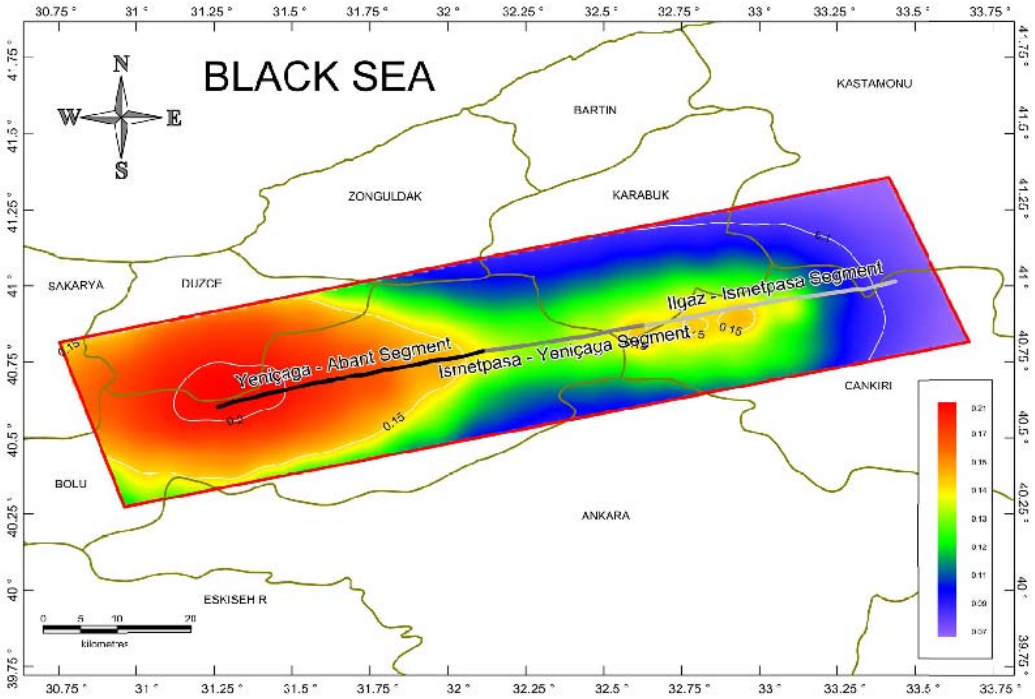

Figure 4.45 Hazard Map for PGA and Vs30 = 760 m/sec at 50% probability of exceedence hazard level

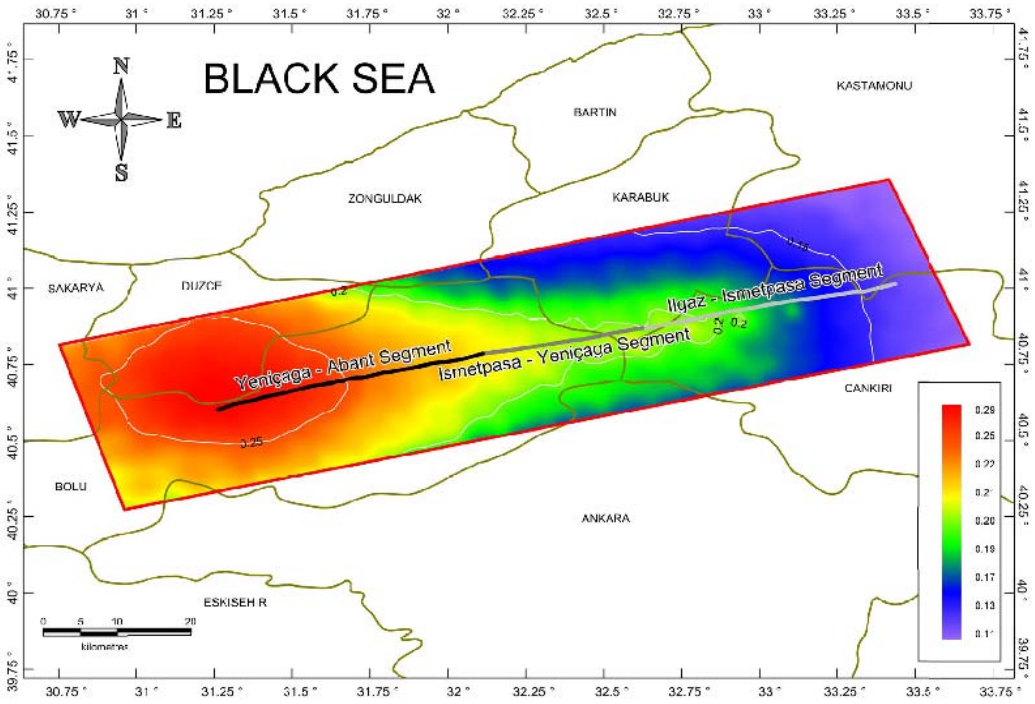

Figure 4.46 Hazard Map for PGA and Vs30 = 270 m/sec at 50% probability of exceedence hazard level

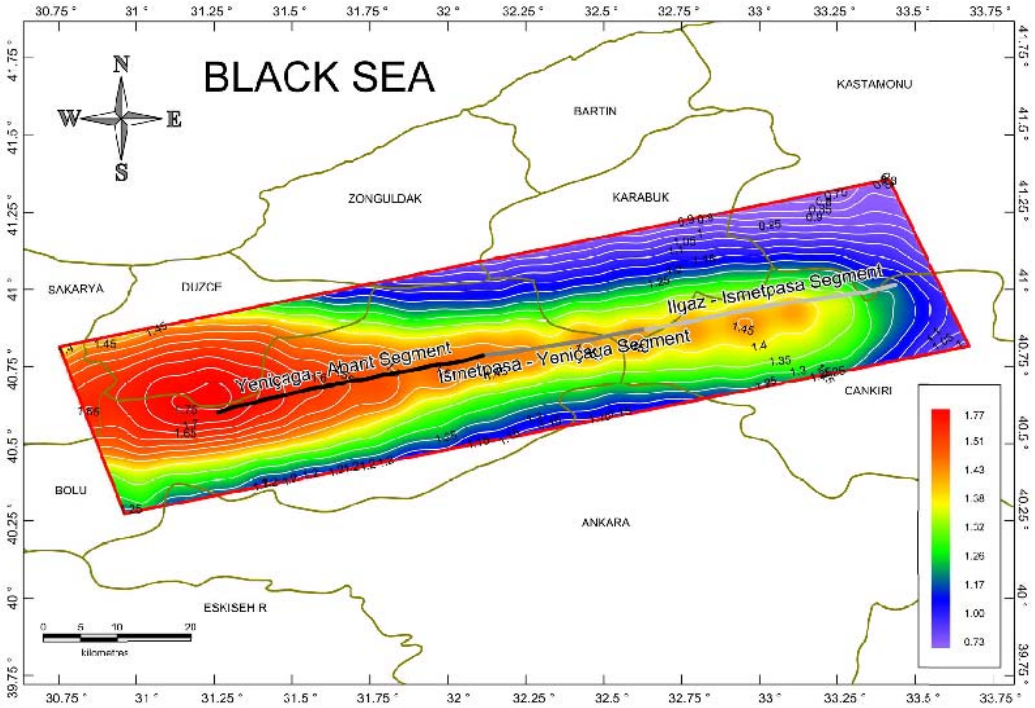

Figure 4.47 Hazard Map for T = 0.2 second Vs30 = 760 m/sec at 2% probability of exceedence hazard level

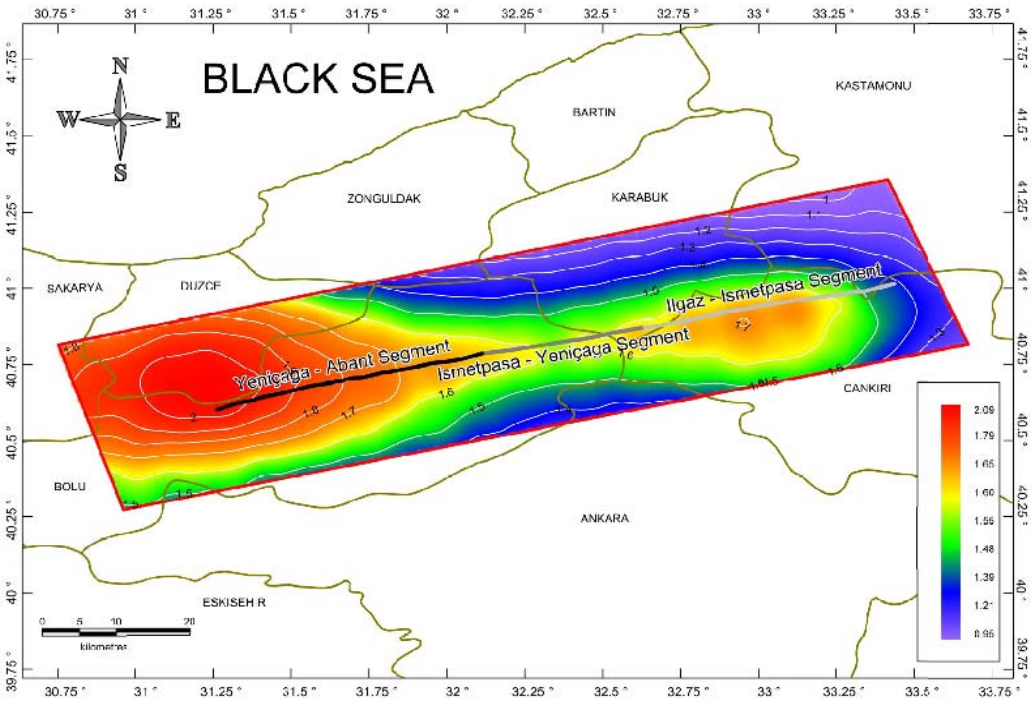

Figure 4.48 Hazard Map for T = 0.2 second Vs30 = 270 m/sec at 2% probability of exceedence hazard level

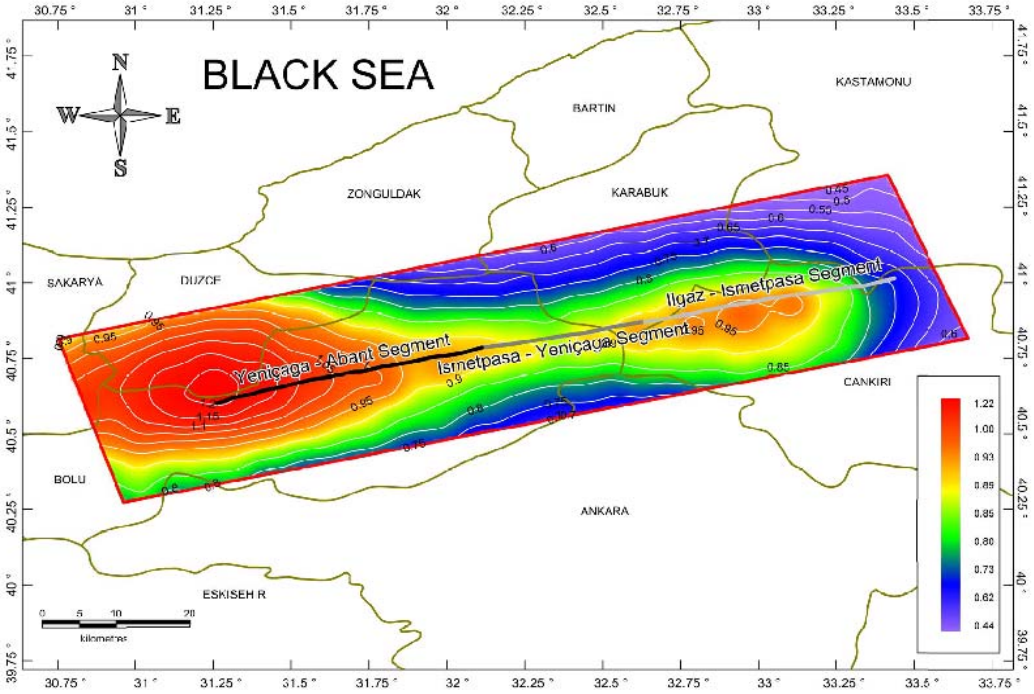

Figure 4.49 Hazard Map for T = 0.2 second Vs30 = 760 m/sec at 10% probability of exceedence hazard level

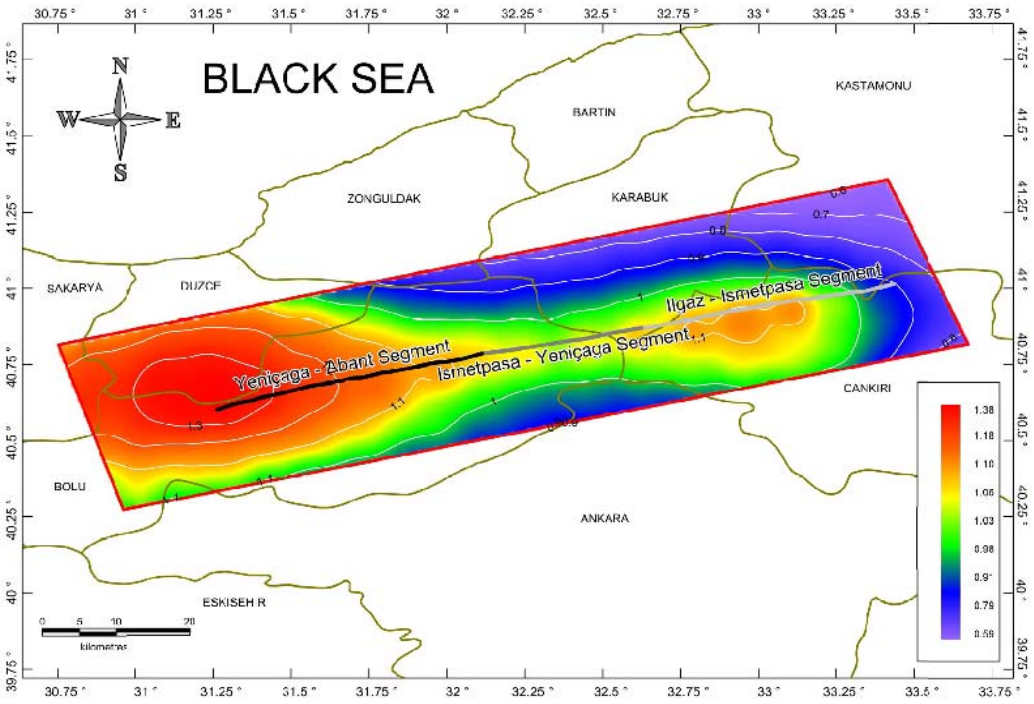

Figure 4.50 Hazard Map for T = 0.2 second Vs30 = 270 m/sec at 10% probability of exceedence hazard level

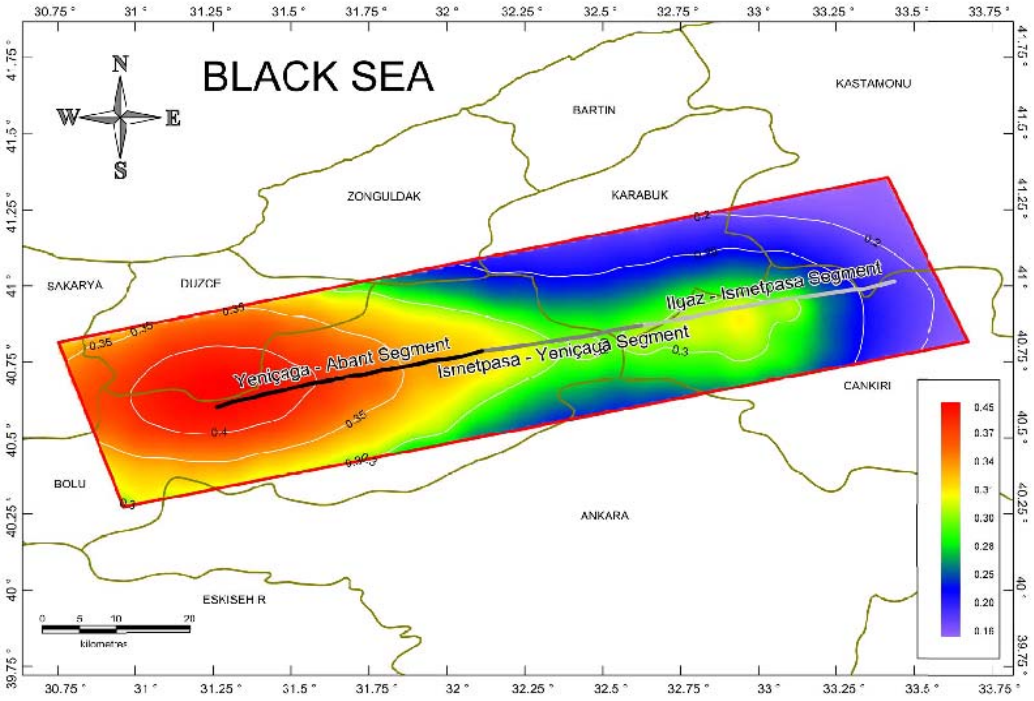

Figure 4.51 Hazard Map for T = 0.2 second Vs30 = 760 m/sec at 50% probability of exceedence hazard level

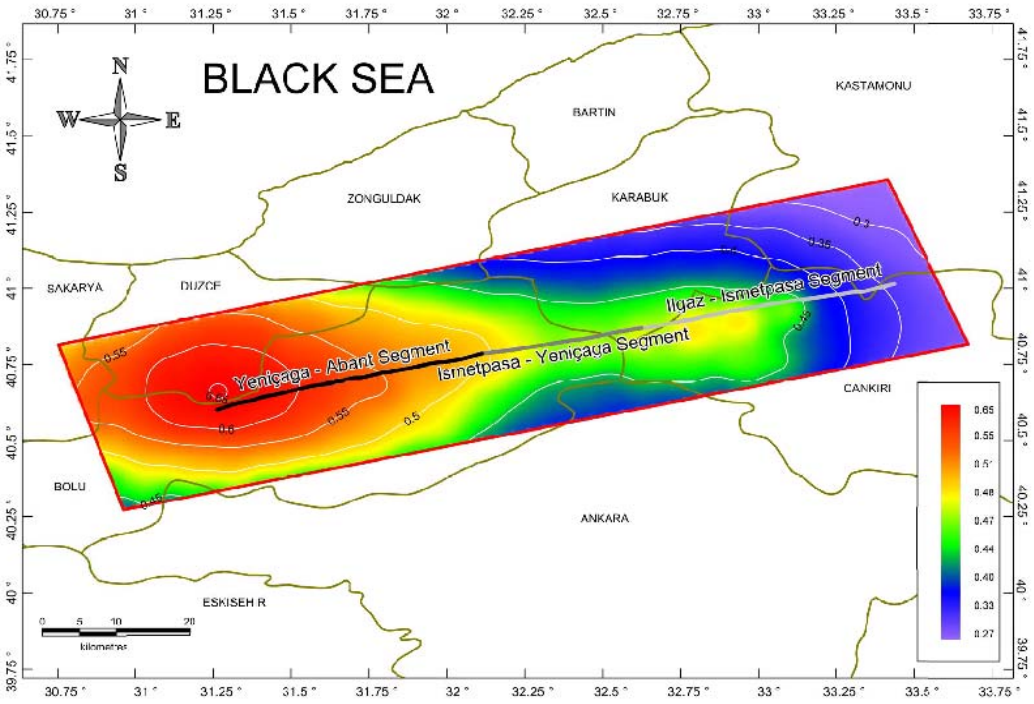

Figure 4.52 Hazard Map for T = 0.2 second Vs30 = 270 m/sec at 50% probability of exceedence hazard level

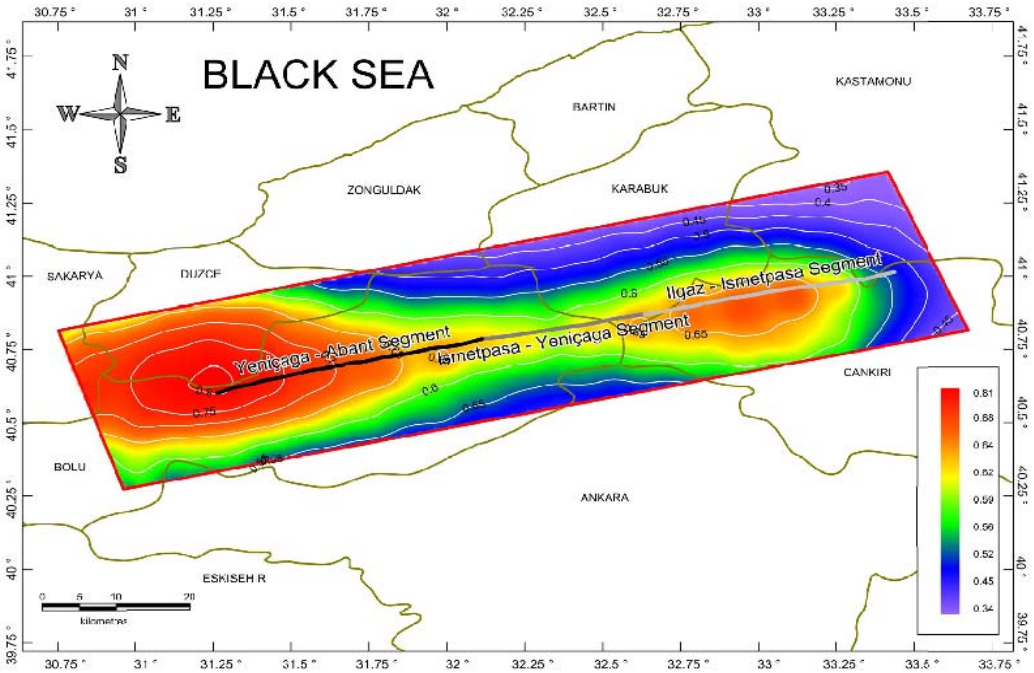

Figure 4.53 Hazard Map for T = 1.0 second Vs30 = 760 m/sec at 2% probability of exceedence hazard level

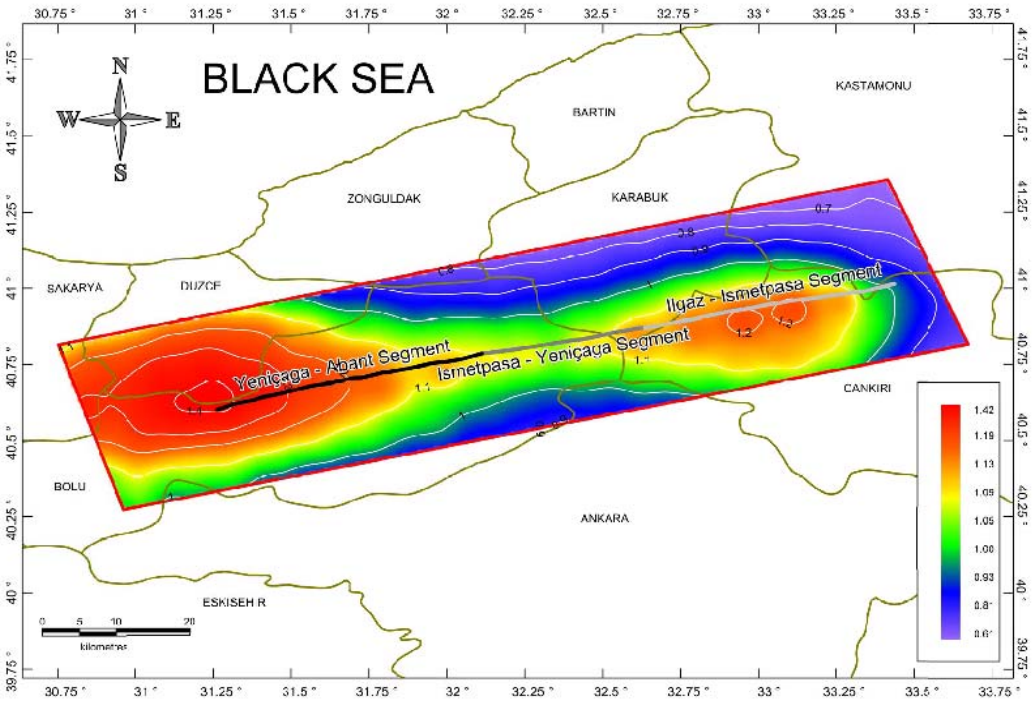

Figure 4.54 Hazard Map for T = 1.0 second Vs30 = 270 m/sec at 2% probability of exceedence hazard level

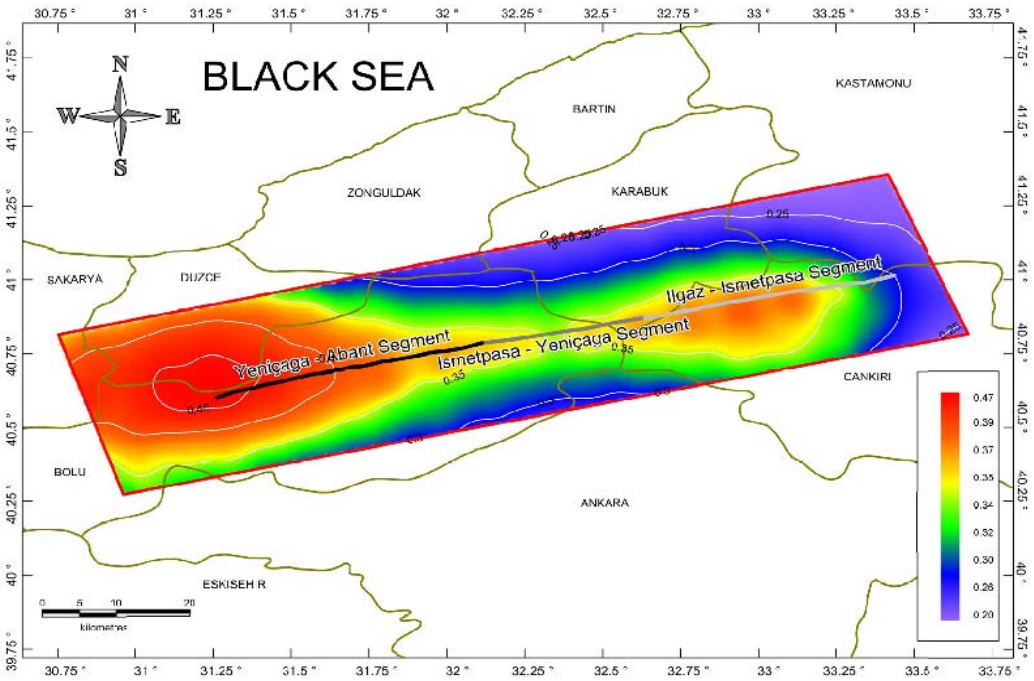

Figure 4.55 Hazard Map for T = 1.0 second Vs30 = 760 m/sec at 10% probability of exceedence hazard level

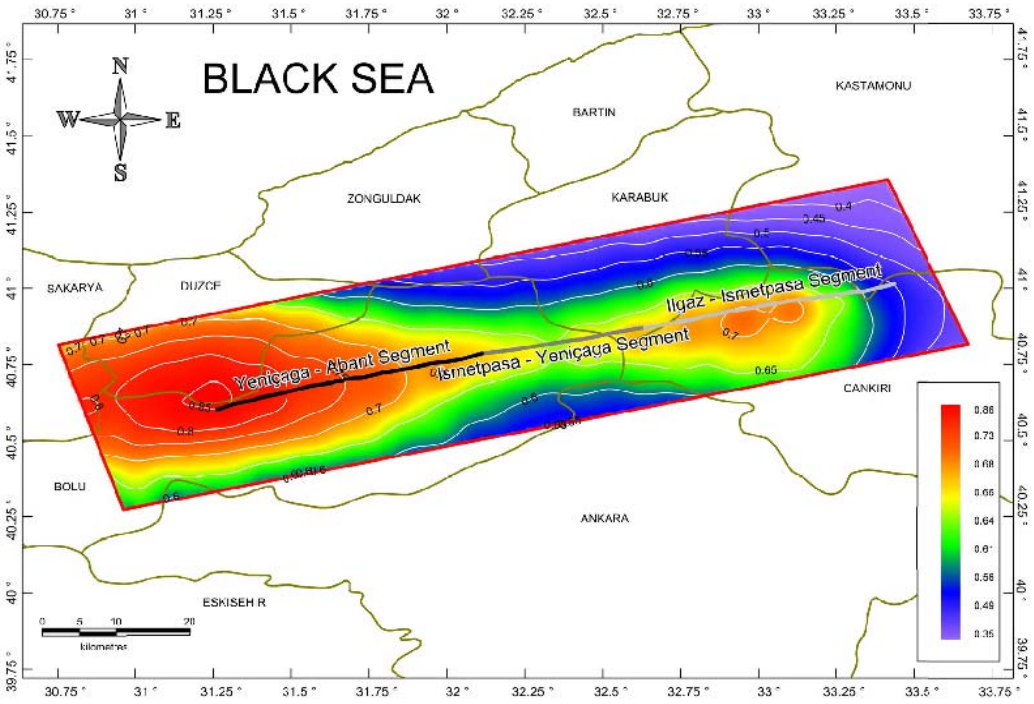

Figure 4.56 Hazard Map for T = 1.0 second Vs30 = 270 m/sec at 10% probability of exceedence hazard level

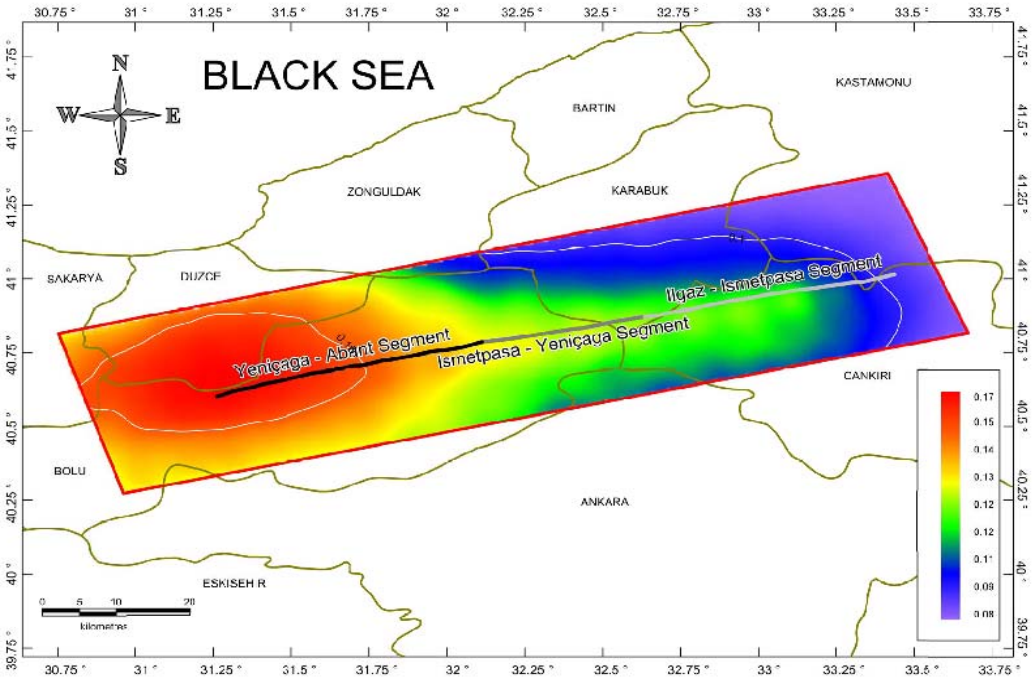

Figure 4.57 Hazard Map for T = 1.0 second Vs30 = 760 m/sec at 50% probability of exceedence hazard level

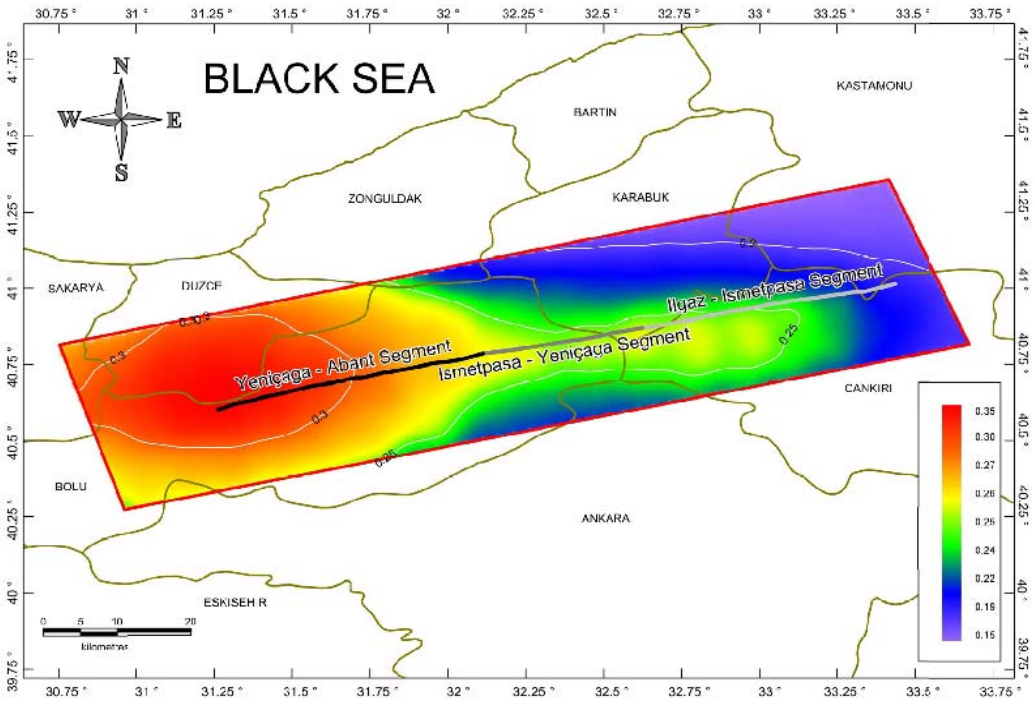

Figure 4.58 Hazard Map for T = 1.0 second Vs30 = 270 m/sec at 50% probability of exceedence hazard level

CHAPTER 5

SUMARY AND CONCLUSION

Bolu-Ilgaz is one of the seismically active regions of Turkey, located on the second degree earthquake zone according to the earthquake zonation map of Turkish Earthquake Code (2007). Being in the cross section of Düzce, Bolu-Ilgaz and Mudurnu-Abant segments of North Anatolian Fault (NAF) system, the region was damaged by several large earthquakes in the last century, however the structural damage in Bolu and its surroundings were substantial especially after the 1944 Bolu-Gerede Earthquake (Mw = 7.2) and 1999 Düzce Earthquake (Mw = 7.1). Therefore, to reduce the damage in the structures and loss of lives in future earthquakes beside a sensible and economical design practice, accurate evaluation of seismic hazard for this region is vital.

When compared to the Marmara Region and Istanbul Metropolitan Area, the number of PSHA studies in the Bolu-Gerede Region is quite inadequate. Actually, published PSHA studies for Turkey were limited (Erdik et al. 1985; Gülkan et al. 1993) before the 1999 events. Several researchers published estimates of seismic hazard and hazard for Marmara Region and for Istanbul after these events. Seismic source characterization was typically based on earthquake catalogue data using areal sources in early seismic hazard assessment studies and the magnitude distributions of these areal sources were modeled with truncated exponential (GR) relationship. In more recent studies (Erdik et al. 2004; Crowley and Bommer 2006; Kalkan et al. 2009), seismic sources were modeled by defining linear fault segments with the assumption that the seismic energy along these fault segments was released by characteristic events. The magnitude distribution functions of linear sources were considered to be fully characteristic. In addition, a background source representing the small-to-moderate magnitude earthquakes were added to the source model and the earthquake reoccurrence of the background source was modeled using truncated exponential magnitude distribution model. Due to the lack of local predictive models, early-stage GMPEs such as Boore et al. (1997), Campbell (1997), and Sadigh et al. (1997) were used in earlier studies to represent the ground motion variability. Only the recent study by Kalkan et al. (2009) used NGA-W1 ground motion prediction models along with a regional GMPE developed for Turkey after the 1999 events by Kalkan and Gülkan (2004).

The main components of PSHA methodology and framework for PSHA are rapidly improving by increase in the number of studies about seismic source and ground motion characterization for special structures and awareness of earthquake hazard reduction. The primary objective of this study is to evaluate the seismic hazard around the 1944 Bolu-Gerede Earthquake Rupture Zone using improved seismic source models and regionalized global ground motion prediction equations within a probabilistic framework. Once published, this study will be one of the foremost probabilistic seismic hazard analysis studies performed on the rupture zones of 1939-1944 earthquake sequence on NAF system.

The development of advanced seismic source models in terms of source geometry and reoccurrence relations is one of the major improvements over the previous seismic hazard assessment practice accomplished in this study. Three linear fault segments are defined for 1944 earthquake rupture zone: Ilgaz – Ismetpaşa Segment, Ismetpaşa – Yeniçağa segment, and Yeniçağa – Abant segment. Geometry of these sub-segments (length, width, and

segmentation points) are determined and incorporated with the help of available studies (Kondo et al., 2005 and Koçyiğit and Ayhan, 2009) and updated active fault maps of General Directorate of Mineral Research and Exploration (2012). Since speciality on structural geology, tectonics and seismology is a necessity to achieve an accurate and proper modeling of the seismic sources as an input to PSHA, expert evaluation of Dr. Şaroğlu for the fault geometry and source-epicenter matching for 1944 rupture zone is adopted for this study.

Composite magnitude distribution model (Youngs and Coppersmith, 1985) is used for all seismic sources in the study area to appropriate representing of the characteristic behavior of NAF without an additional background zone. The key feature of this model is; 94% of seismic moment is released by the characteristic earthquakes whereas the rest of the total seismic moment is released by the smaller size earthquakes due to the constraints of the distribution equation. The recurrence models for each source are bounded by minimum and maximum magnitude values. The minimum moment magnitude value is selected as 4.5 considering the engineering interest and the characteristic magnitude with one standard deviation is assigned to each source as maximum magnitude. The recurrence parameter b-value of the area is calculated as 0.60 using maximum likelihood method. The b-value used by the previous studies in the literature is in good agreement with the value estimated in this study. In order to evaluate the contribution of the variability in the b-value to the total hazard output, a sensitivity analysis is performed for Bolu City Centre and it is found that the hazard results are quite insensitive to the changes in b-value especially for high hazard levels when the composite magnitude recurrence model is employed. Fault segments, rupture sources, and rupture scenarios are determined using the WG-2003 terminology and a full rupture model is developed for each source considering single and multi-segment ruptures. Events in the earthquake catalogue are attributed to the individual seismic sources and scenario weights are determined by balancing the accumulated seismic energy by the catalog (A revised and extended earthquake catalog for Turkey since 1900 (M≥4.0), Kalafat, 2010) seismicity.

Activity rates for each source should be estimated for a complete source characterization model. The annual slip rate of each source is the main parameter to be estimated for calculating activity rate. The long period slip rate of the NAF system is found as 10 mm/year using geological observations (details are provided in Chapter 2). However, the short term slip rate of NAF branch in the area is assumed as 20 mm/year based on the geodetic measurements and assigned to each sub-segment. Several studies indicated that aseismic deformation is measured in İsmetpaşa therefore, in order to estimate the creep rate of Ismetpaşa-Yeniçağa segment, creep amount, time period, and measurement errors proposed in the previous studies from 1957 to 2010 are collected in a catalog of creep rates. Average creep rate measured by recent studies is found as approximately 8 mm/year. The slip rate assigned to the fault segment is reduced by this value for Ismetpaşa-Yeniçağa Segment and a total slip rate of 12 mm/year is assigned to that segment.

A weight is assigned to each rupture scenario and the weighted average of these scenarios are calculated by assigning a weight to each scenario in the logic tree. To establish the best fit between the cumulative rates of historic earthquakes and weighted average lines, the weights of individual scenarios are modified. In order to evaluate the contribution of the weights for rupture scenarios, a sensitivity analysis is performed by arbitrarily changing the weights of rupture scenarios. Analysis results showed that the selected weighted average combination is slightly above the median but lies between ± 1 δ range.

Gülerce et al. (2013) explained that Next Generation Attenuation (NGA-W1) models are renewed and improved in terms of supplement prediction parameters (such as depth of the source, basin effects, magnitude dependent standard deviations, etc.), statistical approach,

and a well constrained global database. Turkey-Adjusted NGA-W1 prediction models are employed by to represent for the first time on NAF system. Moreover, a sensitivity analysis is performed to evaluate the effect of weights assigned to different TR Adjusted NGA-W1 models. A less than 0.02g difference in the hazard for small annual probability of exceedance levels (0.03 or less) caused by using different attenuation models. However, as the level annual probability of exceedance getting smaller, the effect of ground motion prediction model getting larger. The hazard curves obtained using TR Adjusted BA-2008 and TR Adjusted CB 2008 models are quite similar since only magnitude adjustment was applied to these models (Gülerce et al., 2013). In addition to the magnitude adjustment, the site amplification terms of AS 2008 and CY 2008 models were also modified. Therefore, these two models result in lower hazard curves for rock site conditions. To fully represent the ground motion predictability equal weights are assigned to each model.

The hazard curves and uniform hazard spectra for different soil conditions (soil and rock) and for different hazard levels (2%, 10% and 50% probability of exceedence in 50 years) are provided for the four specific locations in the region (Bolu City Centre, Bolu Mountain Tunnel, Hasanlar Dam, Sarıyar Dam). In the PSHA analysis, the seismic sources on the west, Duzce Fault and NAF Southern Strand (Gülerce and Ocak, 2013), are also taken into consideration. The seismic source models of fault segments on the east are not completed yet, therefore these sources are not included in PSHA analyses. Highest hazard levels were obtained at Bolu City Centre and Bolu Mountain Tunnel and Sarıyar Dam has the lowest hazard curves for all of the different hazard levels since Sarıyar Dam is far away from the fault sources when compared with Bolu City Centre and Bolu Mountain Tunnel. The study area is located in first seismic zone according to TEC 2007 and 475 years return period design peak ground acceleration is 0.4g for regular buildings.

The hazard maps for the region for the rock site and soil site conditions at the applicable hazard levels in Turkish Earthquake Code (2007) are built for PGA, T=0.2 second and T=1 second spectral periods. Generally, the fault lines followed by the contours of the maps as expected. The assigned segmentation locations on the sources and the overlap locations of the seismic sources are the locations where hazard level increase. The west of the study area always has bigger hazard values since the sources on the west are included in PSHA. The highest value of PGA is around 0.95g for 2475 years return period for soil site (Vs30 = 270 m/sec) and 0.77g for rock site (Vs30 = 760 m/sec). High spectral accelerations at 0.2 second spectral period were observed at high return periods for sites very close to the active faults. The uncertainty level assigned to the ground motions for this study is median± 3σ as the new seismic hazard practice command which is significantly higher than the uncertainty level in TEC-2007.

Detailed in-situ geotechnical tests are definitely required to make a comprehensive site classification. However, using the geology, tectonics and geomorphology of the study area, an empirical rock classification model is constructed by dividing the study area into two parts; hard rock and soft rock. Since, no site specific measurements are available; the rocks are classified with respect to their neotectonic period or paleotectonic period. The rocks from the neotectonic period are assumed as units that did not face enough diyasine and classified as soft rock on the map. On the contrary, the rocks from the paleotectonic period assumed as units that faced enough diyasine and classified as hard rock on the map. The emprical rock classification map given in Chapter-2 and the hazard maps for PGA for acceptable hazard levels given in Chapter-4 are correlated in Figures 5.1 to 5.3. The resulting site specific hazard maps for PGA at 2%, 10% and 50% probability of exceedance hazard levels in 50 years are presented in Figure 5.1, 5.2 and 5.3, respectively. In order to construct these draft site specific hazard maps, the hazard values obtained from the soil rite runs (Vs30 = 270 m/sec) are attributed to the soft rock regions and the hazard values obtained from the rock

rite runs (Vs30 = 760 m/sec) are attributed to hard rock regions. Following interprepations can be made:

- The highest value of PGA is around 0.77g at 2% probability of exceedence hazard level, 0.49g at 10% probability of exceedence hazard level and 0.21g at 50% probability of exceedence hazard level for rock site conditions (Vs30 = 760 m/sec).
- The highest value of PGA is around 0.95g at 2% probability of exceedence hazard level, 0.62g at 10% probability of exceedance hazard level and 0.29g at 50% probability of exceedence hazard level for soil site conditions (Vs30 = 270 m/sec).
- In the draft site specific hazard map, the highest value of PGA is around 1.17g at 2% probability of exceedence hazard level, 0.77g at 10% probability of exceedance hazard level and 0.39g at 50% probability of exceedence hazard level. (Figure 5.1 to Figure 5.3)
- The draft site specific hazard map has higher hazard levels when compared to other hazard maps. When contouring the site with full of soil or rock, the results are close to each other and in order to not having large errors, the GIS software eliminates some of extremely high values at regions close to the faults. Therefore, the resulting map does not show the result of real extremely high values at regions close to the faults.
- The highest value of PGA at all of the different hazard levels are always West side of the study area for rock or soil maps since, the seismic sources on the west are taken into consideration but the seismic sources on the east are not included in PSHA analyses. As a result, the East side of the study area has smaller value of PGA at different hazard levels. However, for site specific hazard maps, the regions at the East side of the study area and close to the faults are assigned as soft rocks and assumed with Vs30 = 270 m/sec. Therefore, the resulting map shows higher PGA values at the East side of the study area.
- The West side of the study area shows a huge region like a circle with higher PGA values for soil map. However, for site specific hazard maps, the West side of the study area shows again a region with large PGA values and the diameter of the circle shape get smaller. The East side is assigned as both rock and soil, the regions which are assigned as rocks resulting with lower PGA values and this is effecting the West side of the maps getting a smaller diameter circle shaped.
- For both of the soil or rock maps, smaller hazard levels are observed in the regions close to segment-2. The region is the slip rate of segment-2 which is smaller than the other segments due to the creep observed in Ismetpaşa.
- To say repeatedly because of big importance, detailed in-situ geotechnical tests are definitely required to make a comprehensive site classification. The results given in this study can be used to give an idea before in-situ geotechnical tests. The site specific results have larger errors for the regions close the fault because the type of soil assigned is changing in short distances. However, for the regions far away from the faults, the soil type assigned is not changing so much and generally hard rock definitions are assigned to these regions. Therefore, the results are with smaller errors when compared to the near fault sites.

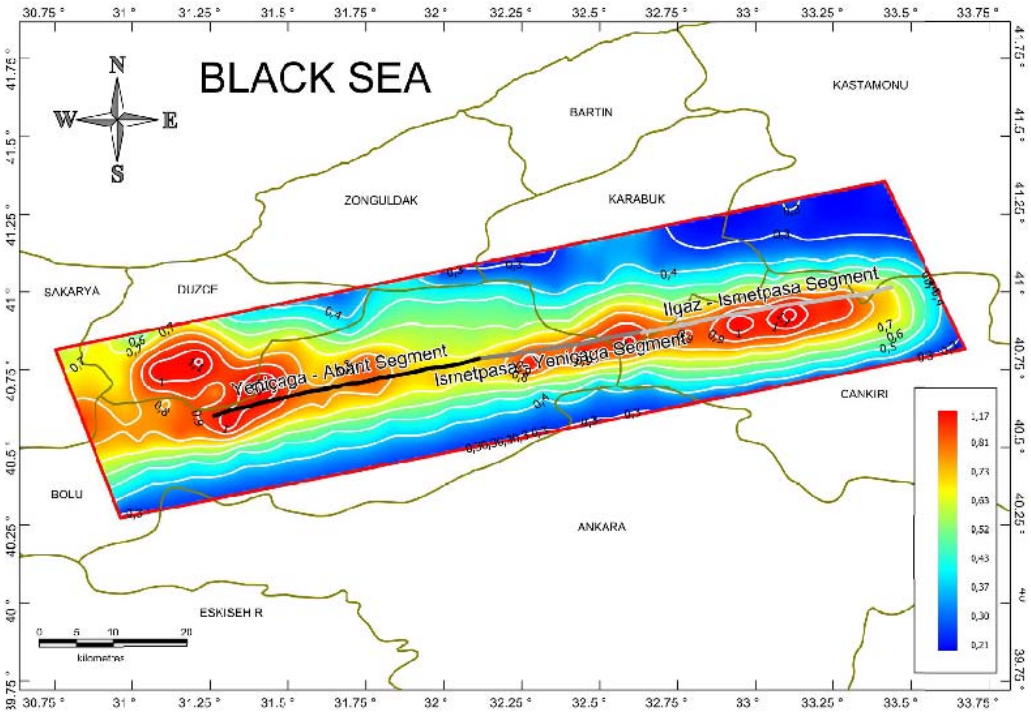

Figure 5.1 Site specific hazard map for PGA at 2% probability of exceedance hazard level

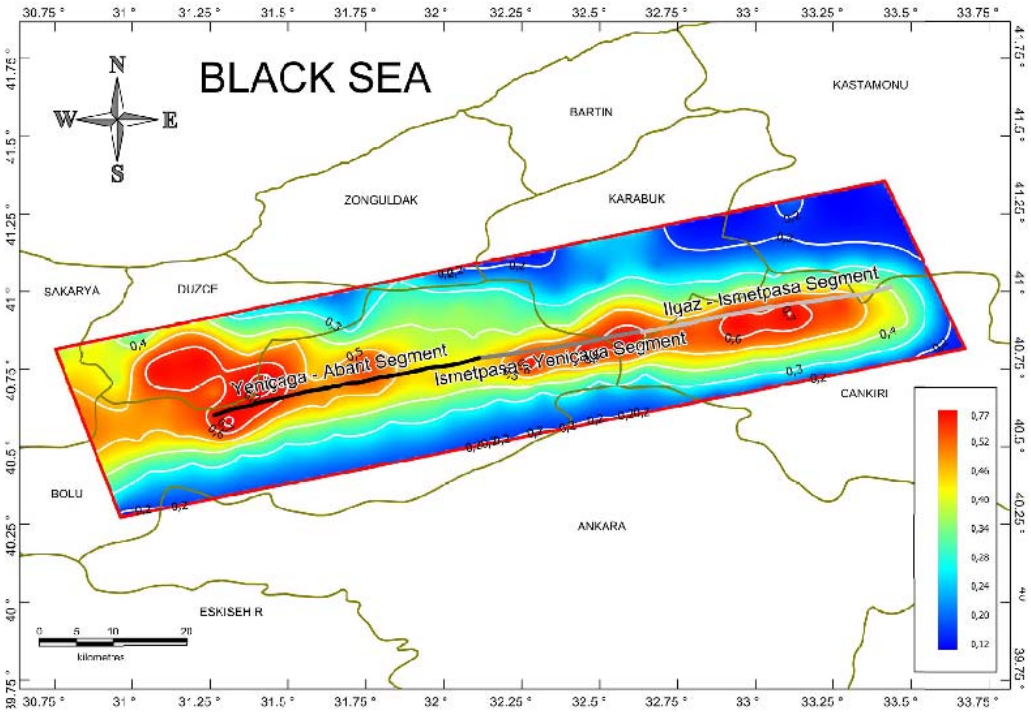

Figure 5.2 Site specific hazard map for PGA at 10% probability of exceedance hazard level

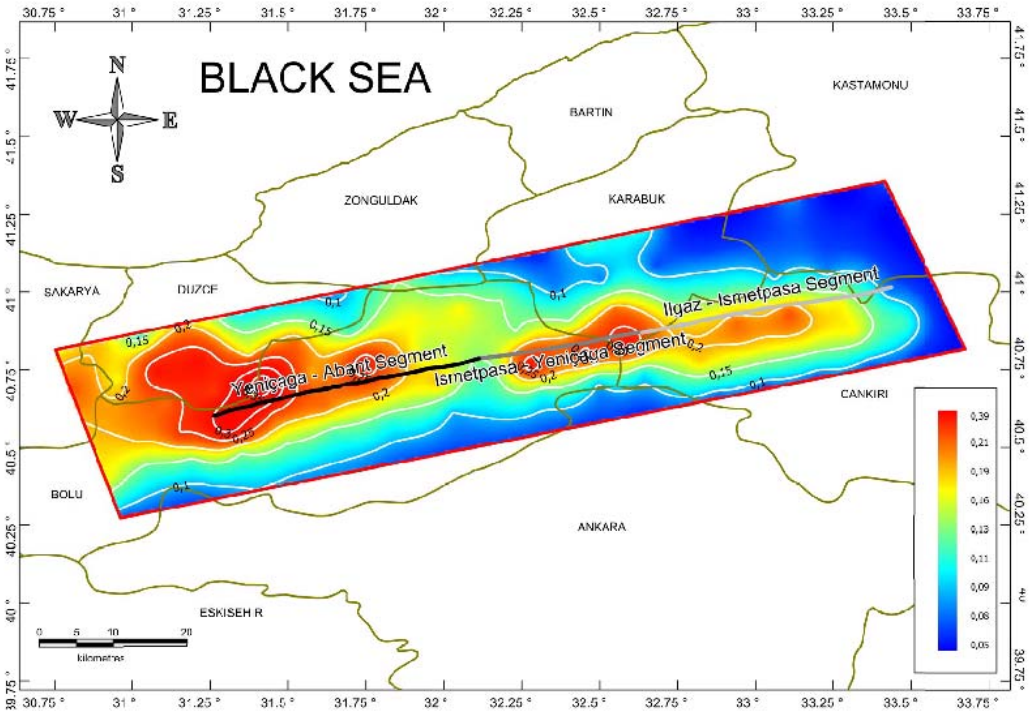

Figure 5.3 Site specific hazard map for PGA at 50% probability of exceedance hazard level

The seismic design of the special structures in the study area may be done with the help of the results of this study. Site-specific hazard assessment for local site conditions and site-specific design spectrum may be constructed by the hazard maps of the study area for rock site and soil site conditions at the applicable hazard levels of TEC-2007. Alternatively, the emprical rock classification map and site specific hazard maps will give an idea about the future seismic hazard in the study area with a must of site-specific in-situ tests. Assigning the seismic sources outside the study area into the analysis may improve the results of this study.

REFERENCES

Abdüsselamoğlu, Ş. (1959) : Yukarı Seyhan Bölgesinde Doğu Toroslar'ın Jeolojik Etüdü. M.T.A. Rap. no. 2668 [in Turkish].

Abrahamson, N. A., State of The Practice of Seismic Hazard Evaluation, 2000

Abrahamson, N.A. (2006) Seismic Hazard Assessment: Problems With Current Practice And Future Developments, First European Conference on Earthquake Engineering and Seismology(a joint event of the 13th ECEE & 30th General Assembly of the ESC)Geneva, Switzerland, 3-8 September 2006.

Abrahamson, N. A. and Silva, W. (2008) Summary of the Abrahamson & Silva NGA Ground-Motion Relations, Earthquake Spectra, Volume 24, No. 1, 67 – 97.

Aki, K. (1965). Maximum likelihood estimate of b in the formula log N = a - bM and its confidencelimits, Bull. Earthquake Res. Inst., Tokyo Univ. 43, 237-239.

Akkar et al. (2010) The Recently Compiled Turkish Strong Motion Database: Preliminary Investigation for Seismological Parameters, Seismicity, Volume 14, Issue 3, 457-479.

Ambraseys, N. N. (1970). Some characteristic features of the Anatolian fault zone, Tectonophysics 9, 143–165.

Ambraseys and Jackson, Faulting associated with historical and recent earthquakes in the Eastern Mediterranean region, Geophysical Journal International, Volume 133, Issue 2, pages 390–406, May 1998.

Armijo, R., Meyer, B., Hubert, A., Barka, A. (1999) Westward propogation of the North Anatolian fault into the nothern Aegean: Timing and kinematics, Geology, vol. 27,no. 3, 267-270.

Atakan, K., A. Ojeda, M. Meghraoui, A. A. Barka, M. Erdik, and A. Bodare (2002). Seismic hazard in Istanbul following the 17 August 1999 Izmit and 12 November 1999 Düzce earthquakes, Bull. Seismol. Soc. Am. 92, no. 1, 466–482.

Atkinson, G. M. and Boore, D. M. (1997) Some comparisons between recent ground-motion relations, Seism. Res. Lett. 68, 24–40.

Ayhan, M.A., Demir, C., Kilicoglu, A., Sanli, I., Nakiboglu, S.M. (1999). Crustal motion around the western segment of the northAnatolian fault zone: geodetic measurements and geophysicalinterpretation. Abstr. Int. Union Geod. Geophy. 99, 77–78.

Ayhan, M.E., Bürgmann, R., McClusky, S., Lenk, O., Aktug, B., Herece, E., Reilinger, R.E. (2001). Kinematics of the Mw=7.2, 12November 1999, Düzce, Turkey earthquake. Geophys. Res. Lett.28 (2), 367–370.

Ayhan, M. E. & Koçyiğit, A. (2009). Displacements and Kinematics of the February 1, 1944 Gerede Earthquake (North Anatolian Fault System, Turkey): Geodetic and Geological Constraints: Turkish Journal of Earth Sciences (Turkish J. Earth Sci.), Vol. 19, 285–311.

Barka, A.A., and Kadinsky-Cade, K., 1988, Strike-slip fault geometry in Turkey and its influence on earthquake activity. Tectonics, 7, 663-684.

Barka, A. A. (1996), Slip distribution along the North Anatolian fault associated with large earthquakes of the period 1939 to 1967, Bull.Seismol. Soc. Am., 86, 1234–1238.

Barka, A.A.and 22 others, 2002, The surface rupture and slip distribution of the 17 August 1999 İzmit earthquake (M 7.4), North Anatolian Fault. Bulletin of the Seismological Society of America, 92, 43-60.

Bender, B. (1983) Maximum Likelihood Estimation Of b Values For MagnitudeGrouped Data, Bull. Seism. Soc. Am. 73, no. 3, 831–851.

Blumenthal, M., 1948, Bolu Civari ile Aşağı Kızılırmak Mecrası Arasında Kuzey Anadolu Silsilelerinin Jeolojisi: MTA Pub., Serie B, No. 13, 265 [in Turkish].

Boore, D. M., Lamprey, J. W., Abrahamson, N. A. (2006) Orientation-Independent Measures of Ground Motion, Bull. Seism. Soc. Am. 96, no. 4A, 1502 - 1511.

Boore, D. M., Atkinson, G. M. (2008) Ground-Motion Prediction Equationsfor the Average Horizontal Componentof PGA, PGV, and 5%-Damped PSAat Spectral Periods between 0.01 sand 10.0 s, Earthquake Spectra, Volume 24, No. 1, 99 – 138.

Campbell, K. W., Empirical Near-Source Attenuation Relationships for Horizontal and Vertical Components of Peak Ground Acceleration, Peak Ground Velocity, and Pseudo-Absolute Acceleration Response Spectra, 1997

Campbell, K. W. and Bozorgnia, Y. (2008) NGA Ground Motion Model for theGeometric Mean Horizontal Componentof PGA, PGV, PGD and 5% DampedLinear Elastic Response Spectrafor Periods Ranging from 0.01 to 10 s, Earthquake Spectra, Volume 24, No. 1, 139 – 171Balaam, N. P., & Poulos, H. G. (1983). The behavior of foundations supported by clay stabilized by stone columns. Proc. 8th European Conf. on Soil Mechanics and Foundation Engineering, Helsinki, Vol. 1, pp.199-204.

Chiou, B. Darragh, R., Gregor, N. and Silva, W. (2008) NGA Project Strong-Motion Database, Earthquake Spectra, Volume 24, No. 1, 23 – 44.

Chiou, B. S. J. and Youngs, R. R. (2008) An NGA Model for the Average HorizontalComponent of Peak Ground Motionand Response Spectra, Earthquake Spectra, Volume 24, No. 1, 173 – 215.

Cornell, C. A. (1968) Engineering siemsic hazard analysis, Bull. Seism. Soc. Am., 58, 1583-1606. Erratum: 59,1733.

Crowley, H., and J. J. Bommer (2006). Modeling seismic hazard in earthquake loss models with spatially distributed exposure, Bull. Eq. Eng. 4, 249–273.

Çakir, A., M. Akoglu, S. Belabbes, S. Ergintav, and M. Meghraoui (2005), Creeping along the Ismetpasa section of the North Anatolian fault (Western Turkey): Rate and extent from InSAR, Earth Planet. Sci. Lett., 238, 225–234, doi:10.1016/j.epsl.2005.06.044.

Dewey, J. W. (1976). Seismicity of Northern Anatolia, Bull. Seism. Soc. Am. 66, 843-868.

Erdik, M., Doyuran, V., Akkas, N., and P. Gulkan (1985): A probabilistic assessment of the seismic hazard in Turkey, Tectonophysics, No. 117, 295-344.

Erdik, M., M. Demircioğlu, K. Şeşetyan, E. Durukal, and B. Siyahi (2004) Earthquake hazard in Marmara region, Turkey, Soil Dyn. Earthq. Eng.24, 605–631.

Gülkan, P., A. Koçyiğit, M.S. Yücemen, V. doyuran and N. Başöz (1993): En son verilere göre hazırlanan Türkiye deprem bölgeleri haritası, *Report No: METU/EERC 93-1 [in Turkish].*

Genç, G. (2004) Probabilistic Seismic Hazard Assessment for Eskişehir. Master Thesis, Middle East Technical University, Ankara.

Herece E. and Akay E., 2003, Atlas of North Anatolian Fault (NAF). General Directorate of Mineral Research and Exploration, Special Publication series-2, Ankara, 61 p+13 appendices as separate maps.

Herece, E. 2005. Neotectonics of the Western Section of the North Anatolian Fault Zone. PhD Thesis, Ankara University, Ankara.

Idriss I. M. (2008) An NGA Empirical Model for Estimatingthe Horizontal Spectral ValuesGenerated By Shallow Crustal Earthquakes, Earthquake Spectra, Volume 24, No. 1, 217 – 242.

Jackson, J., and McKenzie, D., 1988, The relationship between plate motions and seismic moment tensors, and the rates of active deformation in the Mediterranean and Middle East. Geophys. J., 93, 45-73.

Kalafat, D., Statistical Evaluation of Turkey Earthquake Catalog: Case Study, 2010

Kalkan, E. and Gülkan, P. (2004) Site-Dependent Spectra Derived from Ground Motion Records in Turkey, Earthquake Spectra, Volume 20, No. 4, 1111 – 1138.

Kalkan, E., Gülkan P., Yilmaz N. and M. Çelebi (2009): Reassessment of probabilistic seismic hazard in the Marmara Region, Bull. Seismol. Soc. Am. 99, no. 4, 2127-2146.

Karabacak, V., Altunel, E., Çakır, Z. (2011) Monitoring aseismic surface creep along the North Anatolian Fault (Turkey) using ground-based LIDAR: Earth and Planetary Science Letters**,** Vol.304, Issues 1–2, 1 April 2011, Pages 64–70

Ketin, L. (1948) Son on yılda Türkiye'de vukua gelen büyük depremlerin tektonik ve mekanik neticeleri hakkında, TJK Bült. 2/1, 1-13 [in Turkish].

Ketin, I. (1969). Uber die nordanatolishe horizontal verschiebung, Bull. Mineral Res. Explor. Inst. Turkey 72, 1–28.

Kondo, H., Awata, Y., Emre, Ö., Doğan, A., Özalp, S., Tokay, F., Yıldırım, C., Yoshioka, T., Okumura, K. (2005) Slip Distribution, Fault Geometry, and Fault Segmentation of the 1944 Bolu-Gerede Earthquake Rupture, North Anatolian Fault, Turkey: Bulletin of the Seismological Society of America, Vol. 95, No. 4, 1234–1249

Kondo, H., Özaksoy, V., Yıldırım, C. (2010) Slip history of the 1944 Bolu-Gerede earthquake rupture along the North Anatolian fault system: Implications for recurrence behavior of multisegment earthquakes: Journal of Geophysıcal Research, vol. 115,

Kramer, S. L., Geotechnical Earthquake Engineering, Prentice Hall, 1996

Kutoğlu, H. S., Akcin, H., Kemaldere, H., Görmüş, K. S. (2008) Triggered creep rate on the Ismetpasa segment of the North Anatolian Fault: Nat. Hazards Earth Syst. Sci., 8, 1369–1373.

Lienkaemper, J.J. (1984) Statistical relations among earthquake magnitude, surface rupture length, and surface fault displacement, Bulletin of the Seismological Society of America , vol. 74, no. 6, 2379-2411.

McClusky, S.27 coauthors (2000). Global Positioning System constraintson plate kinematics and dynamics in the eastern Mediterranean andCaucasus, J. Geophys. Res. 105, 5695–5719.

Meade, B.J., Hager, B.H., McClusky, S.C., Reilinger, R.E., Ergintav, S., Lenk, O., Barka, A., Ozener, H., 2002, Estimates of seismic potential in the Marmara Sea region from Block modles of secular deformation constrained by global positioning system measurements. Bulletin of the Seismological Society of America, 86, 1238-1254.

Ministry of Publicworks & Settlement, (2007). Turkish Earthquake Resistant Design Code - TEDRC, Ankara, Turkey.

Oztürk, A., S. Inan, and Z. Tutkun (1985). Abant-Yeniçağa Yöresinin Tektoniği, Bull. Earth Sci. Cumhuriyet Univ. 2, 35-52.

Papazachos, B.C., Papaioannou, Ch.A., Papazachos, C.B. and Savvaidis, A.S., 1999, Rupture zones in the Aegean region. Tectonophysics, 308, 205-211

Pınar, N. (1953) : Preliminary Note on The Earthquake of Yenice - Gönen, Turkey, 18 March 1953. Bull. Seism. Soc. Am. 43, s. 307-310.

Reilinger, R.; McClusky, S.; Vernant, P.; Lawrence, S.; Ergintav, S.; Cakmak, R.; Ozener, H.; Kadirov, F.; Guliev, I.; Stepanyan, R.; Nadariya, M.; Hahubia, G.; Mahmoud, S.; Sakr, K.; ArRajehi, A.; Paradissis, D.; Al-Aydrus, A.; Prilepin, M.; Guseva, T.; Evren, E.; Dmitrotsa, A.; Filikov, S. V.; Gomez, F.; Al-Ghazzi, R.; Karam, G., 2006, GPS constraints on continental deformation in the Africa-Arabia-Eurasia continental collision zone and implications for the dynamics of plate interactions. J. Geophys. Res., Vol. 111, No. B5, B05411.

Reiter L 1990: Earthquake hazard analysis. Columbia University Press, New York

Sadigh, K., Chang, C.-Y., Egan, J. A., Makdisi, F. and R.R. Youngs (1997): Attenuation relationships for shallow crustal earthquakes based on California strong motion data, Seismological Research Letters, January/February 1997, v. 68 no. 1, 180-189

Schwartz, D. P. and K. J. Coppersmith (1984). Fault behavior and characteristic earthquakes: examplesfrom the Wasatch and San Andreas faults, J. Geophys. Res. 89, 5681-5698.

Stein, R. S., Barka,A. A. and Dieterich, J. H. (1997), Progressive failure onthe North Anatolian fault since 1939 by earthquake stress triggering,Geophys. J. Int., 128, 594–604.

Şaroğlu, F., Emre, Ö. and Boray, A., 1987, Türkiye'nin diri faylarıve depremsellikleri, MTA Rap No 8174 (unpublished) [in Turkish].

Şaroğlu, F. (1988) Age and Offset of North Anatolian Fault: METU Journal of Pure and Applied Sciences, Vol.31, No.1-3, 65-79.

Şaroğlu, F., et al. "Yeniçağa-Gerede-Eskipazar arasının jeolojisi ve Kuzey Anadolu Fayı'nın genel özellikleri." MTA Derleme 9873 (1995) [in Turkish].

Şaroğlu, F. (2010) Neotektonik ve Türkiye'nin Neotektoniğinden Örnekler: TPAO Arama Daire Başkanlığı Seminer Notları, [in Turkish].

Taşman, C. E. (1944). Gerede-Bolu depremi, Bull. Mineral Res. Explor. Inst. Turkey 1/31, 134 [in Turkish].

Tatar, O., Piper, J.D.A., Gürsoy, H., and Temiz, H., 1996, Regional significance of neotectonic counterclockwise rotation in Central Turkey. International Geology Review, 38, 697-700.

Tokay, M., 1952, Karadeniz Ereğlisi-Alaplı-Kızıltepe-Alacaağzı Bölgesi Jeolojisi: MTA Derg., 42/43, 35-78, Ankara [in Turkish].

Tokay, M. 1973. Geologic observations along the North Anatolian Fault Zone from Gerede to Ilgaz. In: Proceedings of the Symposium on North Anatolian Fault Zone and Earthquake Belt. Mineral Research Institute Publication, Ankara, 12–29 [in Turkish].

Weichert, D. H. (1980), Estimation Of The Earthquake Recurrence ParametersFor Unequal Observation Periods For DifferentMagnitudes, Bull. Seismol. Soc. Am. 70, no. 4, 1337–1346.

Wells, D. L., and K. J. Coppersmith (1994). New empirical relationshipsamong magnitude, rupture length, rupture width, rupture area, and surface displacement, Bull. Seismol. Soc. Am. 84, no. 4,974–1002.

Working Group on California Earthquake Probabilities (USGS Working Group)(2003). EarthquakeProbabilities in the San Francisco Bay Region: 2002–2031, U.S. Geological SocietyOpen File Report 03-214.

Yılmaz Öztürk, N. (2008) Probabilistic seismic hazard analysis: a sensitivity study with respect to different models: A Thesıs Submitted to the Graduate School of Natural and Applied Sciences of Middle East Technical University.

Yoshioka, T., Okumura, K., Kuşçu, İ., Ömer, E. (2000) Datye, K. R. (1982). Recent surface faulting of the North Anatolian fault along the 1943 Ladik earthquake ruptures: Bulletin of Geological Survey of Japan vol.(51) (1), 29-35.

Youngs, R. R., and K. J. Coppersmith (1985). Implications of fault slip rates and earthquake recurrence models to probabilistic seismic hazard estimates, Bull. Seismol. Soc. Am. 75, no. 4, 939–964.